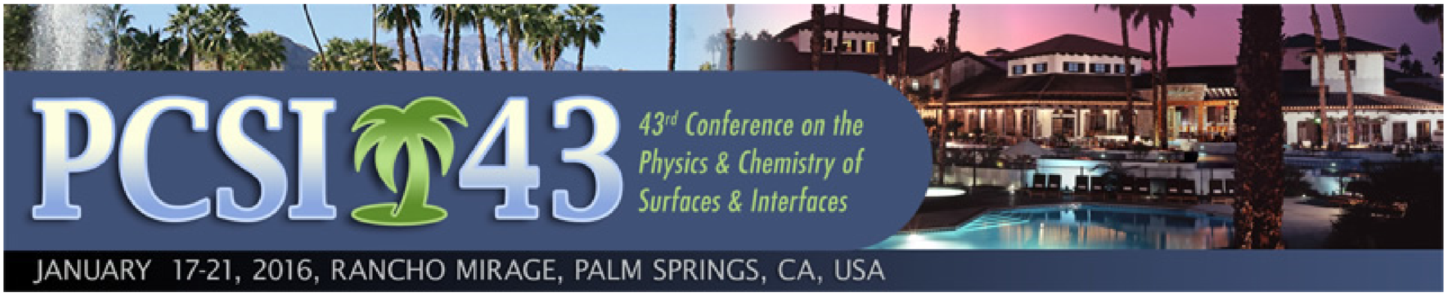

PCSI 43

43rd Conference on the Physics & Chemistry of Surfaces & Interfaces

JANUARY 17-21, 2016, RANCHO MIRAGE, PALM SPRINGS, CA, USA

Abstract Book & Schedule

Platinum Sponsors

SIGMA Surface Science Partnered with MANTIS Deposition	kSA
DEPARTMENT OF THE NAVY USN ONR Science & Technology	

Gold Sponsors

MDC VACUUM PRODUCTS, LLC	SPECS™

Silver Sponsors

AMERICAN ELEMENTS	NANOANDMORE USA The Nanotech Facilitator
RIBER	STAIB INSTRUMENTS

PCSI-43 General Information

Conference Hotel:

Omni Rancho Las Palmas Resort, Rancho Mirage (Palm Springs), California

Conference Website: www.pcsiconference.org

Chair:

Len Brillson
The Ohio State University
E-mail: brillson.1@osu.edu

General Chair:

Chris Palmstrøm
University of California, Santa Barbara
E-mail: cpalmstrom@ece.ucsb.edu

Program Committee:

A. Bhattacharya, Argonne National Laboratory
L. Brillson, The Ohio State University
S. Crooker, Los Alamos National Laboratory
A. Demkov, Univ. of Texas, Austin
C. Eddy, Naval Research Laboratory
M. Flatté, University of Iowa
J. Hilton, Mantis
H. Ishii, Chiba University
H. Hwang, Stanford
K. Kavanagh, Simon Fraser University
R. Kawakami, The Ohio State University
P. Koenraad, Eindhoven University of Technology
W. Lampert, Rice University
L. Lauhon, Northwestern University
R. Ludeke, IBM
C. McConville, Warwick University
A. Mikkelsen, Lund University
R. Myers, The Ohio State University
C.J. Palmstrøm, University of California at Santa Barbara
H. Riechert, Paul Drude Institute
J. Rowe, University of North Carolina
N. Samarth, Penn State University
Y. Suzuki, Stanford University
A. Talin, Sandia National Laboratory
A. Toriumi, University of Tokyo
P. Varanasi, Army Research Office
R. Wallace, University of Texas, Dallas
E. Yu, University of Texas at Austin
J. Zhu, Penn State University

JVST Special Issue Editor:

Rudy Ludeke
E-mail: rudy_ludeke@msn.com

Registration:

Della Miller/Heather Korff
AVS, 110 Yellowstone Dr., Suite 120
Chico, CA 95973
E-mail: della@avs.org /heather@avs.org
Phone: 530-896-0477

Presentation Formats:

Invited Talks—35 minute oral presentation, 5 minute discussion, plus poster
Upgraded Talks—17 minute oral presentation, 3 minute discussion, plus poster
Contributed Talks—4 minute oral presentation (max 3 slides, 1 minute discussion, plus poster)
Posters—Displayed all week (46 inches high x 46 inches wide)

PCSI-43 Sponsors

Platinum Sponsors

SIGMA Surface Science
Partnered with MANTIS Deposition

kSA

DEPARTMENT OF THE NAVY
USN
ONR
Science & Technology

Gold Sponsors

MDC
VACUUM PRODUCTS, LLC

SPECS™

Silver Sponsors

AMERICAN ELEMENTS

NANOANDMORE USA
The Nanotech Facilitator

RIBER

STAIB
INSTRUMENTS

PCSI-43 Schedule Overview

Sunday:

Su1300	Registration
Su1425	Welcome Remarks
Su1430	Sunday Afternoon Session: *Magnetism*
Su1530	Sunday Afternoon Session: *Nanostructures I*
Su1630	Poster Setup
Su1800	Welcome Reception
Su1930	Sunday Evening Session: *Energy I*

Monday:

Mo0745	Registration and Continental Breakfast
Mo0830	Monday Morning Session: *Nanostructures II*
Mo1000	Coffee Break and Poster Viewing
Mo1100	Monday Morning Session: *Nanostructures II Continued*
Mo1110	Monday Morning Session: *Energy II*
Mo1205	Lunch and Poster Viewing
Mo1400	Monday Afternoon Session: *Oxides I*
Mo1530	Coffee Break and Poster Viewing
Mo1630	Monday Afternoon Session: *Spintronics I*
Mo1805	Dinner
Mo1930	Monday Evening Session: *Complex Oxides*

Tuesday:

Tu0745	Registration and Continental Breakfast
Tu0830	Tuesday Morning Session: *Semiconductor Interfaces and Devices I*
Tu1000	Coffee Break and Poster Viewing
Tu1100	Tuesday Morning Session: *2D Materials I*
Tu1200	Free Afternoon
Tu1900	Tuesday Evening Rump Session: *Novel Energy Materials*

Wednesday:

We0745	Registration and Continental Breakfast
We0830	Wednesday Morning Session: *Oxides II*
We0925	Wednesday Morning Session: *High K*
We1015	Coffee Break and Poster Viewing
We1100	Wednesday Morning Session: *Novel Semiconductors*
We1120	Wednesday Morning Session: *2D Materials II*
We1200	Lunch and Poster Viewing
We1400	Wednesday Afternoon Session: *Semiconductor Interfaces and Devices II*
We1500	Wednesday Afternoon Session: *New Techniques and Devices*
We1525	Coffee Break and Poster Viewing
We1625	Wednesday Afternoon Session: *Semiconductor Interfaces*
We1830	Conference Banquet

Thursday:

Th0745	Continental Breakfast
Th0830	Thursday Morning Session: *2D Materials III*
Th1000	Coffee Break and Poster Viewing
Th1100	Thursday Morning Session: *Spintronics II*
Th1205	Conference Ends

PCSI-43 Schedule

Sunday Afternoon, January 17:				
Su1300	1:00 p.m.	Registration		
Su1425	2:25 p.m.	Welcome Remarks		
Magnetism				Session Chair: M. Flatte'
Su1430	2:30 p.m.	INVITED: Atomic Spin Chains as Testing Ground for Quantum Magnetism		S. Otte, Delft Univ. of Technology
Su1510	3:10 p.m.	Non-volatile, Strain-driven Switching of Magnetic Anisotropy in Rare Earth Free Composite Multiferroic Devices		C. Zollner, Cornell Univ.; L.Q. Chen, Penn State Univ.; D. Ralph, Cornell Univ.; R. Ramesh, Univ. of California, Berkeley; G. Stiehl, N. Dawley, R. Steinhardt, N. Reynolds, Cornell Univ.; J. Hu, Penn State Univ.; J. Heron, D.G. Schlom, Cornell Univ.
Su1515	3:15 p.m.	Influence of Cap Layers on Perpendicular Magnetic Anisotropy of Ultra-thin Fe/MgO(001) Films		T. Brown-Heft, M. Pendharkar, Univ. of California Santa Barbara; E. Lee, Harvey Mudd College; C.J. Palmstrøm, Univ. of California Santa Barbara
Su1520	3:20 p.m.	The Correlation Between the Magnetic Perpendicular Anisotropy and Orbital Magnetic Moment with Structural Order Parameter of the Epitaxial Fe/Pt Multilayers Under Annealing		Y-S. Chen, C-H. Lee, National Tsing Hua Univ.; J.C.A. Huang, National Cheng Kung Univ.; H.J. Lin, National Synchrotron Radaition Research Center
Su1525	3:25 p.m.	Magnetization Dynamics of Organic-based Magnetic Heterostructures		M. Chilcote, Y. Lu, H. Wang, F. Yang, E. Johnston-Halperin, The Ohio State Univ.
Nanostructures I				Session Chair: P.M. Koenraad
Su1530	3:30 p.m.	INVITED: Analysis of Composition and Strain in Semiconductor Nanostructures by Quantitative HAADF-STEM and Imaging STEM		A. Rosenauer, K. Müller-Caspary, M. Schowalter, T. Grieb, F.F. Krause, T. Mehrtens, Universität Bremen
Su1610	4:10 p.m.	Conductive Atomic Force Microscopy of Piezoelectric InGaN Nanorods		J. Colvin, A. Mikkelsen, R. Timm, Lund Univ.
Su1615	4:15 p.m.	Design Principles and Fabrication Processes of a New Microstripline Small-sized Inductor with Carbon Nanotube Bumps/Silicon MEMS Pillars for MMICs		N. Yuichi, N. Mistuki, A. Yuji, Keio Univ.
Su1620	4:20 p.m.	Incorporation of Sb into Erassb Containing Structures During MBE Growth		K. Eyink, Y. Zhang, J. Peoples, K. Mahalingam, M. Hill, L. Grazulis, Air Force Research Lab
Su1625	4:25 p.m.	Picosecond Thermoreflectance Measurements of High Density Vertically Aligned Carbon Nanotube Forests with a Height of 10 Um for High Performance Thermal Interface Materials		Y. Kurosu, Keio Univ.; T. Yagi, National Institute of Advanced Industrial Science and Technology; Y. Awano, Keio Univ.
Su1630	4:30p.m.	Poster Setup		
Su1800	6:00 p.m.	Welcome Reception		
Sunday Evening, January 17:				
Energy I				Session Chair: J. Redwing
Su1930	7:30 p.m.	INVITED: Bulk Direct Bandgap MoS$_2$ and Hot Electron Injection in Metal/MoS$_2$ and		S.B. Cronin, University of Southern California
Su2010	8:10 p.m.	INVITED: Structures, Devices, and Architectures for Nanoscale Solutions in Electrical Energy Storage		G.W. Rubloff, Univ. of Maryland

Su2050	8:50 p.m.	Surface/Interface Effects on Performance of Thin-film All-solid-state Li-ion Batteries with Al and Si Anodes		A.A. Talin, Sandia National Laboratories; C. Gong, Univ. of Maryland; D. Ruzmetov, Army Research Lab; A. Pearse, D. Ma, J.N. Munday, G. Rubloff, M.S. Leite, Univ. of Maryland
Su2055	8:55 p.m.	Synthesis of Chemically Activated $L_{i2}MnO_3$ Nanowires and Nanobelts with Improved Electrochemical Properties As Cathode Materials for Li-ion Batteries		X. Ma, College of Chemistry and Life Science, Hubei Univ. of Education, Wuhan, China
Monday Morning, January 18:				
Mo0745	7:45 a.m.	Registration and Continental Breakfast		
Nanostructures II				Session Chair: L. Lauhon
Mo0830	8:30 a.m.	INVITED: III-V Nanowires for Next Generation Solar Cells: Advantages and Challenges		A. Fontcuberta-Morral, EPFL
Mo0910	9:10 a.m.	Correlation of the Atomic Scale Surface Structure and the Electronic Properties of InAs and InAs/InSb Nanowires		J. Knutsson, M. Hjort, J. Webb, O. Persson, S. Gorji Ghalamenstani, S. Lehmann, L. Samuelson, K.A. Dick, R. Timm, A. Mikkelsen, Lund Univ.
Mo0915	9:15 a.m.	UPGRADED: How Can Band Offsets in III-V Nanowires Be Determined Correctly by Scanning Tunneling Spectroscopy?		Ph. Ebert, Forschungszentrum Jülich GmbH; P. Capiod, T. Xu, IEMN; M.J. Wei, Shanghai Univ.; A. Dias Alvarez, X.L. Han, D. Troadec, J.P. Nys, M. Berthe, IEMN; G. Patriarche, CNRS-LPN; L. Lymperakis, J. Neugebauer, Max-Planck Institut für Eisenforschung GmbH; I. Lefebvre, IEMN; S.R. Plissard, Universite de Toulouse; P. Caroff, The Australian National Univ.; R.E. Dunin-Borkowski, Forschungszentrum Jülich GmbH
Mo0935	9:35 a.m.	Suppression of Non-radiative Surface Recombination by N Incorporation in GaAs-based Nanowires Grown by Molecular Beam Epitaxy		S.L. Chen, W.M. Chen, Linkoping Univ.; F. Ishikawa, Ehime Univ.; I.A. Buyanova, Linkoping Univ.
Mo0940	9:40 a.m.	Formation of One-dimensional Arrays of Magic In Clusters Using a Vicinal Si Surface As a Template		M. Franz, J. Schmermbeck, M. Dähne, Technische Universität Berlin
Mo0945	9:45 a.m.	InSb Quantum Nano-stripes by Molecular Beam Epitaxy		T. Poempool, Zon, Chulalongkorn Univ.; S. Kiravittaya, Naresuan Univ.; S. Sopitpan, National Science and Technology Agency; S. Thainoi, S. Kanjanachuchai, S. Ratanathammaphan, S. Panyakeow, Chulalongkorn Univ.
Mo0950	9:50 a.m.	Time-deterministic Control of Quantized Conductance of Au Nanowires Using Feedback-Controlled Electromigration with Real-time Operating System		S. Sato, Y. Kanamaru, Y. Katogi, J-I. Shirakashi, Tokyo Univ. of Agriculture and Technology
Mo0955	9:55 a.m.	Atomic Structure of III-V Layers Grown on GaP/Si(001)		C.S. Schulze, Technische Universität Berlin; X. Huang, Yale Univ.; C. Prohl, V. Füllertt, S. Rybank, Technische Universität Berlin; S. Maddox, S. March, S.R. Bank, The Univ. of Texas at Austin; A. Beyer, R. Straubinger, K. Volz, M.L. Lee, Philipps-Univ. Marburg; A. Lenz, Technische Universität Berlin
Mo1000	10:00 a.m.	Coffee Break and Poster Viewing		

Nanostructures II				Session Chair: L. Lauhon
Mo1100	11:00 a.m.	Atomic Structure of InAs(Sb)/GaAs Submonolayer Qunatum Dots for Strong Charge Carrier Localization		H. Eisele, A. Lenz, Z. Diemer, C. Prohl, D. Quandt, A. Trittmatter, U.W. Pohl, M. Dähne, Technische Universität Berlin
Mo1105	11:05 a.m.	Individual iso-electronic N and Bi Centers in Gaas Studied by Scanning Tunneling Microscopy		C.M. Krammel, R.C. Plantenga, Eindhoven Univ. of Technology; V. Kortan, M.E. Flatté, Univ. of Iowa; FJ. Tilly, M. Roy, P.A. Maksym, Univ. of Leicester; J.M. Ulloa, Universidad Politénica de Madrid; T. Kita, Kobe Univ.
Energy II				Session Chair: G. Rubloff
Mo1110	11:10 a.m.	INVITED: Advanced Research Projects Agency-Energy: Innovation for Impact		E.D. Williams, Advanced Research Projects Agency-Energy
Mo1150	11:50 a.m.	Interfacial and Photocatalytic Properties of Zinc Oxide/Gold Nanoparticle Heterostructures		I. Unlu, Y. Wang, J.E. Whitten, Univ. of Massachusetts, Lowell
Mo1155	11:55 a.m.	Magnesium Hydride Film Formation Using a Sub-atmospheric Hydrogen Pressure Plasma at Low Temperature		H. Ohmi, N. Masuya, T. Hori, H. Kakiuchi, K. Yasutake, Osaka Univ.
Mo1200	12:00 p.m.	Ultrafast Multipass Transient Absorption Spectroscopy of Interfacial Excitonic Dynamics of Organic-Inorganic Heterojunctions: Harnessing Triplet Excitons in Organic Semiconductors via Colloidal Quantum Dots		L.R. Weiss, Cambridge Univ.
Mo1205	12:05 p.m.	Lunch and Poster Viewing		
Monday Afternoon, January 18:				
Oxides I				Session Chair: M. Allen
Mo1400	2:00 p.m.	INVITED: Bipolar Oxide Diodes: Role of the Interface for Type-I, -II and -III Heterostructures		M. Grundmann, Universität Leipzig, Institut für Experimentelle Physik II
Mo1440	2:40 p.m.	INVITED: Electrical Properties of ZnO:Ga/Substrate Interfaces: Bad, Good, and Fantastic		D.C. Look, Wright State Univ.
Mo1520	3:20 p.m.	Defect Redistribution and Mobility Enhancement at Highly Doped/Intrinsic-ZnO Interfaces		G.M. Foster, The Ohio State Univ.; G. Faber, Columbus School for Girls; E. Heller, D. Look, Air Force Research Lab; Y.F. Yao, C.C. Yang, National Taiwan Univ.; L.J. Brillson, The Ohio State Univ.
Mo1525	3:25 p.m.	Effect of Ti Sub-oxide Layers on the Switching Properties of ZnO-based ReRAM Cells		J.H. Park, K.R. Son, T.G. Kim, Korea Univ.
Mo1530	3:30 p.m.	Coffee Break and Poster Viewing		
Spintronics I				Session Chair: F. Yang
Mo1630	4:30 p.m.	INVITED: A Study of the Topological Effect in Artificial Magnetic Skyrmions		Z.Q. Qiu, Univ. of California at Berkeley, Berkeley
Mo1710	5:10 p.m.	Theory for the Coherent Detection of Interfacial Defects		N.J. Harmon, M.E. Flatté, Univ. of Iowa
Mo1715	5:15 p.m.	Long-lived Spin Relaxation and Spin Coherence of Electrons in Monolayer MoS_2		L. Yang, N.A. Sinitsyn, Los Alamos National Lab; W. Chen, J. Yuan, J. Zhang, Rice Univ.; K.M. McCreary, B.T. Jonker, U.S. Naval Research Lab; J. Lou, S.A. Crooker, Los Alamos National Lab

Mo1720	5:20 p.m.	INVITED: Co_2MnSi Half-Metal Magnetic Character Studied by Spin-Resolved PhotoEmission Spectroscopy and FerroMagnetic Resonance		T. Hauet, Universite de Lorraine; T. Devolder, Universite Paris-Saclay; A. Hallal, M. Chshiev, CEA-CNRS-Universite J. Fourier; A. Bataille, CEA-SacLay; P. Le Fevre, Synchrotron SOLEIL; S. Andrieu, A. Neggache, Universite de Lorraine
Mo1800	6:00 p.m.	Ultrafast Study of Dynamic Interfacial Exchange Coupling in Ferromagnet/ Oxide/Semiconductor Heterostructures		Y-S. Ou, Y-H. Chiu, The Ohio State Univ.; N.J. Harmon, The Univ. of Iowa; P. Odenthal, Univ. of California, Riverside; M. Sheffield, M. Chilcote, R. Kawakami, The Ohio State Univ.; M.E. Flatté, The Univ. of Iowa; E. Johnston-Halperin, The Ohio State Univ.
Mo1805	6:05 p.m.	Dinner		
Monday Evening:				
Complex Oxides				Session Chair: C.J. Palmstrøm
Mo1930	7:30 p.m.	INVITED: Noncentrosymmetric Metals: A New Materials Class for Artificial Multiferroic Design		J. Rondinelli, Northwestern Univ.
Mo2010	8:10 p.m.	Frustrated Domain Formation and Charged Domain Walls in $PbTiO_3$/$LaNiO_3$/sub> Heterostructures with Preferential (111) Growth		H-J. Jin, S.H. Oh, W. Jo, Ewha Womans Univ.
Mo2015	8:15 p.m.	Built-in Potential in Fe_2O_3-Cr_2O_3 Superlattices for Improved Photoexcited Carrier Separation		T.C. Kaspar, D.K. Schreiber, S.R. Spurgeon, M.E. McBriarty, S.A. Chambers, Pacific Northwest National Lab; G.M. Carroll, D.R. Gamelin, Univ. of Washington
Mo2020	8:20 p.m.	Hybrid Molecular Beam Epitaxy for the Growth of Stoichiometric $BaSnO_3$		A. Prakash, J. Dewey, B. Jalan, Univ. of Minnesota
Mo2025	8:25 p.m.	Structural and Optical Properties of $SrTiO_3$ Thin Films on Semiconductors		S. Zollner, N. Samarasingha, C. Rodriguez, J. Moya, N. Fernando, New Mexico State Univ.; S. Chattopadhyay, Indian Institute of Technology Indore; P. Ponath, Univ. of Texas - Austin
Mo2030	8:30 p.m.	UPGRADED: Tunneling Spectroscopy in Interface Engineered Metal/$SrTiO_3$ Junctions		H. Inoue, A.G. Swartz, T. Merz, Stanford Univ.; Y. Hikita, SLAC National Accelerator Lab; H.Y. Hwang, Stanford Univ./SLAC National Accelerator Lab
Mo2050	8:50 p.m.	Understanding the Origin of Surface Depletion in δ-doped $SrTiO_3$		H. Yoon, H. Inoue, A.G. Swartz, Stanford Univ.; Y. Hikita, SLAC National Accelerator Lab; H.Y. Hwang, Stanford Univ. / SLAC National Accelerator Lab
Mo2055	8:55 p.m.	Iodine Dimerization at Methylammonium Lead Iodide Perovskite Surfaces		L. She, M. Liu, D. Zhong, Sun Yat-sen Univ.
Tuesday Morning, January 19:				
Tu0745	7:45 a.m.	Registration and Continental Breakfast		
Semiconductor Interfaces and Devices I				Session Chair: C.R. Eddy
Tu0830	8:30 a.m.	INVITED: Interfaces in GaN-diamond Integrated Electronics - Thermal and Mechanical Considerations		M. Kuball, J.W. Pomeroy, J. Anaya, H. Sun, R. Baranyai, D. Spiteri, D. Liu, Univ. of Bristol
Tu0910	9:10 a.m.	Reduced Output Power Drop in AlGaN/GaN HFETs on Si(111) by Controlling the Passivation /AlGaN Barrier Interface		S.K. Oh, Sunchon National Univ.; T. Jang, Chonbuk National Univ.; Y.J.Jo, H-Y. Ko, LG Electronics; J.S. Kwak, Sunchon National Univ.
Tu0915	9:15 a.m.	Suppression and Recovery of Nitrogen Dissociation from Surface of Gallium Nitride During High-temperature Annealing by Using New Nitrogen Heat-beam Method		N.S.N.B. Johari, Y. Awano, Keio Univ.

Tu0920	9:20 a.m.	INVITED: Polarization-Engineered Tunneling in III-Nitride Heterostructures		D. Jena, Cornell Univ. and Univ. of Notre Dame; X. Yan, W. Li, K. Pourang, J. EncomenderoRisco, M. Islam, V. Protasenko, Univ. of Notre Dame; S. Keller, Univ. of California Santa Barbara; P. Fay, Univ. of Notre Dame; and H.G. Xing, Cornell Univ. and Univ. of Notre Dame
Tu1000	10:00 a.m.	Coffee Break and Poster Viewing		
2D Materials I				Session Chair: R.K. Kawakami
Tu1100	11:00 a.m.	INVITED: Excitons in 2D Semiconductors and Heterostructures		X. Xu, Univ. of Washington
Tu1140	11:40 a.m.	Exciton Diamagnetic Shifts and Valley Zeeman Effect in Monolayer WS$_2$ and MoS$_2$ to 65 Tesla		A.V. Stier, Los Alamos National Lab; K.M. McCreary, B.T. Jonker, U.S. Naval Research Lab; J. Kono, Rice Univ.; S.A. Crooker, Los Alamos National Lab
Tu1145	11:45 a.m.	Hybrid, Gate-tunable, Van Der Waals P-n Heterojunctions from Pentacene and MoS$_2$		D. Jariwala, S. Howell, K-S. Chen, J. Kang, V. Sangwan, S. Filippone, R. Turrisi, T.J. Marks, L.J. Lauhon, M.C. Hersam, Northwestern Univ.
Tu1150	11:50 a.m.	Nanoscale Chemical and Electronic Properties of Methyl-terminated Germanane		T.J. Asel, X. Yang, S. Jiang, K. Krymowski, O. Restrepo, W. Windl, J. Goldberger, L.J. Brillson, The Ohio State Univ.
Tu1155	11:55 a.m.	In Situ Studies of Thermal Behavior of Exfoliated Black Phosphorus		M. Fortin-Deschênes, Polytechnique Montréal Pierre Levesque, Richard Martel, Université de Montréal; O. Moutanabbir, Polytechnique Montréal
Tu1200	12:00 p.m.	Free Afternoon		
Tuesday Evening, January 19:				
Rump Session: Novel Energy Materials				Session Chair: A.A. Talin
Tu1900	7:00 p.m.	INVITED: Using Nanostructured Assemblies to Control the Physics of Energy Harvesting and Storage		S.H. Tolbert, Univ. of California, Los Angeles
Tu1940	7:40 p.m.	INVITED: Modulating Charge Transport Mechanisms by Tuning the Architectures of Supramolecular Assemblies		J. Batteas, Texas A&M Univ.
Tu2020	8:20 p.m.	INVITED: Additive Printing of Flexible Electronics		T. Ng, Univ. of California, San Diego; D. Schwartz, P. Mei, G. Whiting, J. Veres, Palo Alto Research Center
Wednesday Morning, January 20:				
We0745	7:45a.m.	Registration and Continental Breakfast		
Oxides II				Session Chair: M. Grundmann
We0830	8:30 a.m.	INVITED: Effect of Oxygen Incorporation on the performance of Noble Metal Oxide Schottky Contacts to ZnO		A.M. Hyland, Univ. of Canterbury; R. Makin, S.M. Durbin, Western Michigan Univ.; M.W. Allen, Univ. of Canterbury
We0910	9:10 a.m.	Laser Curing and Ink-jet Processes for Fabricating SiOx RRAM Structures		K. Byun, Univ. of Texas at Austin; Y. Wang, B. Adams, Applied Materials Inc.; J. Lee, Univ. of Texas at Austin
We0915	9:15 a.m.	WITHDRAWN		WITHDRAWN
We0920	9:20 a.m.	Initial Nucleation and Bi-axial Texturing of Mgo Thin-films Assisted by Ion-beam Irradiation on Amorphous Y$_2$O$_3$ Layers		H-J. Jin, W. Jo, Ewha Womans Univ.; J. Jo, M. Kim, Seoul National Univ.; B.M. Kang, G-T. Kim, R-K. Ko, Y-S. Jo, D-W. Ha, Korea Electrotechnology Research Institute

High-K				Session Chair: J. Hilton
We0925	9:25 a.m.	Solution Processed Organic - Inorganic Hybrid Gate Dielectric For Flexible Thin Film Transistors		M.G. Syamala Rao, CINVESTAV
We0930	9:30 a.m.	Self-cleaning and Unexpected Surface Chemistry During Atomic Layer Deposition Revealed by Time-resolved XPS		S. McKibbin, S. Yngman, A. Head, J. Knutsson, J. Schnadt, A. Mikkelsen, R. Timm, Lund Univ.
We0935	9:35 a.m.	Impact of D_2 High-pressure Annealing Onto Ingaas Moscaps with Al_2O_3/HfO_2		J.S. Kim, Kyungpook National Univ.; S.-H. Shin, Univ. of Texas at Austin; D.-K. Kim, Kyungpook National Univ.; Y.D. Cho, C.-S. Shin, W.-K. Park, KANC; E. Chiu, M. Rivera, J.I. Lew, PoongSan Inc.; J.-H. Lee, Kyungpook National Univ.; S.K. Banerjee, Univ. of Texas at Austin; T-W. Kim, SEMATECH; D.-H. Kim, Kyungpook National Univ.
We0940	9:40 a.m.	Impact of Surface Treatments on High-k Dielectric Integration with Ga-polar and N-polar GaN		C.R. English, Univ. of Wisconsin; V.D. Wheeler, U.S. Naval Research Lab; N.Y. Garces, U.S. Patent and Trademark Office; N. Nepal, Sotera Defense Solutions; A. Nath, American Association for Engineering Education; J.K. Hite, M.A. Mastro, C.R. Eddy, Jr., U.S. Naval Research Lab
We0945	9:45 a.m..	WITHDRAWN		WITHDRAWN
We0950	9:50 a.m.	LATE NEWS: Film-substrate Interfacial Engineering for Accurate Determination of the Near-bandgap Optical Properties Using Spectroscopic Ellipsometry		S. Choi, Univ. of California, Santa Barbara, J. Li, Univ. of Toledo; I.L. Repins, National Renewable Energy Lab
We0955	9:55 a.m.	LATE NEWS: Probing Human Pluripotent Stem Cell Neurons: Electrical Modeling and Physiological Measurements		A.T.E. Youssef, R. Chen, R. Liu, S.H. Lee, M.L. Khraiche, Y. Hwang, Y.G. Ro, S.A. Dayeh, Integrated Electronics and Biointerphases Laboratory, Univ. of California, San Diego; S. Hinckley, A. Bang, Conrad Prebys Center of Chemical Genomics, Sanford Burnham Prebys Medical Discovery Inst.; A. Tanaka, K. Matsushita, S.A. Dayeh, Univ. of California, San Diego.
We1000	10:00 a.m.	LATE NEWS: Strain Engineering for Beyond 10 μm Thick Crack-Free GaN Growth on Si for High Power Device Applications		A. Tanaka, R. Chen, S.A. Dayeh, Univ. of California, San Diego
We1005	10:05 a.m.	LATE NEWS: Ex-situ and In-situ TEM Studies of Ni-InGaAs reaction in InGaAs Fins		R. Chen, S.A. Dayeh, Univ. of California, San Diego
We1010	10:10 a.m.	LATE NEWS: Mechanistic Studies for the Development of Thin Si Microwire Solar Cells for Wearable Electronics		Y.G. Ro, R. Chen, A.T.E. Youssef, N. Park, R. Liu, S.A. Dayeh, Univ. of California, San Diego
We1015	10:15 a.m.	Coffee Break and Poster Viewing		

Novel Semiconductors				Session Chair: J.M. Woodall
We1100	11:00 a.m.	Temperature-dependent Photoluminescence Studies of $Ge_{1-y}Sn_y$ Direct Bandgap Semiconductors		M-Y. Ryu, Kangwon National Univ.; T.R. Harris, B. Wang, Y.K. Yeo, Air Force Institute of Technology; J. Kouvetakis, Arizona State Univ.
We1105	11:05 a.m.	Silicon-Germanium-TiN Semiconductors: Growth and Properties		O. Moutanabbir, J.-H. Fournier, S. Mukherjee, B. Meynard, M. Fortin-Deschênes, Ecole Polytechnique de Montreal; S. Wirths, Forschungszentrum Juelich; J. M. Hartmann, LETI; P. Desjardins, Ecole Polytechnique de Montreal; D. Buca, Forschungszentrum Juelich
We1110	11:10 a.m.	Investigation of the Half-Heusler CoTiSb/III-V Heterointerfaces		S.D. Harrington, A. Rice, T. McFadden, J. K. Kawasaki, C.J. Palmstrøm, Univ. of California, Santa Barbara
We1115	11:15 a.m.	Half-Heusler/Heusler Interfaces:Stability and Electronic Properties		A. Rice, S.D. Harrington, J.K. Kawasaki, N. Verma, B.D. Schultz, C.J. Palmstrøm, Univ. of California, Santa Barbara
2D Materials II				Session Chair: T.F. Heinz
We1120	11:20 a.m.	UPGRADED: 2D Nitrides Beyond hBN: The Case of 2D GaN		Z.Y. Al Balushi, The Pennsylvania State Univ.; K. Wang, Materials Research Institute; R.K. Ghosh, R.A. Vilá, The Pennsylvania State Univ; S.M. Eichfeld, The Pennsylvania State Univ. and Materials Research Institute; J.D. Caldwell, P.A. DeSario, U.S. Naval Research Lab; D.F. Paul, Physical Electronics USA; S. Datta, J.M. Redwing, J.A. Robinson, The Pennsylvania State Univ. and Materials Research Institute
We1140	11:40 a.m.	Observation of Friction Between Gold Nanocrystals and Graphene Using Quartz Crystal Microbalance		M. Lodge, B. Blue, Univ. of Central Florida; B.D. Dawson, Western Digital; M. Ishigami, Univ. of Central Florida
We1145	11:45 a.m.	Development of Water Soluble Polyvinyl Alcohol Assisted Transfer Technique for 2-dimensional Materials for High-performance Graphene Field Effect Transistors		H.V. Ngoc, D.J. Kang, Sungkyunkwan Univ.
We1150	11:50 a.m.	Defect-controlled Addition of Nitrogen into Aromatic Configurations in CVD-grown Graphene by Microwave Flowing Afterglow Plasma Exposure		G. Robert-Bigras, L. Vandsburger, L. Stafford, Universite de Montreal; A. Sarkissian, Plasmionique, Inc.
We1155	11:55 a.m.	Etching-free Transfer of Highly-aligned Bottom-up Graphene Nanoribbon Arrays on Au(788) Template		M. Ohtomo, Y. Sekine, NTT Basic Research Lab; H. Hibino, Kwansei Gakuin Univ.; H. Yamamoto, NTT Basic Research Lab
We1200	12:00 p.m.	Lunch and Poster Viewing		
Wednesday Afternoon, July 20				
Semiconductor Interfaces and Devices II				Session Chair: A. Mikkelsen
We1400	2:00 p.m.	INVITED: Phosphorene as a New 2D Material for Device Applications		P.D. Ye, Purdue Univ.
We1440	2:40 p.m.	Interface Improvement in AlGaN GaN Hfets Using TMAH Pre Treatment		D.K Kim, W.S. Park, Y.I. Jang, J.S. Kim, Y.J. Yun, I.M. Kang, D.H. Kim, J.H. Lee, Kyungpook National Univ.
We1445	2:45 p.m.	Assessment of Substrate Surface Pretreatment for Epitaxial Growth of III-nitrides at Low Temperatures		N. Nepal, V.R. Anderson, V.D. Wheeler, J.K. Hite, S.D. Johnson, D.J. Meyer, B.P. Downey, U.S. Naval Research Lab; A. DeMasi, K.F. Ludwig, Boston Univ.; C.R. Eddy, Jr, U.S. Naval Research Lab
We1450	2:50 p.m.	Direct Ohmic Contact to P-AlGaN and Its Application to 365 Nm AlGaInN/InGaN Light-emitting Diodes		T. Lee, T.G. Kim, D.Y. Kang, Korea Univ.

We1455	2:55 p.m.	Epitaxial Lateral Overgrowth of ZnTe on Sapphire Substrates Using SiO_2 Mask		S. Hattori, T. Nakasu, T. Kizu, Y. Hashimoto, W. Sun, F. Kazami, Waseda Univ.; M. Kobayashi, Waseda Univ. and Research Institute for Materials Science & Technology; T. Asahi , JX Nippon Mining & Metals Corporation
New Techniques and Devices				Session Chair: P. Ye
We1500	3:00 p.m.	Nanoscale Imaging of Local Few-femtosecond Near-field Dynamics Within Individual Nanostructures		E. Marsell, A. Losquin, R. Swaerd, M. Miranda, C. Guo, A. Harth, E. Lorek, J. Mauritsson, C.L. Arnold, Lund Univ.; H. Xu, Wuhan Univ.; A. L'Huillier, A. Mikkelsen, Lund Univ.
We1505	3:05 p.m.	Time of Flight Backscattering Spectrometry and Secondary Ion Mass Spectrometry in a Helium Ion Microscope Enabling Chemical Analysis on the Nm Scale		N. Klingner, R. Heller, G. Hlawacek, Helmholtz-Zentrum Dresden-Rossendorf; P. Gnauck, Carl-Zeiss-Microscopy GmbH; S. Facsko, J. von Borany, Helmholtz-Zentrum Dresden-Rossendorf
We1510	3:10 p.m.	Nanoscale Imaging of Defects in Cdte Photovoltaic Devices Using Two Novel Optical Spectroscopies		Y. Yoon, J. Chae, A. Katzenmeyer, H.P. Yoon, Univ. of Maryland, National Institute of Standards and Technology; J. Schumacher, National Institute of Standards and Technology; S. An, Univ. of Maryland, National Institute of Standards and Technology; A. Centrone, National Institute of Standards and Technology
We1515	3:15 p.m.	Overcoming Interface Oxidation Via Melt Mixing During LPE of AlGaAs Multi-layer Structures		J.M. Woodall, Univ. of California, Davis
We1520	3:20 p.m.	Application of Metal-insulator-metal Single Electron Transistors for Characterization of Ultrathin Dielectrics Grown by Atomic Layer Deposition		G. Karbasian, M. McConnell, A. Orlov, A. Mukasyan, S. Rouvimov, G. Snider, Univ. of Notre Dame
We1525	3:25 p.m.	Coffee Break and Poster Viewing		
Semiconductor Interfaces				Session Chair: M. Kuball
We1625	4:25 p.m.	INVITED: Engineering Interfaces for Memristive Devices		J.J. Yang, Univ. of Massachusetts, Amherst
We1715	5:15 p.m.	UPGRADED: Epitaxial Al-InAs Two-dimensional Systems: a Platform for Gate-able Topological Superconductivity		J. Shabani, Univ. of California, Santa Barbara; C.M. Marcus, Univ. of Copenhagen; M. Troyer, ETH Zurich; C. Nayak, S. Kraemer, Univ. of California, Santa Barbara; P. Krogstrup, Univ. of Copenhagen; R. Lutchyn, Microsoft Research; T. Stankevic, Univ. of Copenhagen; K. Pakrouski, ETH Zurich; F. Nichele, Univ. of Copenhagen; Y. Kim, Univ. of California, Santa Barbara; H.J. Sumominen, M. Kjaergaard, Univ. of Copenhagen; C.J. Palmstrøm, Univ. of California, Santa Barbara
We1735	5:35 p.m.	Schottky Barrier Diodes with In-situ Grown Single Crystal Aluminum on GaN by Plasma-assisted Molecular Beam Epitaxy		H.Y. Tseng, W.C. Yang, P.Y. Lee, C.W. Lin, K.C. Hsieh, K.Y. Cheng, National Tsing Hua Univ.
We1740	5:40 p.m.	How Surface Leakage and Dislocations Affect Diode Behavior in Micrometer-sized SiGe/Si Heterostructures		A. Jung, F. Isa, T. Kreiliger, ETH Zurich; Y. Arroyo Rojas Dasilva, R. Erni, Empa-Swiss Federal Laboratories for Materials Science and Technology; P. Niedermann, CSEM; G. Isella, Politecnico di Milano; H. von Kaenel, ETH Zurich
We1745	5:45 p.m.	Hot Electron Transport Studies of W/Si and Cr/Si Diodes Using		C. Durcan, W. Nolting, SUNY Albany; V. LaBella, SUNY Polytechnic

We1750	5:50 p.m.	Charge Transport Mechanisms in P-i-n Anisotype GaSb/GaAs Hetrojunctions		A. Sellai, Sultan Qaboos Univ.; M. Aziz, M. Henini, Nottingham Univ.; A. Mesli, Aix-Univ., Marseille
We1755	5:55 p.m.	Structural Properties of β-fesi$_2$ Thin Films on Si(111) Substrate and Electrical Transport Properties of N-type β-fesi$_2$/P-type Si Heterojunctions Prepared by Radio Frequency Magnetron Sputtering		N. Promros, King Mongkut's Institute of Technology Ladkrabang; R. Baba, H. Kishimoto, Kyushu Univ.; P. Sittimart, W.Kaenrai, King Mongkut's Institute of Technology Ladkrabang; T.Hanada, A. Zkria, Kyushu Univ.; M.Shaban, Aswan Univ.; T.Yoshitake, Kyushu Univ.
We1800	6:00 p.m.	Lead Telluride Through Transformation of Plumbonacrite in CVD Process and Its Behavior As Part of PbTe-Si Diode		I.R. Chávez-Urbiola, Y.V. Vorobiev, R. Ramírez-Bon, Centro de Investigación y de Estudios Avanzados del Instituto Politécnico Nacional
We1830	6:30 p.m.	Conference Banquet		
Thursday Morning, January 21 :				
Th0745	7:45 a.m.	Registration and Continental Breakfast		
2D Materials III				Session Chair: C. Varanasi
Th0830	8:30 a.m.	INVITED: Excitonic Effects in 2D Semiconductor Layers		T.F. Heinz, Stanford Univ.
Th0910	9:10 a.m.	INVITED: Optical Spectroscopy in Monolayer Transition Metal dichalcogenides: Excitonic Properties and Valley Dynamics		B. Urbaszek, Université de Toulouse
Th0950	9:50 a.m.	Imaging Spin Dynamics in Monolayer WS$_2$ by Time-Resolved Kerr Rotation Microscopy		E. Bushong, Y. Luo, The Ohio State Univ.; K.M. McCreary, Naval Research Lab; M. Newburger, S. Singh, The Ohio State Univ.; B. Jonker, U.S. Naval Research Lab; R.K. Kawakami, The Ohio State Univ.
Th0955	9:55 a.m.	Measuring Band Alignment of Transition Metal Dichalcogenides and Graphene Using Low-energy Electron Microscopy		S.C. de la Barrera, P.C. Mende, J. Li, Carnegie Mellon Univ.; Y-C. Lin, The Pennsylvania State Univ.; S. Vishwanath, Cornell Univ.; J. Robinson, The Pennsylvania State Univ.; H. Xing, Cornell Univ.; R.M. Feenstra, Carnegie Mellon Univ.
Th1000	10:00 a.m.	Coffee Break and Poster Viewing		
Spintronics II				Session Chair: S. Crooker
Th1100	11:00 a.m.	INVITED: FMR-Drive Pure Spin Transport in Metals and Antiferromagnetic Insulators		F. Yang, The Ohio State Univ.
Th1140	11:40 a.m.	Spin Injection in Self-assembled InAs/GaAs Quantum-dot Molecular Structures		Y.Q. Huang, Y. Puttisong, I.A. Buyanova, W. Chen, Linköping Univ.
Th1145	11:45 a.m.	The Role of Interface Dipole for Switching Spin State of Spin Crossover Molecules		X. Zhang, Y. Liu, Univ. of Nebraska, Lincoln; A. N'Diaye, Lawrence Berkeley National Lab; J-F. Létard, Université de Bordeaux; B. Doudin, Université de Strasbourg; P.A. Dowben, Univ. of Nebraska, Lincoln
Th1150	11:50 a.m.	Frequency-dependent Current Hysteresis Measurements for Alternating Current (AC) Characterization of Organic/Carbon Nanotube Thin-film Transistors by Applying Sinusoidal Wave Drain Voltage Signals		K. Watanabe, K. Tanoue, Y. Taki, K. Noda, Y. Awano, Keio Univ.
Th1155	11:55 a.m.	Surface Composition and Atomic Structure of Single Crystal Bi$_2$Se$_3$ Investigated by Low Energy Ion Scattering		W. Zhou, H. Zhu, J.A. Yarmoff, Univ. of California, Riverside
Th1200	12:00 p.m.	Topological Surface States in Sb Quantum Wells on Gasb(111)A Substrates		K.S. Wickramasinghe, C.K. Gaspe, S. Cairns, N.D. Teasdale, T.D. Mishima, J.C. Keay, M.B. Johnson, S.Q. Murphy, M.B. Santos, Univ. of Oklahoma
Th1205	12:05 p.m.	Conference Ends		

THE NEW SPECIALISTS IN SURFACE ANALYSIS
SOLUTIONS FOR UHV SPM & ESCA TECHNOLOGY

THE POWERFUL ASPECT ANALYZER AND NEO PLATFORM WILL TAKE YOU TO A NEW LEVEL OF PERFORMANCE.

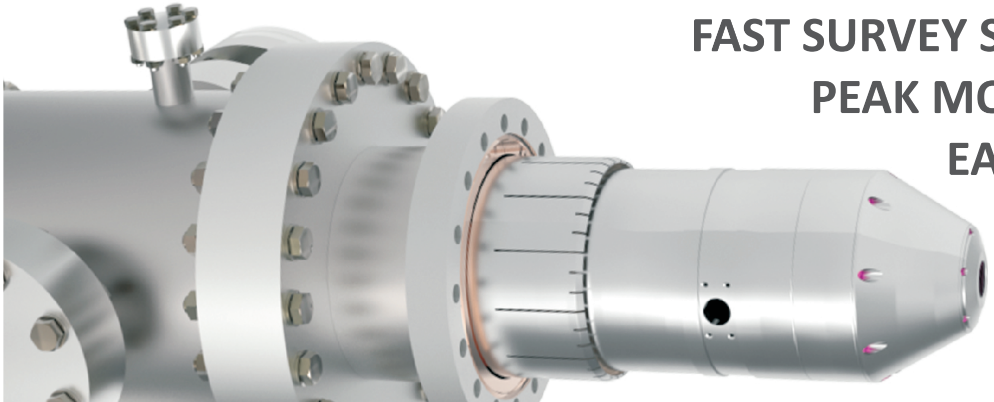

FAST SURVEY SPECTRUM IN 2 SECONDS
PEAK MONITORING IN REAL TIME
EASY ACCESS TO DATABASE
USER FRIENDLY TOOL
GET FASTER RESULTS

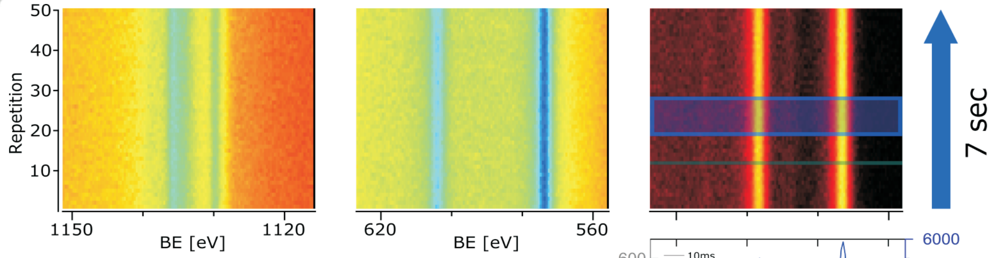

MULTI-PEAK MONITORING IN REAL TIME

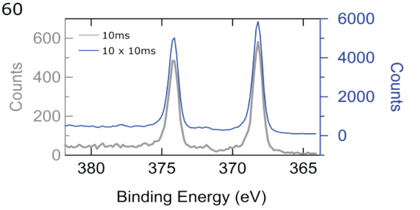

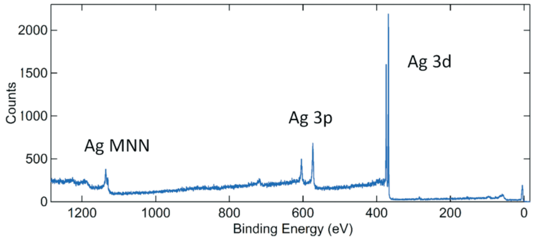

SURVEY SPECTRUM ACQUIRED IN 2 SECONDS

PLEASE VISIT WWW.SIGMA-SURFACE-SCIENCE.COM TO WATCH A VIDEO DEMONSTRATION OF THE SOPHISTICATED SOFTWARE

IDEAL FOR RESEARCHERS AT THE FOREFRONT OF SURFACE SCIENCE AND DEVICE TECHNOLOGY DEVELOPMENT.

MAGNETICS
OPTOELECTRONICS
ENERGY STORAGE
RENEWABLES
CATALYSIS

NANOELECTRONICS
OLEDs
SEMICONDUCTORS
INNOVATIVE 3D MATERIALS

PCSI-43 2016
PLATINUM SPONSOR
PALM SPRINGS, CALIFORNIA

INFO@SIGMA-SURFACE-SCIENCE.COM WWW.SIGMA-SURFACE-SCIENCE.COM

Σ SIGMA Surface Science
Partnered with MANTIS Deposition

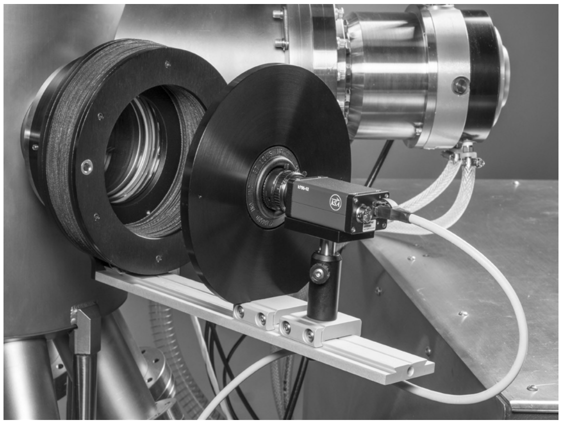


MOS
kSA k-Space Associates, Inc.
Ann Arbor, MI USA

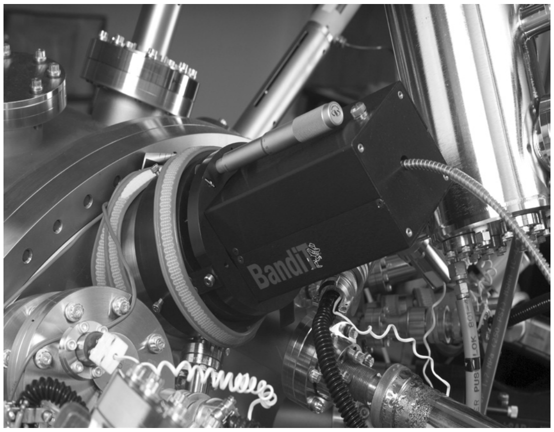
BandiT

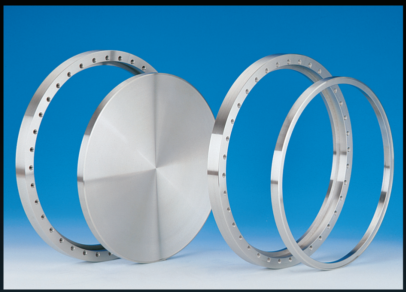

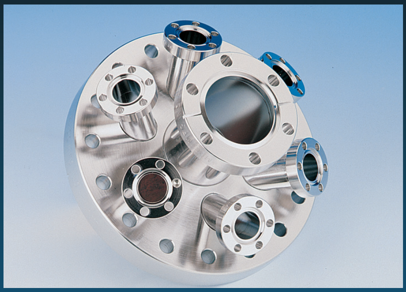

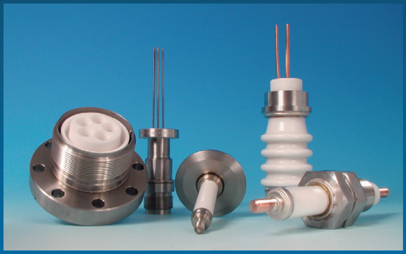

EnviroESCA™

THE BEGINNING OF A NEW ERA

Environmental

- Controllable atmosphere from sample loading to analysis
- Adaptable process gas dosing systems
- Specialized Sample Environments
- Compatible with all kind of samples of sizes up to Ø 60 x 40 mm

Networking

- SampleExplorer
- SmartDock
- AutoLoader
- GloveBox

Versatile

- Revolutionary analyzer technology
- µ-Focus X-ray source
- High resolution XPS
- Automated charge compensation
- Sputter depth profiling

Reliable

- Sample journal for complete documentation
- Reproducable analysis receipes
- Comprehensive system parameter logging
- Uptime focused user support

Integral

- Ergonomic all-in-one design
- Quick installation and setup
- Minimized downtime
- Cost and time efficent servicing
- Easy consumable replacement

Optimized

- Application oriented software package
- Complete remote operation
- Fully automated vacuum system
- Simple sample loading
- Optical 3D sample navigation

SPECS Surface Nano Analysis GmbH
Voltastrasse 5 T + 49 30 46 78 24-0
13355 Berlin / Germany F + 49 30 46 42 083
www.EnviroESCA.com E info@specs.com

SPECS™

pacsurf 2016

Pacific Rim Symposium on Surfaces, Coatings & Interfaces

December 11-15, 2016, Kohala Coast, Hawaii

Hapuna Beach Prince Hotel

This conference is being organized by AVS (United States) with a Steering Committee composed of representatives from Australia, Canada, Chile, China, Japan, Korea, Mexico, New Zealand, Singapore, and Taiwan. Symposium attendees will interact during morning and evening sessions that will include plenary, invited, and contributed presentations.

The main topics for PacSurf 2016 will be focused on the latest advances in **Biomaterial Interfaces**, **Biomaterial Surfaces & Interfaces**, **Energy Harvesting & Storage**, **Nanomaterials**, and **Thin Films**. We will have morning and evening technical sessions with the afternoons free for other activities and discussions.

Energy Harvesting & Storage | Biomaterial Interfaces
Nanomaterials | Thin Films

Program Chair & Scientific Advisory Board:

General Chair: Dave Castner
Program Chair: Charles R. "Chip" Eddy, Jr.

Advisory Committee:

Australia: Sally McArthur
Canada: Adam Hitchcock
Chile: TBD
P.R. China: Hongjun Gao
Japan: Katsuyuki Fukutani
Korea: TBD
Mexico: Alberto Herrera Gómez
New Zealand: Duncan McGillivray
Singapore: Sam Zhang
Taiwan: Jinn P. Chu
United States: Joe Greene

SAVE THE DATE

Call for Abstract Details Coming May 2016
Abstract Submission Deadline: August 5, 2016

Watch for details in early 2016 at **www.pacsurf.org**.

AVS®

bismuth telluride lutetium granules metamaterials electrochemistry solid
strontium doped lanthanum III-IV nitride materials crystal growth nanoribbons
organo-metallics regenerative medicine cerium polishing powder yttrium
thin film dysprosium pellets atomic layer deposition scandium-aluminum
nan ispersions aerospace ultra-light alloys iridium crucibles van m
green technology battery lithium gallium arsenide high ty silic
refrac tals surface functionalized nanoparticles tantal
ite semiconductors palladium shot ermet
catho anode
nucl iron
con liquids
galli

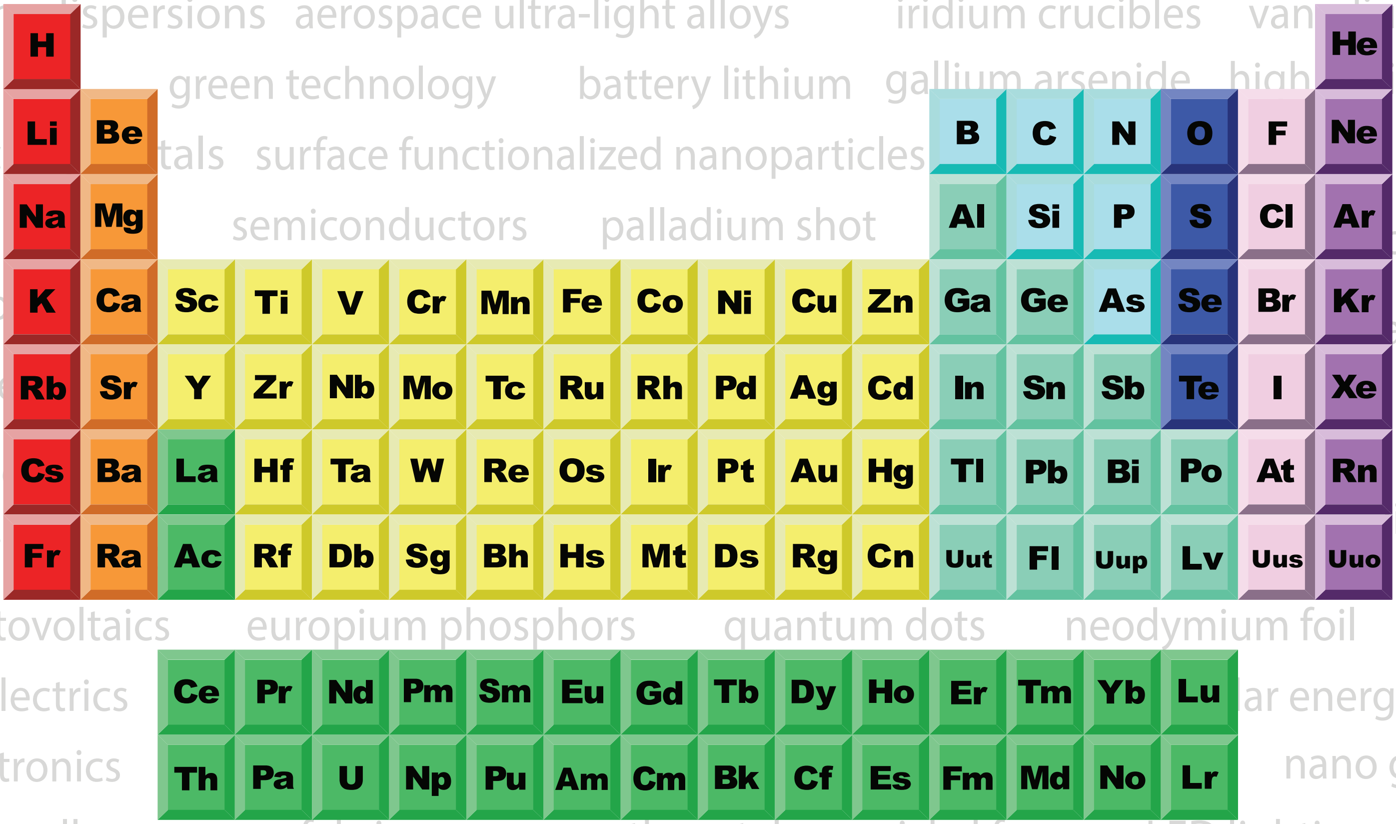

H He
Li Be B C N O F Ne
Na Mg Al Si P S Cl Ar
K Ca Sc Ti V Cr Mn Fe Co Ni Cu Zn Ga Ge As Se Br Kr
Rb Sr Y Zr Nb Mo Tc Ru Rh Pd Ag Cd In Sn Sb Te I Xe
Cs Ba La Hf Ta W Re Os Ir Pt Au Hg Tl Pb Bi Po At Rn
Fr Ra Ac Rf Db Sg Bh Hs Mt Ds Rg Cn Uut Fl Uup Lv Uus Uuo
Ce Pr Nd Pm Sm Eu Gd Tb Dy Ho Er Tm Yb Lu
Th Pa U Np Pu Am Cm Bk Cf Es Fm Md No Lr

photovoltaics europium phosphors quantum dots neodymium foil ionic
dielectrics ar energy
spintronics nano gels
super alloys nanofabrics rare earth metals nickel foam LED lighting
rod platinum ink laser crystals titanium robotic parts tungsten carbide
CIGS stable isotopes carbon nanotubes gold nanoparticles optoelectron

Now Invent.™

optoelectroni mischmetal
es anti-ballistic ceramics fuel cell materials hafnium tubing Nd:YAG
biosynthetics germanium windows superconductors ultra high purity mater
macromolecules 99.999% ruthenium spheres erbium doped fiber optics
sputtering targets gadolinium wire advanced polymers buckey balls
metalloids rhodium sponge shape memory alloys alternative energy
electrochemistry nanomedicine tellurium

AMERICAN ELEMENTS
THE MATERIALS SCIENCE MANUFACTURER®

te osmium

catalog: americanelements.com

©2001-2016. American Elements is a U.S. Registered Trademark.

zirconium single crystal silicon diamond micropowder neodymium foil
gadolinium wire advanced polymers single crystal silicon macromolecules

Sunday Afternoon

Magnetism

Su1430 Invited

Atomic spin chains as testing ground for quantum magnetism

Sander Otte
Department of Quantum Nanoscience, Kavli Institute of Nanoscience, Delft University of Technology, Lorentzweg 1, 2628 CJ Delft, The Netherlands

The field of quantum magnetism aims to capture the rich emergent physics that arises when multiple spins interact, in terms of elementary models such as the spin-½ Heisenberg chain. Experimental platforms to verify these models are rare and generally do not provide the possibility to detect spin correlations locally. In my lab we use low-temperature scanning tunneling microscopy to design and build artificial spin lattices with atomic precision. Inelastic electron tunneling spectroscopy enables us to identify the ground state and probe spin excitations as a function of system size, location inside the lattice and coupling parameter values. Two types of collective excitations that play a role in many dynamic magnetic processes are spin waves (magnons) and spinons. Our experiments enable us to study both types of excitations. First, we have been able to map the standing spin wave modes of a ferromagnetic bit of six atoms, and to determine their role in the collective reversal process of the bit [1]. More recently, we have crafted antiferromagnetic spin-½ XXZ chains, which allow us to observe spinon excitations, as well as the stepwise transition to a fully aligned phase beyond the critical magnetic field. These findings create a promising experimental environment for putting quantum magnetic models to the test.

[1] A. Spinelli *et al.*, Nature Materials **13**, 782 (2014)

Su1510

Non-volatile, strain-driven switching of magnetic anisotropy in rare-earth-free composite multiferroic devices

Authors: **Chris Zollner[1]**, John Heron[2], Jiamian Hu[3], Neal Reynolds[4], Rachel Steinhardt[2], Natalie Dawley[2], Greg Stiehl[4], R. Ramesh[5], D. C. Ralph[4], L.Q. Chen[3], Darrell G. Schlom[2]

[1] Department of Applied and Engineering Physics, Cornell University, Ithaca, New York 14853, USA

[2] Department of Materials Science and Engineering, Cornell University, Ithaca, New York 14853, USA

[3] Department of Materials Science and Engineering, Penn State University, Storrs, Pennsylvania 06269, USA

[4] Department of Physics, Cornell University, Ithaca, New York 14853, USA

[5] Department of Materials Science and Engineering, University of California, Berkeley, California 94720, USA

Abstract: Multiferroics are materials that have more than one “ferroic” order (e.g. ferromagnetism, ferroelectricity and ferroelasticity) [i]. These materials are deemed magnetoelectric when the magnetic and ferroelectric orders are coupled together [ii]. Multiferroics can exist as a single-phase material or in be engineered as heterostructures of materials which are not individually multiferroic. Such is the case for a bilayer of a ferroelectric (piezoelectric) and a ferromagnet (magnetostrictive), in which the two orders are coupled mechanically across the interface via strain/lattice coupling [iii]. Historically, the ferromagnetic layers are $DyFe_2$ and $TbFe_2$ and their optimized mixture, $Tb_{0.3}Dy_{0.7}Tb_{0.3}Fe_2$ known as Terfenol-D, due to their large magnetostriction coefficients [iv]. These intermetallics, however, are costly and relatively brittle; fatiguing easily. Recent interest in $Fe_{1-x}Ga_x$ alloys has been driven by its large magnetostriction coefficient [v], ductility, and natural abundance of source elements.

Here I will discuss the deposition and characterization of epitaxial single-crystalline $Fe_{1-x}Ga_x$ (where x = 0.17 - 0.19) on a ferroelectric $PbMg_{1/3}Nb_{2/3}O_3$—$PbTiO_3$ (PMN-PT) substrate by molecular beam epitaxy. Using lithographically patterned, micron-scale magnetotransport based devices, the interface strain-mediated magnetoelectric coupling is investigated at room temperature. The application of a small electric field (~2-3 kV/cm) can reversibly rotate the magnetic anisotropy of the $Fe_{1-x}Ga_x$. Cycling of the electric field shows hysteresis in the rotation of the magnetic anisotropy, suggesting non-volatile switching. Using polarization versus electric field measurements, we find that the modification of the magnetic anisotropy precedes ferroelectric switching. This result may lead to ultralow-power, non-volatile magnetic devices.

---

[i] H. Schmid, *Ferroelectrics* **162,** 317 (1994).
[ii] R.E. Newnham, *Properties of Materials: Anisotropy, Symmetry, Structure* (Oxford University Press, 2005)
[iii] J. Ma, J. Hu, Z. Li and C.-W. Nan, Adv. Mater. **38**, R123 (2011).
[iv] A.E. Clark “Magnetostrictive Rare Earth-Fe_2 Compounds” in *Ferro-magnetic Materials: A Handbook on the Properties of Magnetically Ordered Substances* edited by E.P. Wohlfarth, Vol. 1 (Elsevier, Amsterdam, 1980) pp. 531-590.
[v] A. E. Clark, K. B. Hathaway, M. Wun-Fogle, J. B. Restorff, T. A. Lograsso, V. M. Keppens, G. Petculescu, R. A. Taylor, J. Appl. Phys. **93**, 8621 (2003)
93:8621

Su1515

Influence of Cap Layers on Perpendicular Magnetic Anisotropy of Ultra-thin Fe/MgO(001) films

T.L. Brown-Heft[1], M. Pendharkar[1], E. Lee[2], C.J. Palmstrom[3]

[1]Materials Department, University of California, Santa Barbara, CA
[2]Engineering Department, Harvey Mudd College, Claremont, CA
[3]Department of Electrical & Computer Engineering, University of California, Santa Barbara, CA

The Fe/MgO(001) system has been predicted to exhibit out-of-plane or perpendicular magnetic anisotropy (PMA) in the ultrathin Fe limit [1], a critical property for the fabrication of magnetic tunnel junctions at dimensions suitable for magnetic random access memory applications [2]. We report a transition from dominant in-plane magnetic anisotropy to PMA in ultrathin Fe/MgO(001) films grown by molecular beam epitaxy on room-temperature substrates after deposited films are capped with Pt and annealed to at least 300˚C in ultra-high vacuum. Interdiffusion of Pt and Fe at this temperature is confirmed by examining changes in peak area from *in-situ* x-ray photoemission spectroscopy (XPS) data, and may indicate the formation of an $L1_0$ ordered PtFe alloy phase, which has previously been shown to exhibit strong PMA [3]. The Pt layer is found to be necessary for the appearance of out-of-plane easy axes by comparing as-deposited, MgO-capped, and Pt-capped Fe/MgO(001) films using an *in-situ* magneto-optic Kerr effect magnetometer in polar and transverse modes.

Additionally, we find that MgO and Pt capping significantly alter the strength of in-plane uniaxial magnetic anisotropy in the ultrathin Fe limit. The Volmer-Weber growth mode for Fe/MgO(001) combined with oblique-incidence Fe deposition 33˚ from sample normal produces elongated Fe islands due to self-shadowing [4]. This morphology is confirmed by *in-situ* atomic force microscopy measurements. The in-plane uniaxial anisotropy arises from the shape anisotropy of the Fe islands, and as a result both MgO and Pt caps alter the overall uniaxial anisotropy by coupling neighboring Fe islands together. This may imply the presence of a thin magnetically active oxide at the upper MgO/Fe/MgO(001) interface, which is corroborated by *in-situ* XPS data.

MgO-capped Fe/MgO(001) films with Fe thickness <10Å exhibit only a superparamagnetic response for all processing conditions. Fe/MgO(001) films with ~11Å thickness exhibit a transition from superparamagnetic to in-plane ferromagnetic behavior after deposition of a 5nm MgO cap. Fe/MgO(001) films with ~13Å thickness often experience a 90˚ rotation of the in-plane uniaxial preferred direction when an MgO cap is deposited. Similar observations are made for Pt-capped films before annealing, which may indicate RKKY coupling of the Fe islands through the conductive Pt.

[1] A. Hallal, H. X. Yang, B. Dieny, and M. Chshiev, *Phys. Rev. B*, vol. 88, no. 18, p. 184423, Nov. 2013.
[2] L. Thomas, G. Jan, J. Zhu, and H. Liu, *J. Appl. Phys.*, vol. 115, no. 17, p. 172615, May 2014.
[3] B. M. Lairson, M. R. Visokay, R. Sinclair, and B. M. Clemens, *Appl. Phys. Lett.*, vol. 62, no. 6, pp. 639–641, 1993.
[4] Y. Park, E. E. Fullerton, and S. D. Bader, *Appl. Phys. Lett.*, vol. 66, no. 16, p. 2140, 1995.

The correlation between the perpendicular magnetic anisotropy and orbital magnetic moment with the structural order parameter of the epitaxial Fe/Pt multilayers under annealing

Y. S. Chen[a], C. H. Lee[a], J. C. A. Huang[b], and H. -J. Lin[c]

[a] Department of Engineering and System Science, National Tsing-Hua University, Hsin-Chu, Taiwan, R.O.C.

[b] Department of Physics, National Cheng-Kung University, Tainan, Taiwan, R.O.C.

[c] National Synchrotron Radiation Research Center, Hsinchu, Taiwan, R.O.C.

The correlation between the perpendicular magnetic anisotropy (PMA) and orbital magnetic moment with the structural order parameter of an epitaxial $L1_0$ Fe/Pt thin film grown from the Fe/Pt multilayer using ion beam sputtering deposition is studied. The Fe/Pt multilayer was grown at 100 ℃ and the multilayer structure was destroyed at an annealing temperature of 500 ℃. When the annealing temperature reached 700 ℃, the $L1_0$ ordered FePt film with growing along (001) orientation epitaxially was obtained. The order parameter reached above 0.95. In addition, c/a ratios of FePt films annealing at different temperatures were below 0.98. This result implies that the interdiffusion of Fe and Pt atoms during the annealing did not distorted the lattice structure too much.

After the sample was annealed at 700 ℃, the out-of-plane order parameter and squareness were close to 1 and magnetocrystalline anisotropy constant reached 3×10^7 erg/cc. It was indicated that the ordered FePt film has strong PMA effect. The ordered FePt film exhibited an out-of-plane coercivity of 1960 Oe after annealing at 600 ℃, but it decreased to 1300 Oe after annealing at 700 ℃.

For the out-of-plane spin-to-orbital ratio, the Fe/Pt multilayer without annealing was 0.088; the Fe/Pt multilayer after annealing at 500 ℃ was 0.149; and the ordered FePt film after 700 ℃ was 0.174. It can be inferred that the higher order parameter, the stronger hybridization and spin-orbital coupling between Fe and Pt atoms occurs. Also, the higher orbital magnetic moment anisotropy implies the out-of-plane spin-to-orbital ratio becomes larger.

Su1525

Magnetization Dynamics of Organic-based Magnetic Heterostructures

Michael Chilcote[1], Y. Lu[2], H. Wang[1], F. Yang[1], and E. Johnston-Halperin[1]
[1]*Department of Physics, The Ohio State University, Columbus, OH 43210-1117, USA*
[2]*Department of Chemistry, The Ohio State University, Columbus, OH 43210-1173, USA*

The low cost, low-temperature conformal deposition of organic-based thin films makes them an attractive class of materials for device applications such as organic light emitting diodes (OLEDs), organic photovoltaics (OPVs), and organic field effect transistors (OFETs). Similarly, organic-based magnets offer the potential for novel applications in high frequency magnetoelectronics and spintronics. Organic-based magnets of the form M[Acceptor]$_x$ (M = transition metal, $x \approx 2$) exhibit room temperature magnetic ordering and provide the opportunity to tailor magnetic properties through the careful selection of the transition metal ions and organic ligands. Ethyl tricyanoethylene carboxylate (ETCEC) and methyl tricyanoethylene carboxylate (MeTCEC) are two such organic ligands that we have recently incorporated into the organic-based ferrimagnets vanadium methyl tricyanoethylenecarboxylate (V[MeTCEC]$_x$) and vanadium ethyl tricyanoethylene carboxylate (V[ETCEC]$_x$). However, despite the promise of these systems, important outstanding questions remain. For example, while these materials are globally disordered structurally, vanadium tetracyanoethylene (V[TCNE]$_x$) exhibits robust magnetism and has been shown to have a Curie temperature as high as 600 K.

Here, we present ferromagnetic resonance (FMR) measurements of both isolated films and bilayers, including all organic and organic/inorganic hybrid heterostructures. Temperature dependent FMR data for isolated films of both V[ETCEC]$_x$ and V[MeTCEC]$_x$ show a switch in the easy axis from in-plane to out of plane coincident with carrier freeze out and a magnetic phase transition. These results are consistent with a mix of ordered and disordered phases within the thin film, with the presence of free carriers mediating exchange between these two subsystems. Temperature dependent FMR measurements are also used to probe the static and dynamic magnetic exchange in V[ETCEC]$_x$/yttrium iron garnet (YIG) hybrid bilayers and V[ETCEC]$_x$/V[MeTCEC]$_x$ all organic magnetic bilayers. These results establish organic magnetic heterostructures as an exciting new materials platform for the exploration of the fundamental mechanisms driving magnetic ordering in organic-based materials and promise the extension of organic spintronics into the regime of dynamically-driven spin currents such as those found in spin pumping driven by FMR or engineered temperature gradients.

Sunday Afternoon

Nanostructures I

Su1530 Invited

Analysis of composition and strain in semiconductor nanostructures by quantitative HAADF-STEM and imaging STEM

A. Rosenauer, K. Müller-Caspary, M. Schowalter, T. Grieb, F.F. Krause, T. Mehrtens

TEM group, Institut für Festkörperphysik, Universität Bremen, D 28359 Bremen, Germany

In this contribution we demonstrate application of quantitative STEM methods to measure composition and strain in semiconductor layers.

The image intensity in high-angle annular dark field (HAADF) STEM images shows a strong chemical sensitivity. As the measured intensity is also influenced by specimen thickness, crystal orientation as well as characteristics of illumination and detector, a standard-free quantification of composition requires a comparison with accurate image simulation. As the largest contribution to the HAADF STEM signal is caused by thermal diffuse scattering (TDS) of electrons, the simulations are carried out with the frozen lattice approach which takes TDS into account.

For the quantification of a STEM image (Fig. 1a) it is subdivided into Voronoi cells in which the intensity is averaged (Fig. 1b). Analysis of composition in a ternary semiconductor layer such as $In_xGa_{1-x}N$ requires measuring the specimen thickness in regions with known composition by comparison with the simulated STEM intensity. Interpolation of the obtained thickness into the layer with unknown composition yields the thickness map (Fig. 1c). Finally, specimen thickness and STEM intensity are compared with simulations computed as a function of composition resulting in a map of In-concentration *x* (Fig. 1d). In alloys containing atoms with different covalent radii (e.g. In and Ga) static atomic displacements occur, which are computed with empirical potentials and included in the simulation. For InGaN, the evaluated composition is compared with atom probe tomography (APT) using InGaN layers with high In concentration as applied in green laser diodes. The results of the STEM measurement are in excellent agreement with composition profiles obtained by APT [1]. As examples of application we demonstrate measurement of segregation efficiency in InGaAs layers buried in GaAs and quantification of few atomic percent of nitrogen in GaNAs. We also show that a combination of measurement of strain and HAADF image intensity can be used to determine both compositions x and y in quaternary $In_xGa_{1-x}N_yAs_{1-y}$. Acquiring two STEM images of the same area with different angular ranges of the detector yields two sources of information which can be exploited, e.g. to evaluate specimen thickness and composition independently. This is demonstrated in Fig. 2 for GaNAs/GaAs.

As material properties such as band gap energy and mobility of charge carriers in semiconductors are governed by strain, it is important to be able to measure strain accurately. In this context, STEM has the disadvantage of scan noise caused by positioning errors of the electron beam. This can be avoided by combining STEM illumination with conventional STEM imaging using an aberration corrected objective lens. This new imaging STEM (ISTEM) mode neither contains scan noise nor is it influenced by the source size. In addition, it has the advantage of spatial resolution beyond the diffraction and information limits [2].

[1] T. Mehrtens et al., Appl. Phys. Lett. 102 (2013) 132112
[2] A. Rosenauer, F.F. Krause et al. Phys. Rev. Lett. 113 (2014) 096101

Su1610

Conductive Atomic Force Microscopy of Piezoelectric InGaN Nanorods

J. Colvin, A. Mikkelsen, R. Timm

NanoLund and Synchrotron Radiation Research, Lund University, Lund, Sweden

The group III-Nitride nanorod family is highly attractive for Light-Emitting Diodes (LEDs) and Laser Diodes (LDs) applications as it covers a wide range of wavelengths, from infrared (InN) to ultraviolet (AlN). InGaN is a prominent example, combining a tunable wavelength range with very efficient light emission [1]. Moreover, having a wurtzite crystal structure with non-central symmetry, InGaN combines piezoelectric and semiconductor properties and opens the door for innovative nanoscale piezo devices, piezotronics [2]. By furthermore inducing a photon excitation, a three way coupling is possible, so-called piezophototronics [2]. Both, piezotronics and piezophototronics are now in the top six future and emerging technologies selected by European Commission for support in the next 10 years [3].

Here, we want to correlate structural, piezomechanical, and electronic properties of individual free-standing InGaN nanorods as shown in Fig. 1 (a). For this we utilize conductive atomic force microscopy (C-AFM), where a metallic AFM tip is used to simultaneously acquire topography (c) and conductivity maps (d) of individual as-grown nanorods. In addition, *I*-*V* curves can be obtained at specific points of the nanorod surface (Fig. 2), which are dominated by the Schottky barrier between the metallic tip and the semiconducting nanorod.

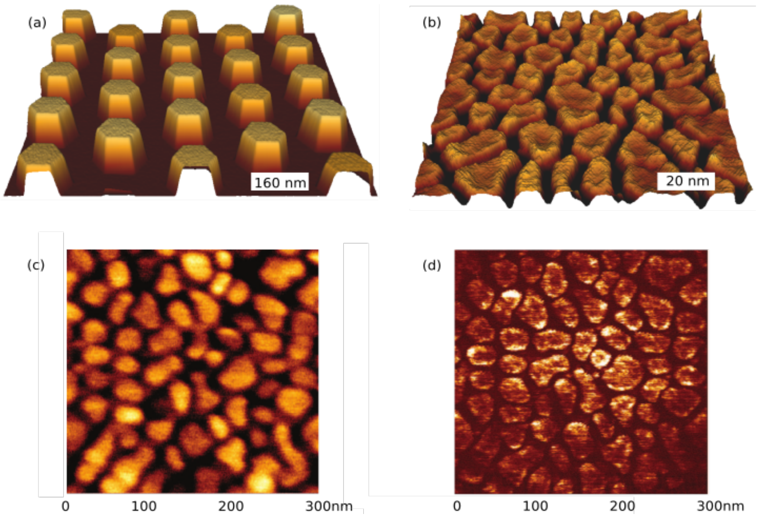

Figure 1: Array of InGaN nanorods (a), dynamic AFM (b), 2D topography (c) and a 2D current map (d) on a c-plane. Here, light paths correspond to higher surface conductivity.

The C-AFM employs small tip loading forces, which can be varied in a controlled fashion, thereby inducing tunable strain on the polar c-plane. By increasing these forces, we observed a shift of the *I*-*V* curves toward lower absolute voltage (Fig. 2), which corresponds to a reduction of the Schottky barrier height (SBH) at increased strain. From comparison with continuum mechanical simulation, we will show that the tuning of the SBH is not determined by contact properties but results from the strain-induced local piezopotential within the nanorod. This opens up new possibilities for investigating piezophototronics and tuning electroluminescence by local strain design.

[1] S. Pereira et al., Phys. Rev. B, 64, 205311 (2001)
[2] Y Zhang et al., Adv. Mater., 23, 4712 (2011)
[3] Y.L. Wang et. al., (2011)

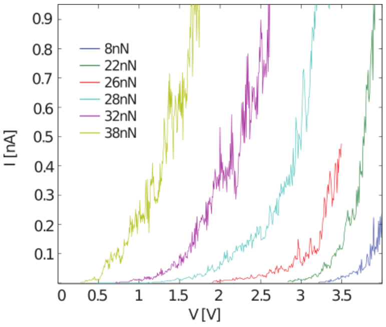

Figure 2: *I*-*V* characteristics of a point on a rod at loads of 8 to 38nN

Su1615

Design principles and fabrication processes of a new microstripline small-sized inductor with carbon nanotube bumps/silicon MEMS pillars for MMICs

Yuichi Nishimoto, Mitsuki Nakamura and Yuji Awano[a)]
Keio University
3-14-1 Hiyoshi, Kohoku-ku, Yokohama, Japan, [a)]E-mail: awano@elec.keio.ac.jp

I. INTRODUCTION

In the present monolithic microwave integrated circuit (MMIC) design, a large area of the chip is taken up by passive components, including spiral inductors. Many efforts have been made to reduce the size of passive components. We proposed a new microstripline structure with carbon nanotube (CNT) bumps for downsizing inductors in MMICs [1]. As shown in Fig.1, in the new structure, CNT bumps are not connected with the grand plane, but with the microstripline. We studied S-parameters of an open-stub with a 1/4 wavelength microstripline having the new structure by 3D simulations and confirmed that it is possible for the new structure to shrink the stub length about 80% to obtain the same resonant frequency [1]. This is due to partly the increase of dielectric constant and magnetic permeability of this structure (i.e., the increase of current path length). The result suggests possible downsizing of distributed filter and other passive circuits. In this paper, we report design principles and fabrication processes of this new inductor technology.

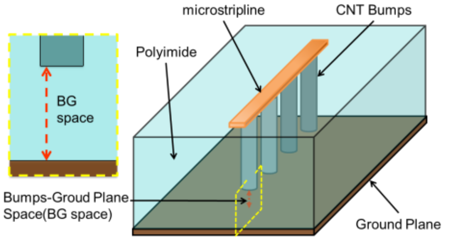

Fig. 1 Schematics of a new microstripline inductor using carbon nanotube (CNT) bumps

II. DESIGN PRINCIPLES:

We simulate several structural dependence (bump number, stub width or bump diameter, stub pitch, etc.) of resonant frequency of the open stub by using Agilent’s Advanced Design System software of method-of-moments (MoM) technique. Figs. 2(a)-(b) show that by introducing 20 bumps, we can shrink the stub length from 1500 to 500 μm to obtain the same resonant frequency of 13 GHz. Figs. 2(c)-(d) suggests that resonant frequency can be controlled by the stub width (or the bump diameter).

III. FABRICATION PROCESS

Fig. 3 shows the fabrication processes for a prototype of microstripline inductors, including bump forming, polyimide filling and planarization, ground plane deposition, silicon substrate polishing and microstripline formation. For a process test, using Si pillars with a height of 100 μm, which are fabricated by MEMS process, we succeeded in filling and planarizing polyimide film, as shown in Figs. 4.

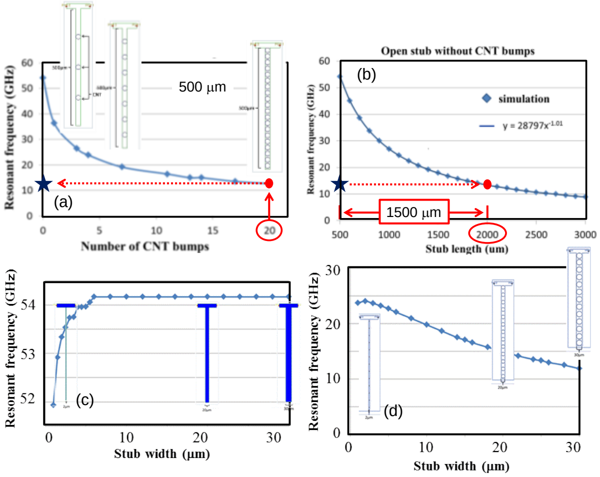

Figs. 2 Bump number (a, b) and bump diameter (c,d) dependence of resonant frequency of open-stub with a 1/4 wavelength microstripline

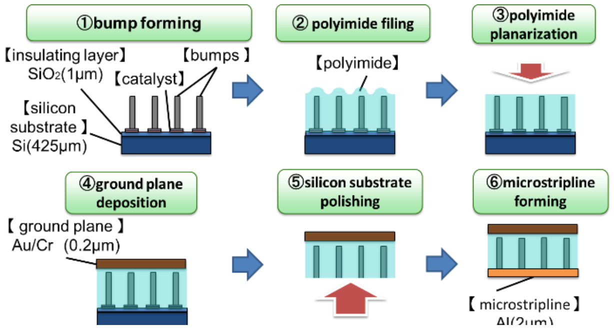

Fig. 3 Fabrication processes for a prototype of the microstripline inductor

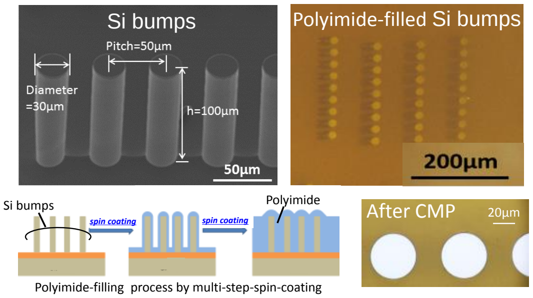

Fig. 4 A SEM image of Si pillars and optical microscope images of polyimide filled Si pillars before and after the planarization process

REFERENCES: [1] T. Iwai, strip line structure JP-A-2006-229297.
[2] C. Caloz et al., IEEE MWCL, vol. 14, no. 4, pp. 133-135, Apr. 2004.
[3] M. Nakamura et al., ADMETA plus 7-6, 2012

Acknowledgement: The authors would like to thank Drs. T. Iwai, S. Sato and D. Kondo of Fujitsu Laboratories Ltd. For their support and discussion.

Su1620

Incorporation of Sb into ErAsSb containing structures during MBE growth

Kurt G. Eyink, Yuanchang Zhang, Joe Peoples, Krishnamurthy Mahalingam, Madelyn Hill, and Lawrence Grazulis
AFRL/RXAN Nanoelectronic Materials Branch, Materials and Manufacturing Directorate, Wright-Patterson AFB, OH 45433

We have been studying the growth of the ErAsSb metal nanoparticle (MNP) on GaAs(001) as a potential plasmonic component in a metal nanoparticle quantum dot hybrid. Modeling suggests strong enhancements in the absorption and luminescent properties of the hybrid compared to a simple quantum dot. In order to maximize these effects, the dot must be precisely placed above the quantum dot with a specific separation between the ErAsSb and the quantum dot. It is known that strain can be used to vertically stack quantum dots to one another if enough strains exists to drive the nucleation event. Modeling has shown the optimum separation is in the range typically seen with vertical stacking of QDs which is less than 40 nm. In the case of ErAsSb, increased strain will require significant Sb in the metal nanoparticle since the lattice constant changes from 5.75Å to 6.15Å as Sb concentration I increases from 0 to 100%. We will present the results of many different growth of ErAsSb that have been analyzed with a combination of high resolution x-ray diffraction and energy dispersive spectroscopy. Our initial attempt was the formation of a multilayer stack of 3 min of ErAsSb MNPs with 40nm GaAs spacer layer. ErAsSb growth was carried out with ~10^{-7} Torr of Sb overpressure on GaAs at 580°C with only residual As in the background. This structure was repeated at a low growth temperature, 500°C and was also done after converting the top GaAs surface to Sb prior to ErAsSb growth. Finally we grew ErAsSb on a relaxed GaSb layer similar to the structures reported by Palmstrom. These results can be summarized that little or no Sb (<9%) was incorporated in any strained growth on GaAs(001) surface where as significant Sb (~64%) is incorporated in the growth of Sb on a relaxed GaSb layer. These results suggest that the strain plays a dominant role in the Sb incorporation into the MNP. We are currently in process of growing a relaxed InAs layer to determine if the amount of Sb is significant. Significant Sb would be expected due to the similar lattice constant between InAs and GaSb.

Su1625

Picosecond thermoreflectance measurements of high density vertically aligned carbon nanotube forests with a height of 10 µm for high performance thermal interface materials

Yuta Kurosu[a], Takashi Yagi[b] and Yuji Awano[a], [c]
[a]Keio University, Yokohama, Japan, [c]E-mail:awano@elec.keio.ac.jp
[b]National Institute of Advanced Industrial Science and Technology, Tsukuba, Ibaraki, Japan

I. INTRODUCTION

Carbon nanotubes (CNTs) have attracted attention as a promising material for thermal management applications in 3D integration, such as Through Silicon Vias (TSVs) and Thermal Interface Materials (TIMs), because of their high thermal conductivity and mechanical strength. For these applications, high density CNT bundles or vertically aligned high density CNT forests are effectively used [1]. Conventional measuring methods for thermal conductivity are not suitable for such a thin-film measurement. A recently developed pulsed optical heating thermoreflectance measurement method can be used as a possible method to measure thermal diffusivity of thin films due to its picosecond time resolution [2]. Nihei et al. reported thermal properties of the CNT forest with a height of a few µm measured by using this method [3]. However, because TIM or TSV heights are typically more than 10 µm, in this paper, we focus on picosecond thermoreflectance measurements for CNT forests with a height of about 10 µm while clarifying issues arising from the measurements.

II. EXPERIMENTAL

High density CNT forests are grown by thermal CVD with slope control of temperature profile (STEP) [4] on silicon substrate. A Fe (3nm) /Al (1nm) layer is used as a catalytic layer for CVD growth. The height of CNT forests is about 12.5 µm. A Mo thin-layer deposited on CNT forests is used to measure the thermal effusivity of CNT forests from the reflectance of the heated Mo surface, as shown in Fig. 1.

III. RESULTS AND DISCUSSION

Fig. 2 shows that the thermal effusivity of the CNT forest on Si is higher than that of SiO_2/Si. Note that the thermoreflectance curve of CNT forest bends with a jagged line at the beginning. One possible explanation of this feature is that a pressure wave is created near the surface of CNT forest by the pump laser pulse. Once the wave is created, the reflectance signal becomes smaller. In order to suppress this phenomenon, it is important to hold the surface of CNT forest. So, we applied spin-on-glass (SOG) filling [5] and chemical mechanical polishing (CMP) for CNT forest [5], as shown in Fig. 3(a). Fig. 3(b) shows a SEM cross-sectional image of a CNT forest partly filled with SOG successfully. We will discuss material selection and process optimization for the SOG filling between CNTs with a height of 10 mm.

CONCLUSIONS We studied picosecond thermoreflectance measurements for CNT forests with a height of more than 10 µm. Both gap filling between CNTs and planarization of the surface of CNT forest are demonstrated.

REFERENCE: [1] T. Iwai et al., IEDM (2005), [2] T. Yagi et al., J. Vac. Sci. Technol. A 23 (2005) 1180, [3] M. Nihei et al., IEDM(2012) 797, [4] A. Kawabata et al., JJAP 54, 045101 (2015), [5] T. Hyakushima et al., Int. Conf. on Planarization/CMP Technology (2009), 197

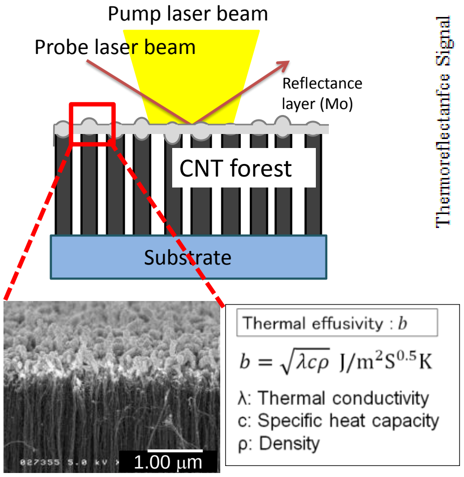

Fig. 1 Schematic of thermoreflectance measurement method and a SEM image of CNT forest

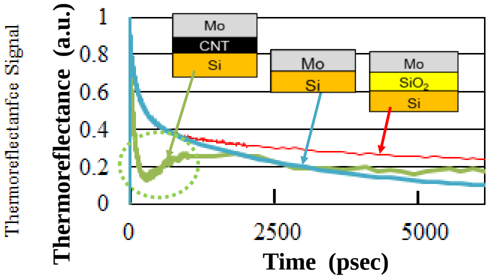

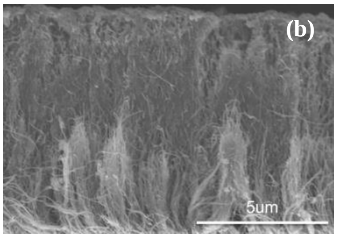

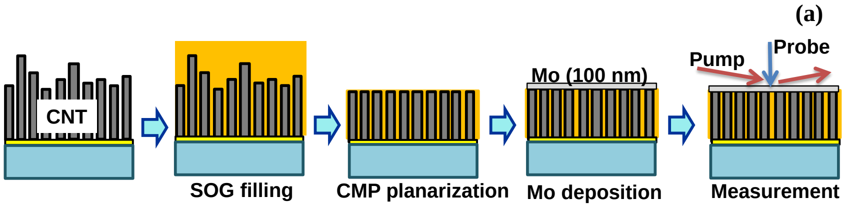

Fig. 3 Advanced sample preparation processes for thermoreflectance measurements (a) and a SEM image after a SOG filling step (b)

Sunday Evening

Energy I

Su1930 Invited

Bulk Direct Bandgap MoS_2 and Hot Electron Injection in Metal/MoS_2 and Metal/WSe_2 Heterojunctions

Stephen B. Cronin (University of Southern California)

In the work presented here, a gentle oxygen plasma treatment is shown to produce a direct bandgap transition in many-layer MoS_2 .The band structure of MoS_2 with more than four layers in thickness is almost identical to that of bulk MoS_2, and flakes thicker than that are considered "many layer" in this work. The data gathered in this work were obtained from samples with thicknesses up to 15 layers (approximately 12 nm), and approximately 5–15 µm in size. This transition is studied using PL spectroscopy, Raman spectroscopy, atomic force microscopy (AFM), and electron energy loss spectroscopy (EELS). Ab initio calculations provide a clear insight into the layer decoupling mechanism responsible for this indirect-to-direct gap transition.[1]

Transition metal dichalcogenides (TMDCs), such as MoS_2 and WSe_2, are free of dangling bonds and therefore make more "ideal" Schottky junctions than bulk semiconductors, which produce Fermi energy pinning and recombination centers at the interface with bulk metals, inhibiting charge transfer. Here, we observe a more than 10× enhancement in the indirect band gap photoluminescence of transition metal dichalcogenides (TMDCs) deposited on various metals (e.g., Cu, Au, Ag), while the direct band gap emission remains unchanged. We believe the main mechanism of light emission arises from photoexcited hot electrons in the metal that are injected into the conduction band of MoS_2 and WSe_2 and subsequently recombine radiatively with minority holes in the TMDC. Since the conduction band at the K-point is 0.5 eV higher than at the Σ-point, a lower Schottky barrier exists for the Σ-point band, making electron injection more favorable. Also, the Σ band consists of the sulfur p_z orbital, which overlaps more significantly with the electron wave functions in the metal. This enhancement in the indirect emission only occurs for thick flakes of MoS_2 and WSe_2 (≥100 nm) and is completely absent in monolayer and few-layer (~10 nm) flakes. Here, the flake thickness must exceed the depletion width of the Schottky junction, in order for efficient radiative recombination to occur in the TMDC. The intensity of this indirect peak decreases at low temperatures, which is consistent with the hot electron injection model.[2]

1. Dhall, R., M.R. Neupane, D. Wickramaratne, M. Mecklenburg, Z. Li, C. Moore, R.K. Lake and S. Cronin, *Direct Band Gap Transition in Many-Layer MoS_2 by Plasma Induced Layer Decoupling* Advanced Materials, **27**, 1573, DOI:10.1002/adma.201405259 (2015).
2. Li, Z., G. Ezhilarasu, I. Chatzakis, R. Dhall, C.C. Chen and S.B. Cronin, *Indirect Band Gap Emission by Hot Electron Injection in Metal/MoS_2 and Metal/WSe_2 Heterojunctions.* Nano Letters, **15**, 3977-3982 (2015).

Su2010 Invited

Structures, Devices, and Architectures for Nanoscale Solutions in Electrical Energy Storage

Gary Rubloff

Director, Nanostructures for Electrical Energy Storage (NEES), a DOE EFRC
Director, Maryland NanoCenter
University of Maryland

Nano science and technology promise enhancement to batteries and capacitors through higher power at given energy, accompanied by new possibilities for better capacity retention and safety. In Nanostructures for Electrical Energy Storage (NEES, www.efrc.umd.edu), we have focused on the latter, seeking to understand how the structure of components and the architecture in which they are arranged determine the multifunctionality required for electrical energy storage: ion transport and storage, electron transport, and structural stability during charge/discharge cycling. Precision multistep synthesis has enabled the creation of heterogeneous nanostructures for energy storage, involving multiple materials to confer the needed multifunctionality, and to understand how design influences electrochemical behavior at the nanoscale and storage performance of nanostructures. Examples include (1) a variety of 3D nanostructure “forests”, (2) nanowire and nanotube structures which integrate electron transport and ion storage components, and (3) solid state electrolyte and battery configurations for scaling safe materials to the nanoscale. Achieving the promise of nanostructures for energy storage will require thin film technologies, either inserted into conventional battery fabrication or as a completely new paradigm.

<table>
<tr>
<td>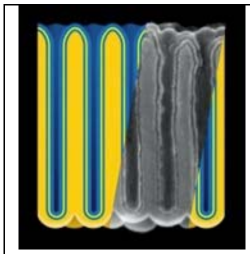</td>
<td>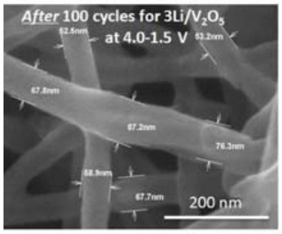 </td>
<td>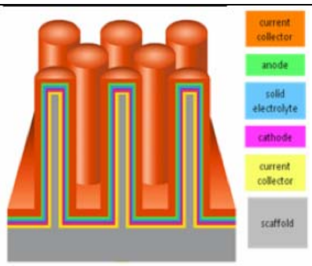 </td>
<td>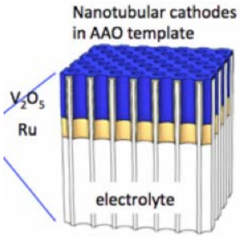 </td>
</tr>
<tr>
<td>Electrostatic nanocapacitor</td>
<td>V2O5/MWCNT sponge electrode</td>
<td>Interdigitated 3-D solid state battery</td>
<td>Nanopore battery</td>
</tr>
</table>

This work has been supported by Nanostructures for Electrical Energy Storage (NEES), an Energy Frontier Research Center funded by the U.S. Department of Energy, Office of Science, Office of Basic Energy Sciences, under Award Number DESC0001160.

Su2050

Surface/Interface Effects on Performance of Thin-Film All-Solid-State Li-Ion Batteries with Al and Si Anodes

A. A. Talin[1,] C. Gong[2], D. Ruzmetov[3], A. Pearse[2], D. Ma[4]
J. N. Munday[4], G. Rubloff[2], M. S. Leite[2]
[1]Sandia National Laboratories, Livermore, CA, United States.
[2]Department of Materials Science and Engineering, Univ. of Maryland, College Park, MD, United States.
[3]Army Research Laboratory, MD, United States.
[4]Department of Electrical and Computer Engineering, Univ. of Maryland, College Park, MD, United States.

Thin film solid state Li-ion batteries employing inorganic, non-flammable electrolytes (TFLIBs) are inherently safe, have negligible self-discharge rates and have demonstrated extremely long cycle life. Using TFLIBs to provide on-chip energy storage would enable concepts such as distributed power wherein components of an integrated circuit (e.g. memory elements) remain powered even upon disconnection from external power, providing one approach for hardware-level information security. Other emerging applications include autonomous MEMS, distributed sensor networks, and medical implants. Metallic Li is currently used as the anode in most commercial TFLIB. However, concerns over semiconductor device contamination and the relatively low melting point (<180 °C) make metallic Li undesirable for on-chip integrated microbatteries. Potential alternatives to elemental Li anodes include Al and Si which reversibly allow with Li at potentials close to that of metallic Li (i.e $Li \rightarrow Li^+ + e^-$). Both Al and Si are compatible with semiconductor processing, inexpensive, and have high Li capacities of ~990 mAhr/g and ~3500 mAhr/g, respectively. Despite their similarities, the cycling behavior of identical solid state batteries fabricated with either Al or Si anodes show significant differences. Batteries with Al anodes degrade rapidly, losing over 80 percent of their initial capacity after just a few charge discharge cycles. Batteries with Si anodes, on the other hand, retain over 90 percent of their capacity after 100 cycles.

In this paper we combine *in situ* cycling of batteries in side a custom scanning electron microscope, X-ray photoelectron spectroscopy (XPS), transmission electron microscopy and local scanning probe electrical conductivity measurements to characterize the processes that occur on the Al negative electrode outer surface during lithiation in thin-film batteries with the aim of gaining deeper understanding for the rapid loss in capacity compared to Si. We find that the lithiation/delithiation process in batteries with Al anodes is restricted to the surface of the anode where highly porous LiAl (*Fd3m* phase) clusters nucleate and grow during charging, and shrink during discharging. The loss in capacity is directly related to the fraction of the Al surface covered with the highly porous LiAl clusters. Using ex situ transmission electron microscopy (TEM) we find that the LiAl clusters form only on the surface of the anode, suggesting that the bulk of the Al film remains essentially strain-free during lithiation/delithiation.We find that the few-monolayer thick Al-Li-O compound formed on top of the Al electrode substantially increases the electrical resistance at its surface, thus hindering surface-bound charge transport processes and degrading the battery's overall performance. We also find that coating the Al electrode with a Cu film *in situ* without breaking vacuum does not resolve the rapid capacity loss. The rapid loss in capacity, even at relatively low lithiation level (<10% of theoretical capacity) is in sharp contrast to similarly prepared TFLIBs with Si thin film anodes which exhibit excellent cycle life, as shown in Fig. 2.

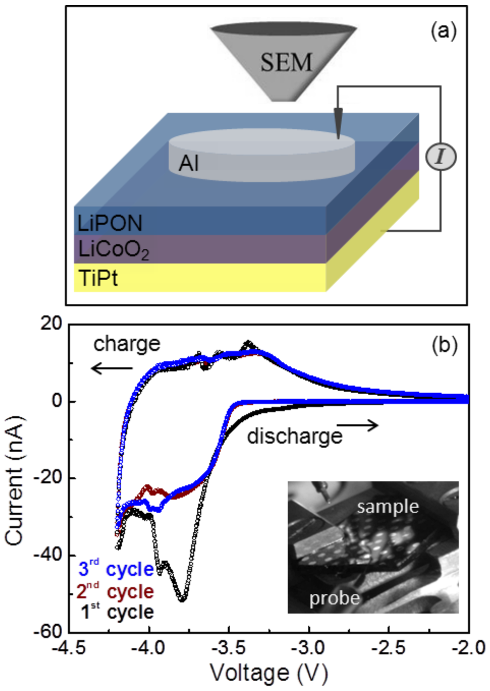

Figure 1: (a) Schematic illustration of *in situ* real-time measurements of electrochemical lithiation/delithiation cycling and morphology evolution of Al-Li alloys on solid state thin film batteries. Layers are represented out of scale for clarity. (b) Cyclic voltammogram from 2.0 V to 4.2 V versus Li/Li$^+$ at a 0.15 mV.s^{-1} scan rate for a representative battery. The first three cycles are shown. Inset: micrograph of sample and electrical probe inside UHV chamber.

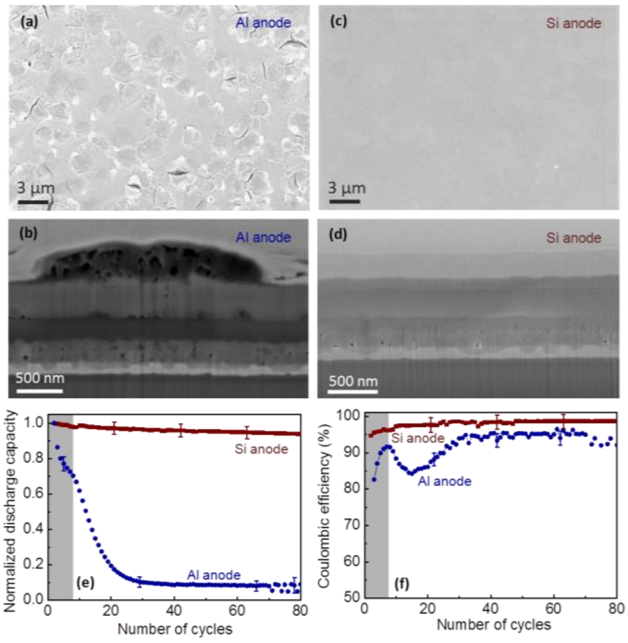

Fig. 2 a.) Plan view and 52° tilted SEM images of (a,b) Al anode and (c,d) Si anode batteries after 10 charging cycles. (e) Discharge capacity at 10 nA for Al anode and 30 nA for Si anode, and (f) Coulombic efficiency as a function of number of cycles.

Synthesis of Chemically Activated Li_2MnO_3 Nanowires and Nanobelts with Improved Electrochemical Properties as Cathode Materials for Li-ion Batteries

Youxiang Zhang[1]*, Xiaoling Ma[2]

1 College of Chemistry and Molecular Science, Wuhan University, Wuhan 430072, China

2 College of Chemistry and Life Science, Hubei University of Education, Wuhan 430205, China

Abstract: Li-rich Mn-based layer-structured $xLi_2MnO_3 \cdot (1-x)LiMO_2$ (M = Mn, Ni, Co, etc.) have been studied very popularly recently as the cathode materials for rechargeable Li-ion batteries due to their high specific capacity. Layer-structured Li_2MnO_3 (x = 1 in the $xLi_2MnO_3 \cdot (1-x)LiMO_2$) has the simplest structure with largest capacity (~458 mAh/g with respect to the initial mass of the sample) in this family of materials. Usually, the Li_2MnO_3 needs to be electrochemically activated in the first charge process in a high cut-off voltage, and this electrochemical activation causes serious capacity decay of the material. In this work, we have synthesized chemically activated Li_2MnO_3 nanowires (Fig. S1a) and nanobelts (Fig. S1b) and measured their properties and performances as the cathode materials for Li-ion batteries. The results show that these directly synthesized nanowires and nanobelts have very good cycling properties (Fig. S1c) and superior high-rate performances (Fig. S1d). The charge-discharge processes of the Li_2MnO_3 as the cathode material are followed and the structural changes are measured.

Monday Morning

Nanostructures II

Mo0830 Invited

III-V nanowires for next generation solar cells: advantages and challenges

E. Alarcon-Llado, A. Fontcuberta i Morral

Semiconductor nanowires are filamentary crystals with a tailored diameter in the order of few to hundred nanometers. Their particular morphology and dimenstions have insipired new applications as well as provided new solutions for existing ones. In this talk we will discuss how the photonic properties of nanowires standing on a substrate provide a path for huge savings in materials [1] (a factor up to 1000) and a more flexible way for highly efficient multi-junction solar cells [2,3]. We will also discuss the challenges for this to become a reality.

[1] P. Krogstrup et al Nature photonics 7, 306 (2013)
[2] A. Kandala et al, PSS A 206, 173 (2009)
[3] A. Dorodnyy et al ACS Photonics 2, 1284 (2015)

Correlation of the Atomic Scale Surface Structure and the Electronic Properties of InAs and InAs/InSb Nanowires

J. Knutsson[1], M. Hjort[1], J. Webb[1], O. Persson[1], S. Gorji Ghalamenstani[1], S. Lehmann[1], L. Samuelson[1], K.A. Dick[1], R. Timm[1], and A. Mikkelsen[1]

[1]*Department of Physics, NanoLund, Lund University, Box 118, 221 00 Lund, Sweden*

III-V semiconductor nanowires (NWs) offer tremendous possibilities for device application in photonics [1], energy conversion [2], and information technology [3]. With their small diameter and their very large surface-to-volume ratio, the NW device behavior is strongly influenced by their surface structure. Thus, it is both essential (but challenging) to investigate their atomic surface structure and to combine this information with electrical measurements on individual NWs. In recent years, we have managed to clean a variety of III-V NWs from their native oxide and revealed the atomic arrangement of their sidewall surfaces with scanning tunneling microscopy (STM). We have now started to combine this with simultaneous nanowire device measurements and operation [4, 5].

Here, we present STM images of various InAs NW surfaces of both wurtzite (Wz) and zincblende (Zb) crystal structure [6]. We find that certain polar NW surfaces exhibit reconstructions not appearing in bulk samples, demonstrating that atomic scale surface structure, and thus surface energies, of NW sidewalls cannot always be expected to behave as on "infinite" planar surfaces [7]. By combining STM imaging with scanning tunneling spectroscopy (STS) measurements, we study local electronic properties across the interfaces of NW heterostructures, both at room temperature [8] and now at 5K. We have previously found that the non-polar facets are unreconstructed, implying that STS data will correspond to the bulk electronic properties of the material without being perturbed by surface states related to reconstructions, allowing for determination of valence and conduction band edges as well as band alignments types. We now investigated the electronic properties of individual defects such as atomic steps and stacking faults on InAs NWs at 5K, and it was found that even single (one atomic layer) stacking faults in the Wz part of a NW had electronic structure corresponding to Zb. Only 1 nm away from the stacking fault Wz behavior is seen, suggesting atomically sharp band alignments between Wz and Zb. Due to the band-offsets between the two crystal phases the stacking fault acts as a quantum well (QW) with measurable confined states.

For correlating local structural and electronic characterization with transport measurements of NW devices, we have developed a novel device setup for direct STM measurements on NW devices that can be Hydrogen cleaned to more than 400C while preserving device performance. The setup allows for simultaneous cleaning of material heterostructures such as NWs with axially stacked segments of InAs and InSb. We will show initial results of atomically resolved STM on InAs NWs in a device setup, where we observe defect migration on the NW surface when an external bias is applied over the NW. By external biasing we were also able to directly observe potential drop over defects such as steps and stacking faults. Finally using this setup, complemented by x-ray photoelectron spectroscopy (XPS) measurements, we were able to investigate how the electronic properties of single NWs are affected by surface oxides, formed natively when transported under ambient conditions. After complete oxide removal by hydrogen cleaning the NW heterostructures, consisting of one InAs bottom segment and one InSb top segment, were found to have an increase in conductivity by two orders of magnitude [9].

[1] D. Saxena *et al.*, Nat. Photonics **7**, 963 (2012)

[2] J. Wallentin *et al.*, Science **339**, 1057 (2013)

[3] M. Egard *et al.*, Nano lett. **10**, 809 (2010)

[4] O. Persson *et al.*, Nano lett. **15**, 3684 (2015)

[5] J. L. Webb *et al.*, Nano Research. **7**, 877 (2014)

[6] M. Hjort *et al.*, Nano Lett. **13**, 4492 (2013)

[7] J. V. Knutsson *et al.*, ACS Appl. Mat. Interfaces **7**, 5748 (2015)

[8] M. Hjort *et al.*, ACS Nano **6**, 9679 (2012)

[9] J. L. Webb *et al.*, Nano lett. **15**, 4865 (2015)

---

* Corresponding author email: johan.knutsson@sljus.lu.se

Mo0915 Upgraded

How can band offsets in III-V nanowires be determined correctly by scanning tunneling spectroscopy?

Ph. Ebert,[1,*] P. Capiod,[2] T. Xu,[2,3], M. J. Wei,[3] A. Díaz Álvarez,[2] X. L. Han,[2] D. Troadec,[2] J. P. Nys,[2] M. Berthe,[2] G. Patriarche,[4] L. Lymperakis,[5] J. Neugebauer,[5] I. Lefebvre,[2] S. R. Plissard,[2,6] P. Caroff,[2,7] R. E. Dunin-Borkowski,[1] B. Grandidier[2]

[1]Peter Grünberg Institut, Forschungszentrum Jülich GmbH, 52425 Jülich, Germany
[2]Institut d'Electronique et de Microélectronique et de Nanotechnologies, IEMN, (CNRS, UMR 8520) Département ISEN, 41 bd Vauban, 59046 Lille Cedex, France,
[3] Key Laboratory of Advanced Display and System Application, Shanghai University, 149 Yanchang Road,Shanghai 200072, People's Republic of China
[4]CNRS-Laboratoire de Photonique et de Nanostructures (LPN), Route de Nozay, 91460 Marcoussis, France
[5]Max-Planck Institut für Eisenforschung GmbH, Max-Planck Str. 1, 40237 Düsseldorf, Germany
[6]CNRS-Laboratoire d'Analyse et d'Architecture des Systèmes (LAAS), Univ. de Toulouse, 7 Avenue du Colonel Roche, F-31400 Toulouse, France
[7]Department of Electronic Materials Engineering, Research School of Physics and Engineering, The Australian National University, Canberra, ACT 0200, Australia
[*] E-mail: p.ebert@fz-juelich.de

Scanning tunneling microscopy (STM) and spectroscopy (STS) allow a unique high resolution insight simultaneously into the structural and electronic properties of III-V semiconductor nanowires. Particularly interesting are heterostructured nanowires with interfaces between different polytypes or different materials. Since the carrier transport through such nanowires is expected to be affected by different band gaps and band offsets, the accurate determination of these values are of critical. Although STM and STS is presented in the literature as the ideal technique for this, we demonstrate that STS measurements (and possibly other measurement techniques) are mostly wrongly interpreted and it is thus unclear if any of the published band offset values are reliable.

In this presentation we demonstrate that the sidewall surfaces of III-V nanowires regularly exhibit a high step density, which induces a pinning the Fermi energy within the fundamental band gap by extrinsic surface states. The pinning level is, however, different on every polytype or on every material Hence, the relative band edge positions between different types of nanowire segments are extrinsically determined by the different pinning levels, but by the intrinsic band offsets. Furthermore, extrinsic band offsets turn out to be much larger than intrinsic one. Hence, extrinsic defects at the sidewall surface likely affect the carrier transport much stronger than intrinsic band offsets. Thus, it is of prime interest to determine pinning levels and extrinsic band offsets at the sidewall surfaces. We demonstrate these extrinsic band offsets using zincblende-wurtzite GaAs nanowire junctions.[1]

In order to nevertheless have experimental access to intrinsic band offsets, we developed a new methodology to determine accurate band offsets between different NW segments.[2] It uses a thin overgrown shell of a material with wider band gap. This allows electron tunneling through this thin surface shell layer directly into the core. The shell furthermore assures that the pinning of both, the overgrown and the pure segment, is identical. Then the differences between the conduction/valence band edge positions of both materials provide the correct band offset values. We applied this methodology to axial GaAs/GaAs$_{81}$Sb$_{19}$/GaAs heterostructure nanowires.

[1] P. Capiod, T. Xu, J. P. Nys, M. Berthe, G. Patriarche, L. Lymperakis, J. Neugebauer, P. Caroff, R. E. Dunin-Borkowski, Ph. Ebert, and B. Grandidier: *Band offsets at zincblende-wurtzite GaAs nanowire sidewall surfaces*. Appl. Phys. Lett. **103**, 122104 (2013).

[2] T. Xu, M. J. Wei, P. Capiod, A. Diáz Álvarez, X. L. Han, D. Troadec, J. P. Nys, M. Berthe, I. Levebvre, G. Patriarche, S. R. Plissard, P. Caroff, Ph. Ebert, B. Grandidier: *Type I band alignment in GaAs81Sb19/GaAs core-shell nanowires*. Appl. Phys. Lett. **107**, 112102 (2015).

Mo0935

Suppression of non-radiative surface recombination by N incorporation in GaAs-based nanowires grown by molecular beam epitaxy

Shula L. Chen[1], Weimin M. Chen[1], Fumitaro Ishikawa[2] and Irina A. Buyanova[1*]

[1] Department of Physics, Chemistry and Biology, Linköping University, 58183, Linköping, Sweden

[2] Graduate School of Science and Engineering, Ehime University, Matsuyama 790-8577, Japan

III-V semiconductor nanowires (NWs) such as GaAs NWs form an interesting artificial materials system promising for applications in advanced optoelectronic and photonic devices, thanks to the advantages offered by the one dimensional architecture and the possibility to combine it with the main-stream silicon technology. Alloying of GaAs with nitrogen can further enhance performance and extend device functionality via band-structure and lattice engineering. However, due to a large surface-to-volume ratio, III-V NWs suffer from severe non-radiative carrier recombination at/near NWs surfaces that significantly degrades optical quality. The contribution of the surface-related recombination is known to be especially severe in GaAs-based NW structures due to a large surface-to-volume ratio and the presence of surface states participating in the non-radiative recombination processes.

In this work we employ photoluminescence (PL) transient spectroscopy to evaluate surface recombination processes in novel GaAs/GaNAs core/shell NWs grown by plasma-assisted molecular beam epitaxy (MBE) on (111) plane Si substrates. It is found that increasing nitrogen composition can strongly suppress the detrimental surface recombination in these structures. This conclusion is based on our experimental finding that lifetimes of photo-generated free excitons and free carriers increase with increasing N composition, as revealed from temperature dependent time-resolved PL studies. This is accompanied by a sizable enhancement in the room temperature PL intensity in the GaAs/GaNAs core/shell NWs as compared with reference GaAs NW structures. The observed N-induced suppression of the surface recombination is suggested to be a result of an N-induced modification of the surface states that are responsible for the nonradiative recombination. Our results, therefore, demonstrate the great potential of incorporating GaNAs in III-V NWs to achieve efficient nano-scale light emitters.

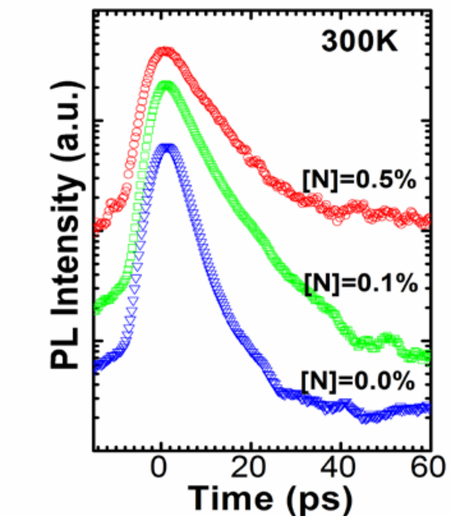

Fig.1. Room temperature PL transients measured from GaAs/GaNAs core/shell NWs with the specified N contents.

Mo0940

Formation of one-dimensional arrays of magic In clusters using a vicinal Si surface as a template

Martin Franz*, Julia Schmermbeck, and Mario Dähne

Institut für Festkörperphysik, Technische Universität Berlin, 10623 Berlin, Germany

*Email address: martin.franz@physik.tu-berlin.de

Self-assembled magic clusters on surfaces are fascinating zero-dimensional nanostructures and promising candidates for the application in future nanodevices and in catalysis.

Here, magic In clusters on the Si(111)7×7 surface were studied using scanning tunneling microscopy (STM) and spectroscopy (STS), in order to investigate fundamental effects in magic cluster system.

These clusters grow in a self-organized way using the 7×7 reconstructed Si(111) surface as a template, resulting in the formation of identical – so-called magic – clusters. Each cluster occupies one half unit cell of the 7×7 reconstruction with a strong preference for the faulted half, due to a lower formation energy of the cluster in this half unit cell.

Using STS, different electronic properties were found for clusters that formed in the faulted half unit cell and in the unfaulted half unit cell of the 7×7 reconstruction. In addition, an influence of clusters forming in neighboring half unit cells on the electronic properties was observed.

Using as a template the Si(557) surface, which is vicinal to Si(111), the possibility to grow one-dimensional arrays of magic clusters was investigated. The Si(557) surface consists of alternating Si(111) terraces with a width of a single 7×7 unit cell and triple steps. It was found that indeed the same magic clusters as on the planar Si(111) surface form on the (111) terraces. Here, the clusters assemble into one-dimensional cluster chains due to the stepped structure of the Si(557) substrate. The strong preference for the faulted half unit cell of the 7×7 reconstruction offers the ability to grow two different one-dimensional arrays of magic In clusters. Similar to the two-dimensional arrays on the planar Si(111) surface, in a first step mainly the faulted half unit cells are occupied by magic clusters, while in a second step all half unit cells are filled.

The authors thank the Deutsche Forschungsgemeinschaft for financial support through FOR 1282 project D.

43rd Physics and Chemistry of Interfaces and Surfaces (PCIS-2016)

InSb Quantum Nano-Stripes by Molecular Beam Epitaxy

***Thanavorn Poempool*[1]*, Zon*[1]*, Suwit Kiravittaya*[2]*, Suwat Sopitpan*[3]*, Supachok Thainoi*[1]*, Songphol Kanjanachuchai*[1]*, Somchai Ratanathammaphan*[1] *and Somsak Panyakeow*[1]**
[1] Semiconductor Device Research Laboratory, Department of Electrical Engineering, Faculty of Engineering, Chulalongkorn University, Bangkok Thailand
[2] Advanced Optical Technology (AOT) Laboratory, Department of Electrical and Computer Engineering, Faculty of Engineering, Naresuan University, Phitsanulok, Thailand
[3] Thailand Microelectronic Center (MTEC), National Science and Technology Agency (NSTDA), Chachoensao, Thailand
Corresponding Author*: Somsak Panyakeow e-mail : somsak.p@chula.ac.th*

Extended Abstract

InSb quantum nano-stripes are grown by molecular beam epitaxy via S-K growth mode. The quantum nanostructure is formed by strain relaxation due to lattice mismatch of InSb and underlying materials.

For the first experiment, InSb is grown on InAs substrate. First, InAs buffer layer is grown at 400°C. Substrate temperature is then decreased to 250°C for the growth of InSb nanostructures. During the interval of temperature decrease process, As shutter is closed to clean up As atmosphere. When the background pressure is below 5×10^{-9} Torr, Sb soaking is conducted for 1 minute by Sb cracker cell operated at 750°C. Then, In shutter is re-opened to create InSb nanostructure at a growth rate of 0.01 monolayer/s (ML/s) for 6 minutes. Spotty RHEED pattern is observed after 2 minutes of In shutter opening. It indicates the formation of three-dimensional nanostructures on the surface. InSb/InAs quantum structure has a configuration of nano-stripe having stripe length, width and height in the range of 270-350, 50-120 and 8-15 nm respectively. Figure 1 shows an AFM image of these InSb nano-stripes on the (001) InAs surface. The nano-stripes are elongated along [110] crystallographic direction.

Another experiment demonstrates the formation of InSb nano-stripes aligned along GaAs anti-phase domains (APD) boundaries. By growing GaAs on Ge substrate, APDs of GaAs are formed. After that the growth of InSb is performed in the same way as the former experiment. AFM image of InSb nano-stripes formed between GaAs APD is shown in Figure 2.

InSb/GaAs and InSb/InAs are considered as type-II and type-III heterostructures, respectively [1]. Only holes are confined in the quantized states in the quantum nanostructure, but electrons are free in the bulk with tunneling behavior due to the broken gap of this separated confinement. This unique property of quantum nanostructure is useful for memory as well as high speed nano-electronic devices.

Keywords: InSb/InAs Quantum Nano-Stripes, Type III Quantum Nanostructures

[1] H. Kroemer, “The 6.1 Å family (InAs, GaSb, AlSb) and its heterostructures: a selective review,” Physica E, Vol. 20, P. 196, (2004)

Time-Deterministic Control of Quantized Conductance of Au Nanowires Using Feedback-Controlled Electromigration with Real-Time Operating System

Shusuke Sato, Yuma Kanamaru, Yu Katogi, and Jun-ichi Shirakashi*

Department of Electrical and Electronic Engineering, Tokyo University of Agriculture and Technology,
Koganei, Tokyo 184-8588, Japan

shrakash@cc.tuat.ac.jp

*Corresponding author

Abstract: Feedback-controlled electromigration (FCE) methods have been successfully and widely used to adjust quantized conductance of metal nanostructures [1-3]. In general, it is considered that the FCE method is commonly performed on general-purpose operating system (GPOS). On the other hand, real-time operating system (RTOS) is known to be designed to run critical applications reliably with precise timing. Hence, we investigate here the FCE methods using RTOS, in order to run FCE algorithms deterministically and to control quantized conductance of Au nanowires precisely, at room temperature in ambient air.

Figure 1 shows conductance G of the Au nanowire as a function of applied voltage V during FCE with RTOS at room temperature in ambient air. The conductance G normalized with the quantum conductance G_0 ($2e^2/h$ = 77.6 μS) is also shown on the right vertical axis of Fig. 1. The conductance G decreased from 17 mS (= around 215 G_0) to less than 2 mS (= around 25 G_0) using the FCE method with RTOS, showing the conductance quantization at integer multiples of G_0, even at room temperature. We fit the Joule heating model [1] to the experimental data. The Joule heating curve with constant power P = 1.7 mW exhibits a good agreement with the experimental data at the wide range of conductance G, as compared with previous reports [1-3]. Thus, it is suggested that Joule heating power during FCE is stably maintained and is precisely regulated with RTOS. Hence, these results imply that FCE methods combined with RTOS can accurately and effectively tune electrical conduction of Au nanowires in quantized conductance regime even at room temperature.

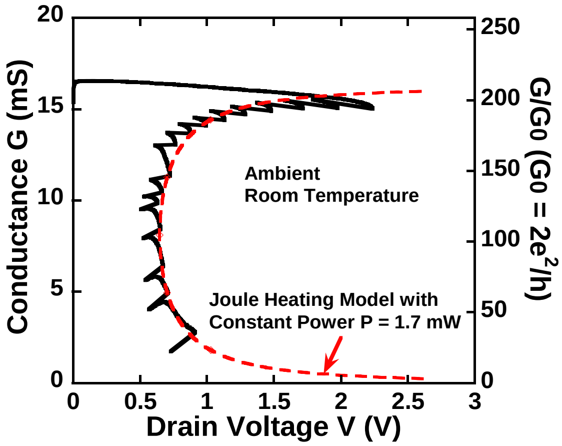

Fig. 1. G-V characteristics of the Au nanowire during FCE with RTOS. Broken line shows the fitting results to the Joule heating model with constant power P = 1.7 mW.

References

[1] D. R. Strachan, D. E. Smith, D. E. Johnston, T.-H. Park, M. J. Therien, D. A. Bonnell, and A. T. Johnson, Appl. Phys. Lett. 86, 043109 (2005).

[2] A. Umeno and K. Hirakawa, Appl. Phys. Lett. 94, 162103 (2009).

[3] R. Hoffmann, D. Weissenberger, J. Hawecker, and D. Stoffler, Appl. Phys. Lett. 93, 043118 (2008).

Session: **Nanostructures for electronics & photonic**

Mo0955

Atomic structure of III-V layers grown on GaP/Si(001)

C.S. Schulze[1], X. Huang[2], C. Prohl[1], V. Füllert[1], S. Rybank[1], S. Maddox[3], S. March[3], S.R. Bank[3], A. Beyer[4], R. Straubinger[4], K. Volz[4], M.L. Lee[2], and A. Lenz[1,2,*]

[1]Institut für Festkörperphysik, Technische Universität Berlin, 10623 Berlin, Germany
[2]Department of Electrical Engineering, Yale University, New Haven, Connecticut 06520, USA
[3]Microelectronics Research Center and ECE Dept., The University of Texas at Austin, Austin, Texas 78758, USA
[4]Material Sciences Center and Faculty of Physics, Philipps-University Marburg, Marburg, Germany
*Email address: alenz@physik.tu-berlin.de

III-V layers for laser structures grown on Si(001) substrates have been of high interest for several decades, but the main challenge is still the high dislocation density. The origin of the dislocations between III-V layers such as GaAs and Si are the lattice mismatch, the different thermal expansion coefficients, and the polar/nonpolar interfaces resulting in anti-phase boundaries (APB). Slightly off-cut substrates are frequently used in order to achieve double steps on the silicon substrate and thus to avoid the formation of APB. However, the growth on exactly oriented Si(001) substrates is highly preferable for successful integration into silicon-based technology.

Here we present a detailed study on InAs/InGaAs quantum-dot-in-a-well (DWELL) structures grown in a GaAs matrix on an exactly oriented GaP/Si(001) template. Cross-sectional scanning tunneling microscopy and spectroscopy (XSTM/XSTS) and high angle annular darkfield images taken in a scanning transmission electron microscope (HAADF-STEM) are used at the same sample to investigate the GaAs/GaP and the GaP/Si interfaces as well as the atomic structure and stoichiometry of InAs/InGaAs DWELL structures.

The GaP/Si interface can be easily identified within XSTM images due to the different step density and orientation of the surface steps or by using XSTS. Images of the GaAs/GaP interface reveal a sharp and strongly undulating electronic contrast due to the different lattice constants and bulk band gaps of the materials, while HAADF-STEM images especially exhibit the high strain between the GaAs and GaP layers. Both XSTM and STEM show a laterally inhomogeneous interface with a vertical extension of about 10 nm. XSTM data of InAs/InGaAs DWELL structures grown on top of the GaP/Si(001) template show lateral quantum-dot sizes of about 20 nm (see Fig. 1), heights up to 8 nm, and an In concentration of up to 100%. In addition, Photoluminescence (PL) spectroscopy was performed for similarly grown samples, revealing a slight blue shift to a ground-state emission wavelength around 1.26 μm, but also an even higher peak intensity for growth on GaP/Si(001) compared with growth on GaAs(001). These structural and electronical properties demonstrate the high potential of such III-V layers for integration in optoelectronics on silicon.

This project was supported by the Deutsche Forschungsgemeinschaft LE3317/1-1, and work at UT-Austin was supported by a Multidisciplinary University Research Initiative from the Air Force Office of Scientific Research (AFOSR MURI Award No. FA9550-12-1-0488).

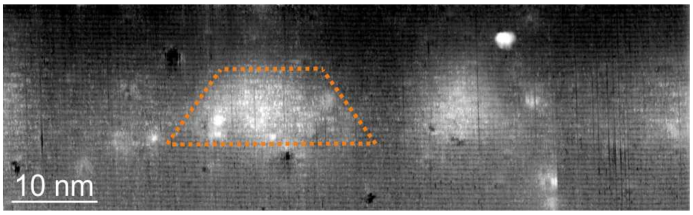

Fig. 1: XSTM filled-state image of an InAs/InGaAsquantum-dot-in-a-well (DWELL) layer, taken at $V_S = -2.7$ V and $I_T = 20$ pA. One quantum-dot structure is indicated by the dashed (orange) line.

Mo1100

Atomic structure of InAs(Sb)/GaAs submonolayer quantum dots for strong charge carrier localization

Andrea Lenz, Zeno Diemer, Christopher Prohl, David Quandt, André Strittmatter,
Udo W. Pohl, Mario Dähne, and Holger Eisele*

Technische Universität Berlin, Institut für Festkörperphysik, 10623 Berlin, Germany
*ak@physik.tu-berlin.de

Submonolayer-grown semiconductor nanostructures are promising for high power and high speed laser devices. They are formed by a cycled deposition of the active material with a thickness well below one monolayer (ML) and also well below the critical thickness for the Stranski-Krastanov-growth mode alternating with several ML thick matrix material. Recently, cross-sectional scanning tunneling microscopy (XSTM) investigations of InAs/GaAs submonolayer quantum dot stacks have shown the formation of InAs agglomerations with lateral sizes of about 5 nm, heights of about 2 nm, and a high density above $10^{12}/\mathrm{cm}^2$ [1]. They were successfully implemented in high speed (>25 Gbit/s) vertical-cavity surface emitting lasers operating up to 120°C.

In this presentation, the cathodoluminescence-proven stronger localization of charge carriers corresponding structural changes upon additional supply of Sb are studied on the atomic scale using XSTM. The InAs(Sb) agglomerations show slightly smaller sizes than equivalent submonolayer structures grown without Sb. From atomically resolved filled-state XSTM images the Sb incorporation could be determined simply by counting the Sb atoms. By an additional comparison with empty-state XSTM images it could be shown that the Sb atoms are mostly incorporated at the InAs agglomerations. Furthermore, by an analysis of the local lattice parameter the In content could be determined, being considerably smaller than the nominally deposited amount of In. Also the size of the submonolayer stacks along growth direction is reduced by about 30%. These reductions from the nominal values are due to reduced growth rates of InGaAs and GaAs on Sb-containing growth surfaces.

This work was supported by the DFG, Sfb 787, TP A2 and A4.

[1] Lenz et al. J. Vac. Sci. Technol. B **29**, 04D104 (2011).

Individual iso-electronic N and Bi centers in GaAs studied by Scanning Tunneling Microscopy

C.M. Krammel[1], R.C. Plantenga[1], V. Kortan[2], M.E. Flatté[2], F.J. Tilly[3], M. Roy[3],
P. A. Maksym[3], J.M. Ulloa[4], T. Kita[5], and P.M. Koenraad[1]

1 Eindhoven University of Technology, Eindhoven, The Netherlands
2 University of Iowa, Iowa City, United States of America
3 University of Leicester, Leicester, United Kingdom
4 Universidad Politécnica de Madrid, Madrid, Spain
5 Kobe University, Kobe, Japan

Nitrogen and bismuth iso-electronic doping centers in GaAs have received considerable interest in the last few years due to their peculiar behavior in dilute nitrides and bismides. In these materials effects such as a strong band bowing (i.e. the a band gap narrowing for low concentrations of nitrogen or antimony) and the formation of resonant states in respectively the conduction and valence band have been reported. This behavior is intimately related with the strong local modification of the lattice around these centers which is due to the fact that their ionic radii differ strongly from that of the As atom they replace. In this contribution we will report our exploration of individual nitrogen and bismuth atoms in the outermost layers of a freshly cleaved (110) GaAs surface by Scanning Tunneling Microscopy. Depending on the tunnel conditions we are able to either visualize the lattice distortion around these centers or image the charge distribution of the resonant state.

We clearly observe that nitrogen pulls its neighboring atoms inwards whereas bismuth pushes its neighboring atoms away. A straightforward geometrical model based on the covalent radii of the dopants and substrate atoms is successfully used to interpret the topographic contrast (crystal deformation) seen in our STM images of nitrogen and bismuth under the appropriate tunnel conditions. This analysis is extended by a comparison of experimental and theoretical STM images, calculated using density functional theory (DFT), for all iso-electronic group III and V dopants on the GaAs (110) surface. We find a good agreement with STM measurements performed on column III and V iso-electronic centers that have been reported in the literature. Our voltage dependent images showed that at small positive voltages we could observe the charge distribution of the resonant state induced by iso-electronic nitrogen atoms in GaAs. Tight Binding Modeling (TBM) was used to explain the observed strongly anisotropic charge distribution. Finally we show that short-range correlations occur in the spatial distribution of bismuth atoms in GaAs. a behavior that we did not observe in dilute nitrides. At the moment we have not identified the mechanism that drives the observed clustering in dilute bismides

Monday Morning

Energy II

Mo1110 Invited

Advanced Research Projects Agency-Energy: Innovation for Impact

Ellen D. Williams
Director of ARPA-E

The Advanced Research Projects Agency – Energy (ARPA-E) is tasked to overcome long-term and high-risk technological barriers in the development of energy technologies. To do so, ARPA-E funds projects with the potential to accelerate break-through technical approaches toward practical applications in reducing US dependence on energy imports, Improving energy efficiency, and reducing energy emissions, including greenhouse gases. ARPA-E has developed a unique program management approach that closely couples technical milestones with commercialization milestones.

ARPA-E's program portfolio includes alternative transportation fuels, energy storage (both vehicular and stationary), low-carbon power, modernization of the electric power grid, and efficiency in buildings, transportation, manufacturing and power generation. Developing and applying advanced materials is an essential component of many of ARPA-E's programs.

The presentation will use program and project examples to illustrate ARPA-E's program development process, and the successful evolution of projects from concept to prototype demonstration.

Mo1150

Interfacial and Photocatalytic Properties of Zinc Oxide/Gold Nanoparticle Heterostructures

Ilyas Unlu, Yiwen Wang, James E. Whitten*
Department of Chemistry, The University of Massachusetts Lowell
Lowell, MA 01854

Abstract

Zinc oxide nanorods (ZnO-NRs) have been decorated with gold nanoparticles (AuNPs) by stirring them with octanethiol-protected gold nanoparticles in the presence of dithiol ligands and subsequently filtering, washing and drying the resulting heterostructure nanocomposite. The formation of the nanocomposite is facilitated by the affinity of thiols for both gold and zinc oxide. Attachment to the AuNPs occurs via a ligand place exchange reaction, and bonding to the ZnO-NRs results from Zn-S covalent bond formation. The ligands were removed by annealing the nanocomposite at 300-450^{o}C, and the optical and electronic properties were evaluated using diffuse reflectance spectroscopy and fluorescence measurements.

Photocatalytic properties of the nanocomposites were evaluated at various wavelengths and compared to undecorated ZnO-NRs by measuring the oxidative decomposition of aqueous rhodamine B and methyl paraoxon dissolved in methanol as a function of light exposure time. The AuNP-decorated ZnO-NRs were found to perform better than undecorated ZnO-NRs, and it was postulated that the enhanced performance is due to slower electron-hole recombination rates.

Toward the goal of understanding the interface between gold nanoparticles and zinc oxide nanorods, fundamental studies on well-defined surfaces have been performed. Gold has been deposited in ultrahigh vacuum onto sputter-cleaned ZnO(0001) single crystals, with its growth followed with X-ray photoelectron spectroscopy. The evolution of the electronic structure of the interface has been studied as a function of gold coverage. The energies of the filled and unfilled electronic states have been measured using ultraviolet photoelectron and inverse photoelectron spectroscopies, respectively. The relevance of these measurements to the photocatalytic performance is discussed.

Magnesium hydride film formation using a sub-atmospheric hydrogen pressure plasma at low temperature

Hiromasa Ohmi, Naoya Masuya, Takahiro Hori, Kakiuchi Hiroaki, and Kiyoshi Yasutake
2-1 Yamadaoka, Suita, Osaka, 565-0871, Japan
Department of Precision Science and Technology, Osaka University
+81-6-6879-7270, ohmi@prec.eng.osaka-u.ac.jp

In recent year, magnesium hydride (MgH_2) has drawn strong attention as hydrogen storage alloys because of resource abundance and relatively large storage capacities (7.6 wt% and 0.11 g/cc). However, since Mg has a low chemical activity to hydrogenation reaction, long hydrogenation time, high temperature, and high hydrogen pressure are necessary for MgH_2 preparation. In steads of increasing the hydrogen pressure with consuming the energy, the utilization of hydrogen plasma is considered to be alternative method to progress the hydrogenation reaction. Furthermore, if the Mg atoms are evaporated into hydrogen plasma, the efficient hydrogenation can be occurred without diffusion-limit reaction.

Recently, we have prepared the hydrogenated Si film by using a chemical transport technique in sub-atmospheric pressure hydrogen plasma. In this plasma, high density atomic hydrogen reaching to 10^{16} atoms/cc can be obtained at relatively low gas temperature. In this study, we attempt to synthesize the MgH_2 film at less than normal pressure by using the sub-atmospheric pressure hydrogen plasma.

In the MgH_2 synthesis experiment, the source Mg metal was put on the electrically grounded susceptor. The susceptor is equipped with electronic resistance heater to control the source temperature (T_{so}). Si plate was used for the substrate to collect the prepared MgH_2 sample. This Si plate was attached to the water-cooled electrode. The sub atmospheric pressure plasma was generated in the plasma gap between Si plate and Mg cube by capacitive coupled plasma. The plasma driven frequency and plasma gap were 150MHz and 2mm, respectively. Total pressure, T_{so}, input plasma power, and plasma exposure time are varied as experimental parameter. The obtained samples on Si plate were weighed to evaluate the transport rate from source to substrate and their structure and purity were evaluated by X-ray diffraction (XRD) and scanning electron microscopy. The hydrogen desorption behavior from the prepared sample was evaluated by thermal desorption spectroscopy. Optical emission spectroscopy of the plasma was also conducted.

As a result, the prepared MgH_2 contained a metallic Mg as impurity. The purity of the prepared MgH_2 strongly depends on the total process pressure, though it is independent on the hydrogen partial pressure at constant total pressure of 200 Torr. The MgH_2 purity and Mg transport rate (R_d) degrade with increasing the total pressure from 100 Torr to 400 Torr. Furthermore, the MgH_2 purity also degrades and the R_d increases exponentially with increasing T_{so}. This seems to be due to the excess Mg atom, which is thermally evaporated, in the plasma gas phase. In contrast, the MgH_2 purity has a little dependence on the plasma input power. The crystallite size was about 30 nm. Furthermore, the prepared MgH_2 film on Si (001) substrate showed the columnar structure preferentially oriented to (200) or (211) planes by decreasing the transport rate. By optimizing a synthesis parameter, the high-purity MgH_2, which is comparable to commercial high-purity MgH_2, can be obtained with a reasonable process time at T_{so} of 300°C and process pressure of 200 Torr.

Abstract Submission, PCSI: 43rd Conference on the Physics and Chemistry of Surfaces and Interfaces

Leah Weiss, PhD Student, Cambridge University (Supervisor: Prof. Sir Richard Friend)
Cavendish Laboratories, Optoelectronics Group
Gates Cambridge Scholar, Winton Scholar for the Physics of Sustainability

Ultrafast Multipass Transient Absorption Spectroscopy of Interfacial Excitonic Dynamics of Organic-Inorganic Heterojunctions: Harnessing Triplet Excitons in Organic Semiconductors via Colloidal Quantum Dots

Recent studies have exhibited the potential for harnessing spin-1 dark triplet excitons via transfer to emissive lead-chalcogenide colloidal quantum dots [1,2]. This process has potential application to solar energy harvesting via singlet exciton fission and LED technology in hybrid phosphorescent organic light emitting diodes. The reverse process of triplet injection from inorganic mixed excitonic spin states into organic systems in triplet-triplet annihilation-based upconversion devices has also proved promising [3,4]. The use of inorganic colloidal quantum dots as either triplet emitters or sensitizers when coupled with organic semiconducting materials promises to allow a greater degree of tunability due to the size-controlled electronic structure of colloidal quantum dots. Using ultrafast cavity-enhanced multi-pass transient absorption spectroscopy and time-resolved photoluminescence spectroscopy we studied the dynamics of charge carriers and triplet excitons at the sub-monolayer interface between pentacene —a canonical small molecular organic semiconductor— and PbSe colloidal quantum dots to understand the underlying factors that determine the rates and efficiencies of these two processes. We determine that there is an asymmetry in time dynamics between triplet injection and collection and delineate its dependence on quantum dot bandgap, choice of ligand, and excitation. The resulting kinetics points to the critical interplay of the asymmetric density of states between the organic and inorganic systems and the importance of energetics in defining a fundamental efficiency limit of the process of triplet injection from quantum dot systems to organic semiconducting surfaces.

[1] Thompson, Nicholas J., et al. "Energy harvesting of non-emissive triplet excitons in tetracene by emissive PbS nanocrystals." Nature materials (2014).
[2] Tabachnyk, Maxim, et al. "Resonant energy transfer of triplet excitons from pentacene to PbSe nanocrystals." Nature materials (2014).
[3] Huang, Zhiyuan, et al. "Nanocrystal size and quantum yield in the upconversion of green to violet light with CdSe and anthracene derivatives." Chemistry of Materials (2015).
[4] Huang, Zhiyuan, et al. "Hybrid Molecule–Nanocrystal Photon Upconversion Across the Visible and Near-Infrared." Nano letters 15.8 (2015): 5552-5557.

Monday Afternoon

Oxides I

Mo1400 Invited

Bipolar Oxide Diodes:
Role of the Interface for Type-I, -II and -III Heterostructures

Marius Grundmann
Universität Leipzig, Institut für Experimentelle Physik II
Linnéstr. 5, 04103 Leipzig, Germany

Our recent advances in highly rectifying all-oxide ZnO/$ZnCo_2O_4$ and ZnO/NiO pn-diodes [1,2] allow the fabrication of JFET's (junction field effect transistors) with bipolar gates [3,4] and high-gain inverters based on such transistors [5]. Also highly rectifying all-amorphous bipolar zinc-tin-oxide/zinc-cobalt-oxide diodes have been reported by us [6]. We discuss the electrical characteristics of these bipolar oxide diodes in terms of their heterostructure band line-up which covers type-I, type-II and also type-III for CdO/NiO diodes [7].

This work is in cooperation with F.-L. Schein, P. Schlupp, R. Karsthof, F. Klüpfel and H. von Wenckstern. We acknowledge financial support of Deutsche Forschungsgemeinschaft (DFG) in the framework of SFB 762 "Functionality of Oxidic Interfaces" and projects Gr 1011/27-1, Gr1011/30-1 and ESF (SAB 100124929) and Sächsische Aufbaubank (SAB 100112104).

References:
[1] F.-L. Schein, M. Winter, T. Böntgen, H. von Wenckstern, M. Grundmann, *Highly rectifying p-$ZnCo_2O_4$/n-ZnO heterojunction diodes*, Appl. Phys. Lett. **104**, 022104 (2014)
[2] M. Grundmann, R. Karsthof, H. von Wenckstern, *Interface Recombination Current in Type II Heterostructure Bipolar Diodes*, ACS Appl. Mat. Interfaces **6**(17), 14785 (2014)
[3] F.-L. Schein, H. von Wenckstern, H. Frenzel, M. Grundmann, *ZnO-based n-channel junction field-effect transistor with room-temperature fabricated p-type $ZnCo_2O_4$-gate*, IEEE Electron Device Letters **33**, 676 (2012)
[4] R. Karsthof, H. von Wenckstern, M. Grundmann, *Transparent JFETs based on p-NiO/n-ZnO heterojunctions*, IEEE Transact. Electr. Dev., *published online* (2015), doi: 10.1109/TED.2015.2490555
[5] F.J. Klüpfel, A. Holtz, F.-L. Schein, H. von Wenckstern, M. Grundmann, *All-Oxide Inverters Based On ZnO channel JFETs with amorphous $ZnCo_2O_4$ gates*, IEEE Transact. Electr. Dev., *published online* (2015), doi: 10.1109/TED.2015.2493361
[6] P. Schlupp, F.-L. Schein, H. von Wenckstern, M. Grundmann, *All Amorphous Oxide Bipolar Heterojunction Diodes from Abundant Metals*, Adv. Electr. Mater. **1**, 1400023 (2015)
[7] R. Karsthof, M. Grundmann, H. von Wenckstern, J. Zuniga-Perez, unpublished

Electrical properties of ZnO:Ga/substrate interfaces: bad, good, and fantastic

D. C. Look[1,2,3]
[1]Semiconductor Research Center, Wright State University, Dayton, OH 45435
[2]Wyle Laboratories, 2602 Mission Point Blvd, Suite 300, Dayton, OH 45431
[3]Air Force Research Laboratory Sensors Directorate, Wright-Patterson AFB, OH 45433
Contact: david.look@wright.edu

Ga-doped ZnO (GZO) is becoming an important transparent conductive oxide (TCO) for solar-cell, display, and LED applications, and may ultimately replace ITO as the most popular TCO material. However, as is the case with any TCO, the GZO/substrate interface quality can influence the electrical properties of the GZO film itself. To quantify this influence, we have earlier introduced phenomenological formulas for sheet concentration n_s and mobility μ that have a fairly general applicability over a wide range of materials: $n_s = n(d - \delta d)$ and $\mu = \mu_\infty/[1 + d^*/(d - \delta d)]$, where n, μ_∞, δd, and d^* are fitting parameters. Here, δd is a "dead-layer" thickness, and d^* is a figure of merit, lower for better interfaces. In some cases, d^* can be given a physical meaning; e.g., $d^* \approx z_0/2$ if μ is degraded by threading dislocations that decrease exponentially from the interface as $\exp[-(d - \delta d)/z_0]$. For GZO on glass, sapphire, and Si, representative values of δd and d^* are 10 and 25 nm, respectively. The use of buffer layers can help considerably; e.g., a ZnON buffer layer in a GZO/ZnON/glass structure, introduced by N. Itagaki and co-workers, can reduce d^* from 23 to ~ 7 nm, and for GZO/bulk-ZnO homoepitaxial structures, we have shown that a low d^* of ~ 3 nm can be achieved. These results indicate that the interface can have an important influence on μ, and in virtually all cases, μ decreases as d decreases. Thus, we were recently surprised to find an exception to this rule in MBE-grown GZO/ZnO/GaN structures from the group of C.C. Yang. For those layers, μ actually *increased* as d_{GZO} decreased. Indeed, for $d_{GZO} = 300$ nm, $\mu_{Hall} = 34$, whereas for $d_{GZO} = 5$ nm, $\mu_{Hall} = 64$ cm^2/V-s. It turns out that this phenomenon is due to "Debye leakage", i.e., the thermodynamically driven transfer of electrons from the GZO to the ZnO buffer layer. Poisson theory shows that for the measured $n_{GZO} = 8.5 \times 10^{20}$ cm^{-3}, about 10% of the electrons in a 5-nm GZO layer will transfer to the ZnO, and scattering theory shows that the ZnO mobility immediately across the interface will be very large, about 206 cm^2/V-s, due to the lower concentration of scattering centers in the ZnO and also the strong screening activity of the transferred electrons. At 2 nm from the interface, theory predicts that μ_{ZnO} will fall sharply to 58 cm^2/V-s, but still the Hall-averaged theoretical mobility over the entire GZO/ZnO structure is 57 cm^2/V-s. (Although this is a little lower than the experimental value of 64 cm^2/V-s, it must be noted that the theory has no adjustable parameters.) More complicated structures can also be theoretically analyzed and, if promising, grown. For example, the hypothetical structure 1-nm-GZO/2-nm-ZnO/6 repeats, would have 43% of the electrons and 84% of the sheet conductance in the ZnO (i.e., in the Debye tails). The sheet resistance of this 18-nm-thick structure would be 130 Ω/sq, much lower than the 358 Ω/sq for 6 nm of GZO alone (i.e., with no ZnO interlayers). Moreover, this large decrease of sheet resistance comes with no added light absorbance, which presumably comes mainly from the GZO material. Finally, the phenomenon of Debye-tail mobility enhancement should apply to many other semiconductor systems since it is a general thermodynamic principle arising from the much higher Fermi level in the heavily-doped, lower-mobility material that forces electrons into the purer, higher-mobility material.

Mo1520

Defect Redistribution and Mobility Enhancement at Highly Doped/Intrinsic-ZnO Interfaces

G. M. Foster[1], G Faber[2],Y. F. Yao[3], C.C. Yang[3], and L.J. Brillson[1,4]

[1] Department of Physics, The Ohio State University, 191 W. Woodruff Ave., Columbus, OH 43210, USA
[2] Columbus School for Girls, 56 S. Columbia Ave, Columbus, OH 43209, USA
[3]Institute of Photonics and Optoelectronics, National Taiwan University, No. 1, Section 4, Roosevelt Road, Taipei 10617, Taiwan
[4] Department of Electrical & Computer Engineering, The Ohio State University, 205 Dreese Lab, 2015 Neil Ave., Columbus, OH 43210, USA

We used a differential depth resolved cathodoluminescence spectroscopy (DDRCLS) to measure the spatial distribution of native point defects at the gallium-doped ZnO (GZO) interface with undoped ZnO. Free electrons in the degenerately-doped GZO leak into the ZnO where mobility is much higher, producing a high electron density, high mobility channel within a few nanometers of the interface [1]. Significantly, Hall Effect measurements reveal mobilities that vary with GZO overlayer thickness on the ZnO, increasing with decreasing thickness to values higher than the mobility of the buffer ZnO (64.1 vs. 41.2 cm^2/Vs). For the same MBE-grown GZO sample on ZnO/GaN/sapphire, incident electron beams with energies E_B = 0.5 -5 keV generated electron-hole (e-h) pairs that recombined to exhibit DRCLS spectra with 3.5 – 3 eV filled conduction band-to-valence band transitions in GZO, 3.27 eV intrinsic band gap transitions in ZnO, and 1.8 eV V_{Zn} transitions in both GZO and ZnO. V_{Zn} become increasingly more stable thermodynamically as Fermi level rises in highly doped GZO, acting to compensate electron densities [2]. DDRCLS enabled us to profile the deconvolved V_{Zn} density across the GZO/ZnO interface on a nm scale as defined by Monte Carlo simulations of electron-hole (e-h) pair creation rate vs. depth by subtracting out contributions from shallower recombination of e-h pairs [3]. This unique defect depth precision revealed monolayer abrupt interfaces with V_{Zn} profiles that extended from GZO into the ZnO and that varied with GZO overlayer thickness for specimens 300, 50, 25, and 5 nm. Profile widths decreased from *ca*. 25 nm to 5 nm between 50 nm vs. 5 nm, respectively, two to the three times the calculated ZnO Debye lengths.

The variation of V_{Zn} density and penetration into ZnO is significant since native defects act as scattering centers that reduce free carrier mobility. The decreasing V_{Zn} density and depth with decreasing GZO overlayer thickness can account for the increasing mobility observed. Both interface electric field gradients and epitaxial growth conditions may influence this systematics. These results suggest that ultrathin GZO/ZnO superlattices may yield high electron density, high mobility structures for high speed electronics. The authors gratefully acknowledge support from National Science Foundation Grant No. DMR-1305193 (Charles Ying and HaiyanWang).

1. D.C. Look, E.R. Heller, Y.-F. Yao, and C.C. Yang, "Significant mobility enhancement in extremely thin high doped ZnO films," Appl. Phys. Lett. **106**, 152102 (2015).
2. D.C. Look, K.D. Leedy, L. Vines, B.G. Svensson, A. Zubiaga, F. Tuomisto, D.R. Doutt, and L.J. Brillson, "Self-compensation in semiconductors: the Zn-vacancy in Ga-doped ZnO," Phys. Rev. B **84**, 115202 (2011).
[3] T.J. Asel, H. Gao, T.J. Heinl, D. Adkins, P.M. Woodward, J. Hoffman, A. Bhattacharya, and L.J. Brillson, "Near-nanoscale-resolved energy band structure of $LaNiO_3/La_{2/3}Sr_{1/3}MnO_3/SrTiO_3$ heterostructures and their interfaces" J. Vac. Sci. Technol. B **33**, 04E103 (2015).

Mo1525

Effect of Ti sub-oxide layers on the switching properties of ZnO-based ReRAM cells

Ju Hyun Park[1], Kyung Rock Son[1], Tae Geun Kim[1]

[1]School of Electrical Engineering, Korea University, Anam-dong 5-ga, Sungbuk-gu, Seoul 136-701, Republic of Korea, tgkim1@korea.ac.kr

Resistive random access memory (ReRAM) has attracted great interest for application in the next-generation nonvolatile memory because of many advantages such as low power consumption, simple structure, fast operation speed, long retention and excellent endurance. Because of these advantages, various oxide-based materials, such as HfO_2, NiO, ZrO_2, ZnO and TiO_2 have been studied for ReRAM device. Among these materials, ZnO-based film is of particular interest because of its excellent switching and reliability behavior as well as high transparency [1]. However, there are several issues (i.e., improved uniformity in operating voltage/current, and the reliability) that should be solved for its practical ReRAM application. To overcome these problems, we need to control the randomness of the filament formed across the electrodes, and as a solution, additional thin films that can help to localize the position of filaments path, have been added to the switching layer [2].

In this work, we report an efficient way to minimize the distribution in switching parameters by inserting two different Ti sub-oxide layers between ZnO and top electrode, respectively. When compared to Pt/Ti/ZnO /Pt structures, the switching operation was more reproducible and reset process more accurately occurred in Pt/TiO_x (or TiO_y) /ZnO/Pt devices because TiO_x and TiO_y layers could serve as oxygen reservoirs to rupture conducting filament. We also analyzed the Ti sub-oxide films using an x-ray photoelectron spectroscopy. Consequently, our proposed ReRAM structure exhibited better uniformity in the electrical property, and Ti sub-oxide films played an important role in terms of reliability by supplying the oxygen ions during the reset process.

[1] M. C. Chen, T. C. Chang, C. T. Tsai, S. Y. Hung, S. C. Chen, C. W. Hu, M. S. Simon and M. J. Tsai, Appl. Phys. Lett. 96, 262110, (2010).

[2] X. Liu, S. M. Sadaf, S. Kim, K. P. Biju, X. Cao, M. Son, S. H. Choudhury, G. Y. Jung, and H. Hwang, ECS Solid State Lett. 1, no. 5, Q35-Q38, (2012).

Monday Afternoon

Spintronics I

Mo1630 Invited

A study of the topological effect in artificial magnetic Skyrmions

Z. Q. Qiu, Dept. of Physics, Univ. of California at Berkeley,
Berkeley, CA 94720

A magnetic Skyrmion is a topological twist of two-dimensional spin texture which exhibits many fascinating properties. In experiment, magnetic Skyrmions were realized in 2009 in several experimental systems as a result of Dzyaloshinsky-Moriya interactions (DMI). However, the Sykyrmion phase in these materials usually exists in a limited region in the phase diagram. With the motivation that non-collinear spins also exist in magnetic vortex disks, we fabricated single crystalline Co circular disks on perpendicularly magnetized Ni/Cu(001) film to create artificial Skyrmions. These artificial magnetic Skyrmions exist at room temperature with their topology easily controled by changing the relative orientation between the vortex core polarity and the surrounding perpendicular magnetization. In this way, we studied the topological effect of the artificial Skyrmions using Photoemission Electron Microscopy (PEEM). By applying an in-plane magnetic field of various strength, we find strong evidence that the annihilation of the vortex core depends on the topological Skyrmion number of the system.

Mo1710

Theory for the coherent detection of interfacial defects

Nicholas J. Harmon and Michael E. Flatté
[1]*Department of Physics and Astronomy and Optical Science and Technology Center, University of Iowa, Iowa City, Iowa 52242, USA*

Defects in semiconductors and insulators can either erode or enhance desired properties. In either case detailed knowledge of defect states is vital to understanding and controlling a material's electronic and optical properties. Characterizing defects at magnet/non-magnet interfaces has become increasingly important in recent years due to interests in spin pumping and thermal spin physics such as the spin Seebeck effect. It has recently been recorded that defects in interface barriers between contacts can be especially important for transport due to the defect acting as an intermediary step for charge current [1]. Contemporary measurements of defects exist but require measurements of defect chains as opposed to a single one [2].

We propose extending three terminal measurements into a coherent regime through which single or small numbers of defects are precisely detected by their local fields even at room temperature. The setup involves the defects being situated between small non-magnetic (NM) and ferromagnetic (FM) contacts under a bias; one advantage over other techniques is that no ESR cavity is required. The FM magnetization is driven periodically around some axis (see upper Figure). Due to the large exchange interaction, the ability for a spin at the defect site to enter the FM is dependent on the spin and FM's relative orientation. Fields, which are likely hyperfine, local to the defect play a role in determining this relative orientation and it is through this relationship that the defect spin environment can be studied via changes in charge current. As long as the axis of the FM rotation is non-collinear with the defect's local field, some portion of the spin will be maintained anti-parallel to the AC magnetization at the resonant precessing frequency. Hence, a dip in current is expected when the AC frequency is equal to the local field. The lower Figure shows the resonance for charge current through two independent defects.

We find that a rich physics extends also into the DC realm where spin may accumulate on the defect as well as in the NM. Lastly we explore the defect-FM system as a means of preparing and reading nuclear spin states.

This work is supported by the Center for Emergent Materials, an NSF MRSEC under award number DMR-1420451.

[1] H. Inoue, A. G. Swartz, N. J. Harmon, M. E. Flatté, T. Tachikawa, Y. Hikita, and H. Y. Hwang, "Origin of the magnetoresistance in oxide tunnel junctions determined through electric polarization control of the interface". Accepted into Phys. Rev. X.
[2] C. J. Cochrane and P. M. Lenahan, "Spin counting in electrically detected magnetic resonance via low-field defect state mixing", Applied Physics Letters **104**, 093503 (2014).

Mo1715

Long-lived Spin Relaxation and Spin Coherence of Electrons in Monolayer MoS_2

Luyi Yang[1], Nikolai A. Sinitsyn[2], Weibing Chen[3], Jiangtan Yuan[3], Jing Zhang[3],
Kathleen M. McCreary[4], Berend T. Jonker[4], Jun Lou[3] & Scott A. Crooker[1]
[1]National High Magnetic Field Laboratory, Los Alamos, NM 87545, USA; [2]Theoretical Division, Los Alamos National Laboratory, [3]Department of Materials Science and NanoEngineering, Rice University, Houston, TX 77005, USA.; [4]Materials Science and Technology Division, Naval Research Laboratory, Washington, DC 20375, USA.

Monolayer MoS_2 and related atomically-thin transition metal dichalcogenides (TMDs) are analogous to graphene in that they are 2D materials with hexagonal structure, but with an extremely important difference: TMDs possess a semiconductor bandgap. This makes TMDs useful for a variety of opto-electronic applications, including solar applications, light-emitting diodes, and semiconductor electronics, spintronics, and valleytronics. Although robust spin and valley degrees of freedom have been inferred from polarized photoluminescence (PL) studies of *excitons*, PL timescales are necessarily constrained by short-lived (3–100 ps) electron–hole recombination. Direct probes of spin/valley polarization dynamics of *resident* carriers in electron (or hole)-doped TMDs, which may persist long after recombination ceases, are at an early stage.

Here we directly probe the coupled spin and valley dynamics in electron-doped monolayer MoS_2 using techniques based on time-resolved Kerr rotation spectroscopy (see Fig. 1) [1]. In contrast to PL studies, these techniques *directly* probe the spin and valley polarizations of electrons alone (rather than excitons), which can persist long after any recombination with photoexcited holes. Using these Kerr-effect methods, we directly and unambiguously measure very long intrinsic electron spin relaxation timescales of 3 ns at zero field (Fig. 2a), which is 2-3 orders of magnitude longer than the exciton recombination time. Crucially, the polarization decay time decreases rapidly with small applied transverse magnetic fields B_y, and no prominent spin precession is observed, indicating that electrons 'see' a strong effective magnetic field due to the large spin-orbit coupling in these 2D materials, and that electrons undergo rapid *K-K'* intervalley scattering [1].

Additionally, a small but very long-lived oscillatory signal commensurate with *g*-factor $|g_0| \simeq 1.86$ is also observed (Fig. 2a & 2b) in some CVD-grown MoS_2 monolayers [2]. This signal, which is not expected from itinerant resident electrons for the reasons just described, likely arises from localized electron states that are not subject to intervalley scattering and which precess only about the bare applied field B_y. The dephasing rate of this oscillatory signal increases linearly with magnetic field (Fig. 2c), suggesting that the coherence arise from a sub-ensemble of localized electron spins having an inhomogeneously-broadened distribution of *g*-factors [2]. These studies provide direct insight into the intrinsic physics underpinning spin and valley dynamics of resident electrons in TMDCs.

[1] L. Yang *et al.*, *Nature Physics* **11**, 830-834 (2015).
[2] L. Yang *et al.*, submitted (2015).

Mo1720 Invited

Co_2MnSi Half-Metal Magnetic character studied by Spin-Resolved PhotoEmission Spectroscopy and FerroMagnetic Resonance

Stéphane Andrieu*(1), Amina Neggache (1), Thomas Hauet (1), Thibaut Devolder (2), Ali Hallal (3) ,Mairbek Cschiev (3) , Alexandre Bataille (4), Patrick Le Fèvre (5), Francois Bertran (5)

1 Institut Jean Lamour, CNRS / Université de Lorraine-, F-54506 Vandoeuvre cedex, France
2 Institut d'Electronique fondamentale, CNRS / Université Paris Saclay, 91405 Orsay France
3 SPINTEC, CEA/CNRS/UJF/Grenoble INP, 38054 Grenoble Cedex, France
4 IRAMIS/LLB, CEA/Saclay, 91191 Gif-Sur-Yvette, France
5 Synchrotron SOLEIL-CNRS, L'Orme des Merisiers, 91192 Gif-sur-Yvette Cedex, France

Half Metal Magnets (HMM) are of great interest in the field of spintronics because of their lack of density of states at the Fermi energy for minority spin. In other words, an HMM material is a metal for majority spins and an insulator for minority spins. Such properties lead to full spin-polarization at the Fermi energy and low magnetization damping. Theoreticians evidenced that some magnetic ternary alloys belonging to the Heusler alloys family can got this HMM behavior [1]. The HMM property was thus claimed for many Heusler alloys thin layers in order to explain transport properties, despite any direct proof of the existence of the spin gap. Moreover, the transport properties of devices using many Heusler alloys were often deceiving. There was renewed interest after large magnetoresistance was obtained in Co_2MnSi/MgO-based Magnetic Tunnel Junctions [2] [3]. High spin polarization was observed very recently on this material using spin-resolved photoemission experiments [4]. This has to be however confirmed for other photon energies to investigate some possible resonant surface state. Moreover, it is essential to assess whether this property persists when covering the surface with MgO and whether the material has also a low magnetic damping.

The half-metallic magnetic character of the Co_2MnSi Heusler alloy is here examined using spin-resolved photoemission and ferromagnetic resonance [5]. In the case of an uncoated surface, a gap in the minority spin channel is actually observed, leading to 100% spin polarization. However, this gap is observed at -0.3 eV below the Fermi level, the polarization becoming even negative at E_F (see figure). This is observed to come from a minority spin states located at E_F. This means that the bare surface is not HMM, contrary to what was claimed before [4]. However, these states can be pushed above from E_F by changing the stoichiometry of the alloy and our study nicely explains magneto-transport results in the literature [6]. We also show that these states are suppressed by covering the surface by Mn, MnSi or MgO, the spin gap then extending to the Fermi level. Magnetic damping coefficients of the order of 10^{-3} were observed with a record value equal to 7.10^{-4}, to our knowledge the lowest damping value ever measured on a conducting film.

[1] see for instance Galanakis, I., Mavropoulos, P., J. Phys. Cond. Mat., 19, 315213 (2007).
[2] Ishikawa T. et al, Appl. Phys. Lett., 95, 232512 (2009).
[3] Liu, H.X., et al. Appl. Phys. Lett., 101, 132418 (2012).
[4] Jourdan, M. et al. Nature Commun., 5, 4974 (2014).
[5] Andrieu,S et al, (2015) submitted to Nat. Mat.
[6] Ishikawa *et al*, Appl. Phys. Lett., 95, 232512 (2009).

Mo1800

Ultrafast Study of Dynamic interfacial Exchange Coupling in Ferromagnet/Oxide/Semiconductor Heterostructures.

Yu-Sheng Ou[1], Yi-Hsin Chiu[1], N. J. Harmon[2], Patrick Odenthal[3], Matthew Sheffield[1], Michael Chilcote[1], R. K. Kawakami[1,3], M. E. Flatté[2], E. Johnston-Halperin[1]

1. Department of Physics, The Ohio State University, Columbus, OH; 2. Department of Physics & Astronomy, The University of Iowa, Iowa City, IA; 3. Department of Physics & Astronomy, University of California, Riverside, CA

Time-resolved Kerr/Faraday rotation (TRKR/TRFR) is used to investigate GaAs spin dynamics in the regime of strong and dynamic exchange coupling to an adjacent Fe layer. This study reveals a dramatic, resonant suppression in the inhomogeneous spin dephasing time (T_2^*) in the GaAs layer. Further investigation of the magnetization dynamics of the neighboring Fe layer, also using TRKR/TRFR, reveals not only the expected Kittel-dispersion but also additional lower frequency modes with very short lifetime (~65 ps) that are not easily observed with conventional ferromagnetic resonance (FMR) techniques. These results suggest the intriguing possibility of resonant dynamic spin transfer between the two spin systems. We discuss the potential for this work to establish GaAs spin dynamics as an efficient detector of spin dissipation and transport in the regime of dynamically-driven spin injection in ferromagnet/semiconductor heterostructures.

Monday Evening

Complex Oxides

Mo1930 Invited

Noncentrosymmetric Metals: A New Materials Class for Artificial Multiferroic Design

James M. Rondinelli
Northwestern University, Department of Materials Science and Engineering, Evanston, IL, 60208, USA
jrondinelli@northwestern.edu

The metallic features in materials, which provide low-resistance channels for electrical conduction, lead to effective screening of local electric dipole moments. Itinerant electrons disfavor both dipole formation and cooperative ordering. Consequently, most metals with a finite density of states and partial band occupation exhibit centric (inversion symmetric) crystal structures. Despite this contraindication, noncentrosymmetric metals (NCSM) lacking inversion were proposed more than fifty years ago with some examples discovered serendipitously later [1]. In the first part of the talk, I describe a design framework to alleviate such property disparities and accelerate NCSM discovery: The primary ingredient relies on the removal of inversion symmetry through displacements of atoms whose electronic degrees of freedom are decoupled from the states at the Fermi level. Density functional theory calculations validate our crystal-chemistry strategy, and predict a polar-NCS perovskite ruthenate superlattice to be metallic and robust to spin-orbit interactions [2]. Next, I discuss a superlattice composed on the polar metal $\mathrm{LiOsO_3}$ that shares a similar electronic configuration [3], *i.e.*, half-filled Os t_{2g} orbitals weak electron-electron interactions that essential to sustaining the metallic state in bulk. I then propose how to turn this non-magnetic polar metal into a multiferroic through the design of a superlattice, which increases the degree of correlation, leading to Mott localization of the Os orbitals [4]. I conclude by summarizing new technology opportunities where noncentrosymmetric metals may serve as an ideal materials platform.

[1] P. W. Anderson and E.I. Blount, "Symmetry Considerations on Martensitic Transformations: 'Ferroelectric' Metals?" *Phys. Rev. Lett* , **14**, 217 (1965).

[2] D. Puggioni, and J. M. Rondinelli, "Designing a robustly metallic noncenstrosymmetric ruthenate oxide with large thermopower anisotropy," *Nat. Commun.*, **5**, 3432 (2014).

[3] Y. Shi *et. al.*, "A ferroelectric-like structural transition in a metal," *Nat. Mater.*, **12**, 1024 (2013).

[4] D. Puggioni, G. Giovannetti, M. Capone, J. M. Rondinelli, "Design of a Mott Multiferroic from a Nonmagnetic Polar Metal," Phys. Rev. Lett., **115**, 087202 (2015).

Frustrated domain formation and charged domain walls in $PbTiO_3/LaNiO_3$ heterostructures with preferential (111) growth

Hye-Jin Jin, Seol Hee Oh, and William Jo*

Department of Physics, Ewha Womans University, Seoul, 120-750, Korea

*E-mail: wmjo@ewha.ac.kr

Domain configurations determine ferroelectric properties and it can be controlled inner structure of the ferroelectric thin films. In particular, direction of polarization can give interesting phenomena in domain dynamics. Domain wall conductivity can be originated depending on arrangement of the polarization. Conductive domain wall is very attractive issues in application of ferroelectric thin films in electronic devices. $PbTiO_3$ is one of the ferroelectric materials which have large polarization values and high Curie temperature. Because of asymmetry along (111) direction induced by tetragonal structure, a variety of polarization arrangements can be achieved. Conducting $LaNiO_3$ as a bottom electrode can induce different ferroelectric behavior by controlling the interface between $PbTiO_3$ and $LaNiO_3$. Phase formation and inner structure of the thin films were obtained by X-ray diffraction patterns and transmission electron microscopy. Local ferroelectric characteristics are investigated by using piezoresponse force microscopy. Domain configurations as well as electrical responses from the domain walls were attained with the method. In addition, conductive atomic force microscopy was also used to describe the conducting properties at domain walls in the thin films. Frustrated configuration of domain formation and conducting states near domain walls are extensively investigated.

Mo2015

Built-in potential in Fe_2O_3-Cr_2O_3 superlattices for improved photoexcited carrier separation

Tiffany C. Kaspar,[1] Dan K. Schreiber,[2] Steven R. Spurgeon,[1] Martin E. McBriarty,[1] Gerard M. Carroll,[3] Daniel R. Gamelin,[3] Scott A. Chambers[1]

[1]Physical Sciences Division, Pacific Northwest National Laboratory, Richland, WA

[2]Energy and Environment Directorate, Pacific Northwest National Laboratory, Richland, WA

[3]Department of Chemistry, University of Washington, Seattle, WA

Hematite, α-Fe_2O_3, is an ideal photocatalyst to split water as a source of H_2 fuel because it is non-toxic, Earth-abundant, stable in aqueous environments, and possesses a bandgap in the visible wavelength range (~2.1 eV). However, fast photogenerated electron-hole recombination, facilitated in part by slow carrier transport kinetics, has long been identified as a major obstacle in the utilization of hematite photocatalysts. A direct method to reduce photogenerated carrier recombination is to employ heterojunctions to spatially separate excited electrons and holes. Our approach is to engineer built-in electric fields by exploiting the band alignment characteristics of epitaxial Fe_2O_3/Cr_2O_3 heterojunctions. The Fe_2O_3-Cr_2O_3 system exhibits non-commutative band offsets which differ by approximately 0.4 eV depending on the order of deposition. The non-commutative band offset properties of Fe_2O_3-Cr_2O_3 interfaces can be utilized in a superlattice structure, deposited by oxide molecular beam epitaxy, to build up an intrinsic electric field; this potential may be sufficient to spatially separate photogenerated electrons and holes. We demonstrate precise control over the Fe_2O_3-Cr_2O_3 interface structure with atomic-resolution atom probe tomography and scanning transmission electron microscopy. Direct evidence that Fe_2O_3-Cr_2O_3 superlattice layers generate an intrinsic built-in potential is observed with x-ray photoelectron spectroscopy. The individual interfacial band offset values, and thus the overall potential, can be tailored by altering the cation stoichiometry at the interfaces. To illustrate how the built-in potential in optimized Fe_2O_3-Cr_2O_3 superlattice structures can be harnessed to drive holes to the surface and electrons into the bulk, photoconductivity results will be presented.

Mo2020

TITLE: Hybrid molecular beam epitaxy for the growth of stoichiometric $BaSnO_3$
CONFERENCE FOCUS AREA: Epitaxial oxide heterostructures
AUTHORS: Abhinav Prakash, John Dewey, and Bharat Jalan
AFFILIATION: Department of Chemical Engineering and Materials Science, University of Minnesota

We will present on the growth of phase-pure, epitaxial $BaSnO_3$ films using a hybrid molecular beam epitaxy (MBE) approach with scalable growth rates [1] (see Fig. 1). In this approach, we use a metal-organic precursor (hexamethylditin) as a tin source, a solid effusion cell for barium and an rf plasma source to supply oxygen. $BaSnO_3$ films were grown on $SrTiO_3$ (001), $LaAlO_3$ (001) and LSAT (001) substrates. The substrate temperature and oxygen pressure were kept fixed at 900 °C and 5×10^{-6} Torr respectively whereas Ba/Sn beam equivalent pressure (BEP) ratio was varied to optimize cation stoichiometry. The unstrained lattice parameter determined using high-resolution X-ray diffraction, and the Rutherford backscattering spectroscopy (RBS) were used to optimize cation stoichiometry. Stoichiometric composition yielded an unstrained lattice parameter value of 4.116 ± 0.001 Å, which is identical to that of bulk $BaSnO_3$. Remarkably, this value was found to increase irrespective of whether films were Ba- or Sn-deficient. Time-dependent reflection high-energy electron diffraction (RHEED) intensity oscillations were observed during film growth indicating films grew in a layer-by-layer fashion (see Fig. 2). The average spacing between 0^{th} order and 1^{st} order diffraction streaks of a time-dependent RHEED pattern recorded during growth were used to investigate the evolution of strain relaxation. A critical thickness of ~ 1 nm for strain relaxation was thus observed for films grown on $SrTiO_3$ (see Fig. 2). Similar to the hybrid MBE of $SrTiO_3$ [2], the use of tin chemical precursor also resulted in a MBE "growth window" where cation stoichiometry was self-regulating, i.e. for a range of Ba/Sn BEP ratio only stoichiometric films grow. Atomic force microscopy confirmed smooth surface morphology for stoichiometric films, with a root mean square roughness value of 1-2 u.c., whereas non-stoichiometric films showed nano-crystallites on film surface indicating a correlation between surface morphology and film stoichiometry. Scanning transmission electron microscopy combined with electron energy-loss spectroscopy and energy dispersive X-ray spectroscopy confirmed the cube-on-cube epitaxy and composition (Fig. 3). Finally, we will also discuss transport properties of these films as a function of cation stoichiometry, film thicknesses and dopant concentrations.

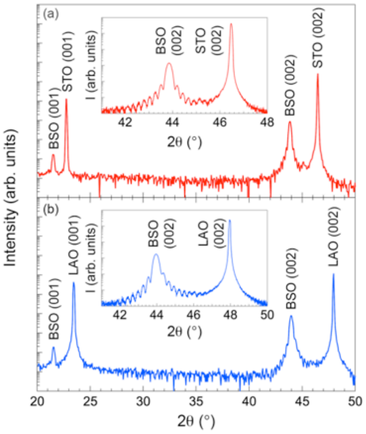

Figure 1: High-resolution X-ray diffraction patterns for films grown on (a) $SrTiO_3$ (001) and (b) $LaAlO_3$ (001) substrates indicating phase-pure, and single crystalline films. Thickness fringes suggest that films are smooth on short lateral length scales.

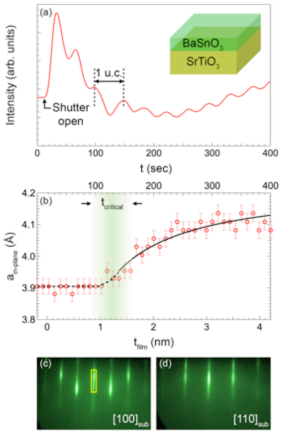

Figure 2: (a) RHEED intensity oscillations showing layer by layer growth mode, (b) variation of in-plane lattice parameter as a function of film thickness, and (c) RHEED patterns after film growth along [100] and [110] azimuth of the substrate.

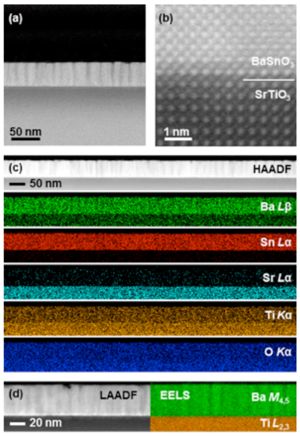

Figure 3: (a) High-angle annular dark field image of a 40 nm thick $BaSnO_3$ on $SrTiO_3$ showing evenly spaced regions of different contrast, (b) atomic resolution images showing cube-on-cube epitaxy, and (c,d,e) EDX and EELS maps confirming phase purity. STEM measurements were performed in collaboration with Prof. Mkhoyan group at UMN.

References:

[1] A. Prakash, J. Dewey, H. Yun, J.S. Jeong, K.A. Mkhoyan, and B. Jalan, "Hybrid molecular beam epitaxy for growth of stoichiometric $BaSnO_3$", J. Vac. Sci. Technol. A, **accepted** (2015).

[2] B. Jalan, P. Moetakef, and S. Stemmer, "Molecular beam epitaxy of $SrTiO_3$ with a growth window," Appl. Phys. Lett. **95**, 032906 (2009).

Mo2025

Structural and Optical properties of $SrTiO_3$ thin films on Semiconductors

Nuwanjula Samarasingha,[1] **Cesar Rodriguez**[1] **,** Jaime Moya,[1] Stefan Zollner,[1] Nalin Fernando,[1]

Sudeshna Chattopadhyay,[2] Patrick Ponath,[3] A.A.Demkov[3]

[1] New Mexico State University
[2] Indian Institute of Technology Indore
[3]University of Texas at Austin

$SrTiO_3$ (STO) films were grown epitaxially by molecular beam epitaxy (MBE) on different semiconductor substrates (Si, Ge, STO). STO is a perovskite and has drawn much attention due to its wide range of applications in microelectronics. X-ray diffraction (XRD) and X-ray reflectivity (XRR) were used to characterize the structural properties of STO on Si, Ge and STO. The lattice constant and strain were obtained using high resolution X-ray diffraction with two types of scans (ω and ω-2θ). Most technological applications require thin films of definite thickness with a known density/depth profile. Hence, determination of film thickness and corresponding density profile is very crucial for these technologies. Using a simulation (theoretical model based on Parratt formalism) of the X-ray reflectivity pattern, a highly accurate measurement of thickness, roughness and electron density profile can be obtained. X-ray reflectivity data indicate that the $SrTiO_3$ thin film on Si thickness is approximately 17 nm with 2.9 nm SiO_2 layer with a constant electron density. Also, the $SrTiO_3$ thin film on Ge thickness is approximately 16 nm with 3 nm GeO_2 layer with a varying electron density . According to our X-ray reflectivity results, it can be clearly seen that the electron density values of STO films depends on the choice of substrate. The optical constants of our STO films were studied using variable angle spectroscopic ellipsometry. This technique allowed us to study the films using a broad energy range of 0.76 - 6.6 eV, at a range of incident angles from 65, 70 and 75 degrees. We used a parametric oscillator model to fit the data of the STO films and added a Lorentzian term to fit the region near the IR. After obtaining a reasonably good fit for our data we determined the thickness of each film from which we then extracted the optical constants epsilon (dielectric function) and the absorption coefficient. The thickness for each film obtained from XRR and spectroscopic ellipsometry agree very well with each other which gives us confidence our results are correct. From these results we compared the behavior of the dielectric function of STO on a chosen substrate to that of bulk STO. The critical point amplitudes at 3.8, 4.2, 4.6 and 6.2 eV have been dampened and became much broader which was expected for our thin films (less than 200 Angstroms).

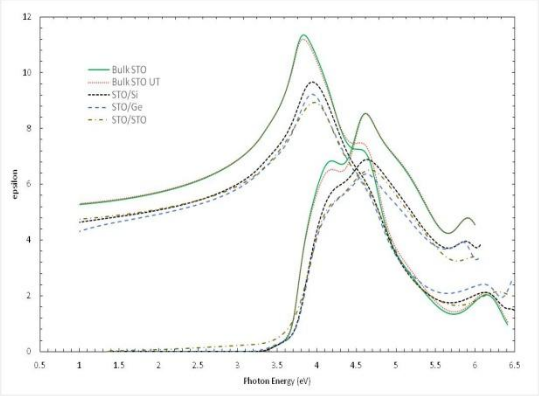

Figure 1: Comparison of the dielectric function of STO films on various substrates compared to that of bulk STO.

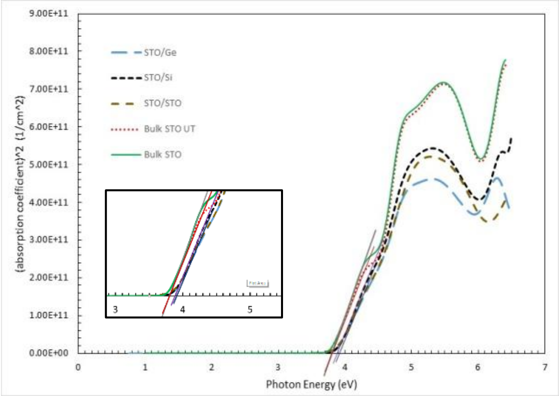

Figure 2: The absorption coefficient squared was plotted versus photon energy to approximate our direct band gap.

Tunneling spectroscopy in interface engineered metal/$SrTiO_3$ junctions

H. Inoue[1], A. G. Swartz[1], T. Merz[1], Y. Hikita[2], and H. Y. Hwang[1,2]

1. Geballe Laboratory for Advanced Materials, Department of Applied Physics, Stanford University, Stanford, CA 94305, USA

2. Stanford Institute for Materials and Energy Sciences, SLAC National Accelerator Laboratory, Menlo Park, CA 94025, USA

e-mail: hinoue6@stanford.edu

$SrTiO_3$-based heterostructures have received intense interest since the discovery of a two-dimensional gas of high mobility electrons, magnetism, and superconductivity, with properties highly dependent upon the interface and bulk structure. While reduced dimensional heterostructures have revealed a host of interesting phenomena, bulk $SrTiO_3$ is a unique semiconducting superconductor with the lowest known bulk carrier density. Despite 60 years of research, the origin of the superconductivity is not well understood. Tunneling spectroscopy, enabling a direct measurement of the density of states, is a powerful probe of the superconducting ground state. While this approach has been instrumental in the study of strong coupling [1] and unconventional [2,3] superconductors, its implementation in semiconducting $SrTiO_3$ has been limited [4] due to the large dielectric constant ($\varepsilon \sim 20{,}000$) and the thick interfacial charge depletion layer ($W > 100$ nm) obscuring the tunneling process.

By exploiting atomic scale control over epitaxial interface dipoles, we suppress this depletion layer allowing access to the intrinsic properties of $SrTiO_3$ in tunneling experiments. We fabricated high quality elemental metal / $LaAlO_3$ / Nb:$SrTiO_3$ (001) junctions by pulsed laser deposition, where the dipole in ultrathin $LaAlO_3$ (001) alters the band alignment between the metal and Nb:$SrTiO_3$ (see Fig. (a,b)) [5-6]. The junction resistance decreases over three orders of magnitude as $LaAlO_3$ thickness is increased from 0 to 2 unit cells, indicating the suppression of the depletion layer. At the same time, the signal to noise ratio of the tunneling spectrum is significantly improved. Using this approach, we have observed inelastic tunneling arising from interactions with the $SrTiO_3$ longitudinal optic (LO) phonon modes, and the superconducting gap of $SrTiO_3$ with a spectral resolution of a few μeV (see Fig. (c)). These results provide significant insight relevant to the electron-phonon coupling and the superconducting pairing mechanism. Furthermore, this example of interface engineering by electric dipole layers is a rather general technique and can be applied to a wide variety of oxide systems.

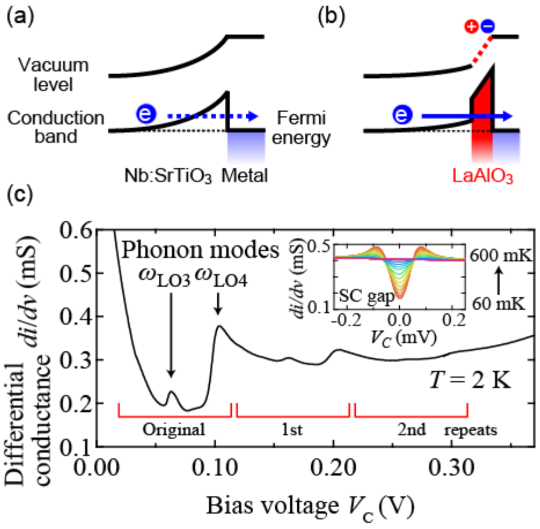

Fig. (a) (b) Schematic diagram of band alignment tuning using an $LaAlO_3$ dipole layer. (c) Tunneling spectrum in normal state showing $SrTiO_3$ phonon modes. Inset: Superconducting gap spectrum.

[1] J. M. Rowell and W. L. McMillan, *Phys. Rev. Lett.* **16**, 453 (1966).
[2] Ø. Fischer *et al.*, *Rev. Mod. Phys.* **79**, 353 (2007).
[3] Y. Tanaka *et al.*, *J. Phys. Soc. Jpn.* **81**, 011013 (2012).
[4] G. Binnig *et al.*, *Phys. Rev. Lett.* **45**, 1352 (1980).
[5] H. Inoue *et al.*, submitted.
[6] T. Yajima *et al.*, *Nano Lett.* **15**, 1622 (2015).

Mo2050

Understanding the Origin of Surface Depletion in δ-doped $SrTiO_3$

Hyeok Yoon[1], Hisashi Inoue[1], Adrian G. Swartz[1], Yasuyuki Hikita[2], Harold Y. Hwang[1, 2]

[1] Geballe Laboratory for Advanced Materials, Department of Applied Physics, Stanford University, Stanford, California 94305, USA
[2] Stanford Institute for Materials and Energy Sciences, SLAC National Accelerator Laboratory, Menlo Park, California 94025, USA

Surface symmetry breaking can generate new physical phenomena not seen in the parent bulk material. The charge depletion layer stemming from a surface pinning potential is a well-known example in traditional group IV and III-V semiconductors. Unlike the most of the conventional semiconductors, the large dielectric constant of the incipient ferroelectric $SrTiO_3$ results in a pronounced depletion width [1]. In thin films, the effect of surface depletion is even more dramatic: reduction of mobility and two-dimensional (2D) carrier density. To avoid this surface effect, capping and buffering a narrow channel of doped $SrTiO_3$, so called δ-doping, is designed to make the channel free from surface scattering, resulting in highly mobile carriers [2][3][4]. Despite its importance for oxide thin film engineering such as electrostatic-gating and nanowires, a comprehensive understanding of the physical origin for the surface depletion in $SrTiO_3$ is lacking. In particular, whether or not this depletion layer is due to a particular electronic surface state, or is driven by some chemical process arising from materials synthesis remains unclear.

To address this longstanding problem, we have investigated systematic changes in electronic transport by tuning the thicknesses of the undoped surface buffering cap (t_{cap}) and the δ-doped layer (t_{δ}). All samples are grown by pulsed laser deposition in a step-flow growth mode. Resistivity and Hall measurements in the low-field limit are used to extract the three-dimensional (3D) carrier density and mobility. This has allowed us to map the electronic phase diagram as a function of t_{cap} and t_{δ}, where we find regions consisting of a 3D metal, 2D metallic behavior, and an insulating phase. In addition, in order to understand the role of the capping layer and its contribution to transport, we study the surface depletion width in cap-less samples as a function of doping density. We find that the depletion width is temperature independent, which is inconsistent with a simple model based on the intrinsic $SrTiO_3$ dielectric constant and a traditional picture of a fixed surface state pinning potential.

[1] A. Ohtomo and H. Y. Hwang, *Appl. Phys. Lett.* **84**, 1716 (2004).
[2] Y. Kozuka *et al.*, *Appl. Phys. Lett.* **97**, 222115 (2010).
[3] Y. Kozuka, M. Kim *et al., Nature* **462**, 487 (2009).
[4] M. Kim *et al., Phys. Rev. Lett.* **107,** 106801 (2011).

Mo2055

Iodine dimerization at methylammonium lead iodide perovskite surfaces

Limin She, Meizhuang Liu, and Dingyong Zhong*

State Key Laboratory of Optoelectronic Materials and Technologies, School of Physics and Engineering, Sun Yat-sen University, 510275 Guangzhou , China

**Email: dyzhong@mail.sysu.edu.cn*

Organic-inorganic hybrid perovskites, consisting of organic cations intercalated in the metal-halogen octahedron frameworks, have attracted much interest due to their promising applications in electronics and optoelectronics. In the last few years, their crystallographic structures and electronic properties have been intensively investigated experimentally and theoretically. However, the information about the surface and interface structures, which are of importance for device performances, is so far very rare. In this work, we report on the atomic structures of methylammonium (MA) lead iodide ($CH_3NH_3PbI_3$) perovskite surfaces, based on a combined scanning tunneling microscopy and density functional theory calculation study. A reconstructed surface phase with iodine dimers, coexisting with the pristine zigzag phase, was found at the MA-iodine terminated (001) surfaces of the orthorhombic perovskite films grown on Au(111) surfaces. The reorientation of surface MA dipoles, which strengthens the interactions with surface iodine anions, resulting in a slight energy reduce of 34 meV per unit cell, is responsible for the surface iodine dimerization. According to our calculation, the surface MA dipoles weaken the surface polarity and are therefore considered stabilizing the surface structures.

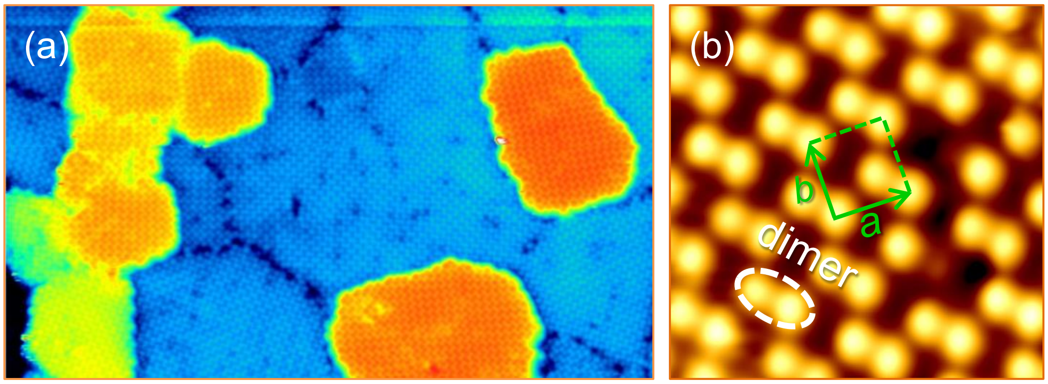

Figure 1 STM image of $CH_3NH_3PbI_3$ perovskite surfaces with iodine dimers. (a) 64.7 × 37.2 nm^2; 1.6 V; 30 pA. (b) 4.3 × 4.3 nm^2; 2.5 V; 50 pA.

Tuesday Morning

Semiconductor Interfaces & Devices I

Tu0830 Invited

Interfaces in GaN-diamond integrated electronics - Thermal and mechanical considerations

M. Kuball, J.W. Pomeroy, J. Anaya, H. Sun, R. Baranyai, D. Spiteri, D. Liu
Affiliation: Center for Device Thermography and Reliability (CDTR), University of Bristol, United Kingdom

Abstract: GaN is a material of great interest for high electron mobility transistors for microwave and power applications. One current topical driver is the integration of GaN with diamond, to enable even higher device power densities than possible with the more common GaN-on-SiC transistor technology. This is a technological challenge. Interfacial effects on heat transfer across GaN-diamond interfaces however also across diamond-diamond grain boundary interfaces will be discussed, in additional to the mechanical stability of this interface.

Reduced output power drop in AlGaN/GaN HFETs on Si(111) by controlling the passivation /AlGaN barrier interface

Seung Kyu Oh[1], Taehoon Jang[2], Young Je Jo[3], Hwa-Young Ko[3],
and Joon Seop Kwak[1]*,

[1]Department of Printed Electronics Engineering, Sunchon National University, Jeonnam 540-742, Korea
[2]Semiconductor Physics Research Center, Department of Semiconductor Science and Technology, Chonbuk National University, 567 Baekje-daero, Deokjin-gu, Jeonju-Si, Jeonbuk, 561-756, Korea
[3]IGBT part, System IC R&D, LG Electronics, 38, Baumoe-ro, Seocho-Gu, Seoul 137-724, Korea.

Corresponding author: jskwak@sunchon.ac.kr, +82-61-750-3559

Purpose of Work

Reduction of output power has been observed in AlGaN/GaN heterostructure field effect transistors (HFETs) with inorganic passivation layer such as SiO_2 and SiN_x after TO-220 plastic package due to the passivation layer cracking and metal deformation caused by thermal stress and filler-induced stress. In order to solve this problem, thick organic polyimide layer was passivated on AlGaN/GaN HFETs. However, the output power was also decreased after the passivation process as shown Fig. 1, because of the diffusion of fluorine ions during curing of the polyimide layer followed by the reduction of 2DEG concentration due to the strong electronegativity of fluorine ions[1]. In this paper, we have demonstrated reduced output power drop in AlGaN/GaN HFETs on Si(111) by controlling the passivation/AlGaN barrier interface with inorganic/organic hybrid passivation layers. The inorganic/organic hybrid passivation layers will suppress the diffusion of fluorine ions as well as prevent the passivation layer cracking during the TO-220 plastic package process.

Results and Conclusions

In order to suppress output power drop of the AlGaN/GaN HFETs with inorganic passivation layer after plastic package process, the 5 μm thick polyimide layer was formed on AlGaN/GaN HFETs instead of the inorganic passivation layer. The result shows that although the output power of polyimide passivatied AlGaN/GaN HFETs was not decreased after the plastic package, it was reduced after curing of the polyimide passivation layer. A shown in Fig. 2(a), the XPS spectrum with/witout the polyimide passivation layer on the AlGaN barrier layer showed that the fluorine ions in polyimide layer were incorporated into the AlGaN surface during curing process of the polyimide layer, followed by the reduction of 2DEG concentration due to the strong electronegativity of fluorine ions, as illustrated in Fig. 2.

To avoid fluorine ion diffusion into AlGaN surface during the curing of the polyimid passivation layer, a 100 nm thick SiN_x layer was inserted between the AlGaN barrier and organic polyimide layer by PECVD. The resultas showed that the drain current and leakage current were not changed even after passivation and TO-220 plastic package process, as well. This result clearly show that the inorganic/organic hybrid passivation layer consisted of a thin SiNx layer and a thick polyimide layer sucessfully suppressed the diffusion of fluorine ions into the AlGaN surface during the curing process due to the SiN_x inorganic passivation layer as well as prevented the passivation layer cracking during the TO-220 plastic package process by the thick polyimide layer.

[1] Yong Cai, Yugang Zhou, Kevin J. Chen, Kei May Lau, "High-performance enhancement-mode AlGaN/GaN HEMTs usinfluoride-based plasma treatment," *IEEE Electron Device* , vol. 26, p. 435, 2005

Tu0915

Suppression and recovery of Nitrogen dissociation from the surface of Gallium Nitride during high temperature annealing by a new Nitrogen heat-beam method

Nur Syafiqah Nadia binti Johari[a)] and Yuji Awano
Keio University
3-14-1 Hiyoshi, Kohoku-ku, Yokohama, Japan, [a)]E-mail: syafiqah08_nad@z8.keio.jp

INTRODUCTION: Gallium Nitride (GaN) based High Electron Mobility Transistors (HEMTs) have attracted considerable interests due to their outstanding electronic properties for the high-speed and high-power electronics applications that require a combination of high break-down voltage, high efficiency, high linearity and high operation frequency. To achieve these requirements, lower source and drain resistance, lower thermal resistance [1] and suppression of current collapse effects are unavoidable challenges to be addressed. Previous studies encountered material loss or thermal decomposition at the surface of GaN related materials during high temperature annealing, which is often used for fabricating alloyed ohmic contacts or for electrical activations of impurities after ion-implantation. These phenomena lead to carrier traps at the surface, which are strongly related to the issues mentioned above. This paper is focused on a new fabrication process to lower ohmic contact resistance [2] and current collapse with a minimum damage to GaN related materials' surface by using a new annealing method named "Heat-Beam (HB) annealing" [3].

EXPERIMENTAL: In Heat-Beam (HB) annealing method, a flowing high temperature inert gas is used to anneal samples at higher gas flow rate, resulting substrate temperature as high as 960℃. N_2 gas is utilized as an inert gas for applying excess nitrogen pressure during annealing, as shown in Fig. 1. The advantages of HB annealing method include (i) high process throughput, due to the larger diameter of heat beam compared to a laser annealing, (ii) high controllability of nitrogen excess pressure and annealing time, and (iii) differ from conventional high N_2-pressure annealing, HB annealing is obviously contribute higher temperature at near-surface region only, resulting slightly lower substrate temperature than heat-beam temperature. In this work, HVPE-grown non-doped Gallium Nitride epitaxial layer on sapphire substrate is employed.

RESULTS AND DISCUSSIONS: The annealing temperature, which is measured by thermocouples placed on the substrate surface, is 879℃. X-ray Photoelectron Spectroscopy (XPS) analysis is carried out to measure the depth profiles of Ga and N atoms in annealed and non-annealed samples. Based on the calculations of intensity ratio of Ga (2p, 3s, 3p, 3d) to N 1s from XPS spectra, a nitrogen loss region is observed in original sample (before annealing) near the surface of less than a hundred nanometers in depth. Then, after the HB annealing, it seems that the nitrogen loss region has disappeared and there is a flat profile of nitrogen from the surface to as deep as about 500 nm, except in the very vicinity of the surface, as shown in Fig. 2. It is suggested that the oxygen either binds on gallium sites or form V_{Ga}-O_N complexes when it is incorporated into the GaN lattice before annealing, but the vacancies at Ga and N lattices possibly decorated with N atoms or maybe O atoms during HB annealing process, which need further investigations. Comparing with the conventional annealing method [4], the percentage of nitrogen loss was successfully reduced, which suggests a better opportunity to achieve a lower contact resistance. We will report results on nitride loss phenomena at shallower surface region and under higher anneal temperature. In addition, HB annealing of Si-doped Gallium Nitride grown on sapphire substrate is carried out and substrate temperature of 765℃ is observed. Dynamic Secondary Ion Mass Spectroscopy (D-SIMS) analysis is carried out to measure the depth profile of dopant concentration. At near-surface region, D-SIMS profile shows Si doping concentration of $2x10^{17}$ cm^{3} loss by $1x10^{17}$ cm^{3} only after HB annealing, as shown in Fig. 3. This loss is negligibly small for higher doping layer in HEMT, which promising better device performance.

CONCLUSION: As a conclusion, a newly proposed annealing method is demonstrated as the first approach for real application of GaN-based HEMTs to lower nitrogen loss from the surface using a nitrogen-gas Heat Beam with nitrogen excess pressure, which is viable and highly promising for the high frequency power electronics applications.

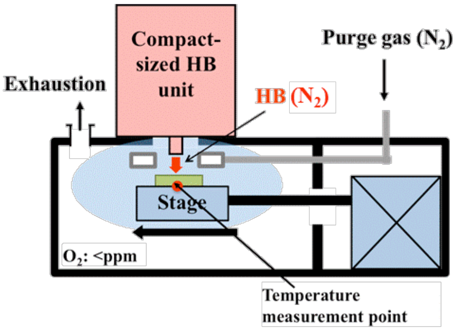

Fig.1 Schematic of Heat-beam (HB) annealing

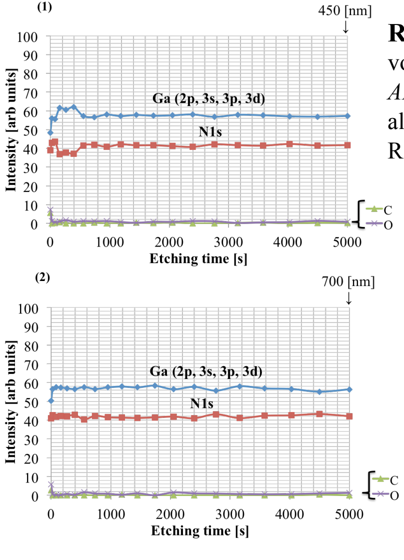

Fig. 2 Depth profiles of Ga(2p, 3s, 3p, 3d) and N1s intensities of XPS obtained from the samples (1) before and (2) after HB annealing process (879℃)

References: [1] M. J. Tadjer, IEEE *EDL,* vol. 33, Issue 1 (2012), [2] M. H. Wong, et al., *APL*, vol. 91 pp 232103 (2007), [3] K. Ito, et al., *APEX,* vol. 6, pp 115101 (2013), [4] M. A. Rana, et al., *CPL*, 380, pp. 105-110 (2003)

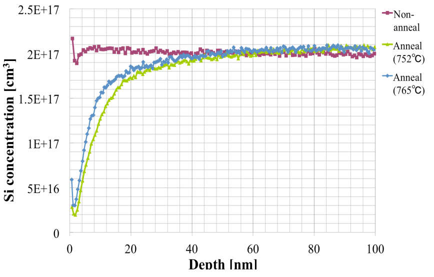

Fig. 3 D-SIMS profile of Si-doped samples before and after HB annealing process

Polarization-Engineered Tunneling in III-Nitride Heterostructures

Debdeep Jena[1,2], Xiaodong Yan[2], Wenjun Li[2], Kasra Pourang[2], Jimy EncomenderoRisco[2],
Moudud Islam[2], Vladimir Protasenko[2], Stacia Keller[3], Patrick Fay[2], and Huili Grace Xing[1,2]

[1]ECE and MSE Departments, Cornell University, USA
[2]EE Department, University of Notre Dame, USA
[3]ECE Department, University of California Santa Barbara, USA

The wide energy bandgaps of III-Nitride semiconductors should prohibit interband tunneling, which they do – and in the process help sustain very large breakdown voltages, enabling power electronics and high voltage devices. But for certain device applications, we wish to turn on large tunneling currents on demand. Such applications range from various embodiments of two-terminal interband Zener tunnel diodes, three-terminal tunneling field-effect transistors (TFETs), to intraband resonant tunneling diodes (RTDs). In this presentation, we discuss how the spontaneous and piezoelectric polarization in III-Nitride heterostructures is the *key enabler* of tunneling transport physics [1,2]. The high spontaneous and piezoelectric polarization fields that originate without the introduction of impurity dopants is a change in paradigm which can be exploited unlike in other III-V semiconductors. Exploiting this concept, nitride interband tunnel junctions are being explored for reducing the p-type contact resistance in visible and UV light emitters [3, 4].

Pushing the concept of the polarization-induced Zener tunnel diode further, it was realized that there is a unique potential to gate this sort of a diode and make a three-terminal Tunneling Field-Effect Transistor (TFET). Conventional wisdom would suggest this to be a low-current transistor because of the large bandgap of the nitrides. But a careful choice of heterostructures materials-by using large Indium mole fractions and high polarization fields, the tunneling currents in GaN TFETs are projected to exceed those of the much narrower III-V arsenide and antimonide counterparts [5]. This is rather remarkable: preliminary experimental work towards realizing such devices will be presented [6].

Obervation of intraband *resonant* tunneling in III-Nitride heterostructures has been plagued by defects and hysteretic behavior. The recent availability of single-crystal bulk GaN substrates has now enabled the demonstration of clear and repeatable NDR in GaN/AlN RTDs, and points towards a new and strong effect of polarization on the transport physics. Preliminary results will be presented. The discussion will conclude with a summary of current challenges and potential future directions in exploiting tunneling with polarization in III-Nitride heterostructures. The work presented in this talk is was supported in part by the Center for Low Energy Systems Technology (LEAST), one of the six SRC STARnet Centers, sponsored by MARCO and DARPA, and the ONR DATE MURI.

REFERENCES:

[1] M. Grundmann et al., "Multicolor light emitting diode using polarization-induced tunnel junctions", Physica Status Solidi C, Vol. 4, pp 2830-2833, 2007.
[2] J. Simon et al., "Polarization-Induced Zener Tunnel Junctions in Wide-Band-Gap Heterostructures", Physical Review Letters, Vol. 103, pp 026801 1-4, 2009.
[3] S. Krishnamoorthy et al., "Low resistance GaN/InGaN/GaN tunnel junctions", Applied Physics Letters, Vol. 102, pp 113503 1-5, 2013.
[4] M. Kaga et al., "GaIn N-Based Tunnel Junctions in n-p-n Light-Emitting Diodes", Japanese Journal of Applied Physics, Vol. 52, pp 08JH06 1-4, 2013.
[5] W. Li et al., "Polarization-Engineered III-Nitride Heterojunction Tunnel Field-Effect Transistors", IEEE Journal of Exploratory Solid-State Comp. Devices and Circuits, 1, 28, 2015.
[6] X. Yan et al., "Polarization-induced Zener tunnel diodes in GaN/InGaN/GaN heterojunctions", Applied Physics Letters, 107, 163504, 2015.

Tuesday Morning

2D Materials I

Excitons in 2D semiconductors and heterostructures

Xiaodong Xu
Department of Physics,
Department of Materials Science and Engineering
University of Washington

Abstract

Electronic valleys are energy extrema of Bloch bands in momentum space. Having multiple valleys gives the electron states pseudospin degrees of freedom in addition to their real spin. In this talk, I will discuss our experimental progress on the investigation of valley excitons in monolayer semiconductor and heterostructures. I will first show a strong phonon-exciton interactions in monolayer WSe_2, which manifests as excitonic anti-stokes enhanced by doubly resonant Raman scattering with valley selectivity and electrical control. I will then discuss interlayer exciton in $MoSe_2/WSe_2$ heterostructures, which is analogous to spatially indirect excitons in double quantum wells, but with additional valley pseudospin properties.

Tu1140

Exciton diamagnetic shifts and valley Zeeman effect in monolayer WS_2 and MoS_2 to 65 Tesla

Andreas V. Stier[1], Kathleen M. McCreary[2], Berend T. Jonker[2], Junichiro Kono[3], Scott A. Crooker[1]

[1]*National High Magnetic Field Laboratory, Los Alamos National Laboratory, Los Alamos, NM*
[2]*Naval Research Laboratory, Washington D.C.*
[3]*Department of Physics and Astronomy, Rice University, Houston, TX*

Monolayer transition-metal dichalcogenides (TMDs) are a new class of 2D semiconductors that feature direct bandgaps at the extreme *K/K'* points of their hexagonal Brillouin zone. Strong spin-orbit coupling and broken inversion lead to valley-selective optical selection rules for right/left circularly polarized light, permitting direct optical studies of valley physics [1]. As bands in *K* and *K'* are related by time reversal symmetry, they have equal-but-opposite magnetic moment ($\boldsymbol{\mu}^K = -\boldsymbol{\mu}^{K'}$), so that in applied magnetic fields a *valley Zeeman splitting* can be observed optically. Recent low-field PL studies have indeed reported the valley Zeeman effect of the 'A' exciton in $MoSe_2$ and WSe_2, but measurements of their di*sulphide* counterparts (MoS_2 and WS_2) have not been reported to date. Nor have studies of the higher-energy 'B' exciton been reported for any monolayer TMD material.

To this end we study magneto-*reflection* spectroscopy of large-area WS_2 and MoS_2 monolayers in unprecedentedly large pulsed magnetic fields to 65 T, which allows the first observation of the valley Zeeman effect, for both the A *and* B excitons, in the monolayer transition-metal disulphides [2]. Valley splittings of approximately -230 μeV/T ($g \approx -4$) are observed for both A and B excitons, which agrees unexpectedly well with straightforward expectations from a simple two-band tight-binding model.

Even more importantly, the very large magnetic fields used in these studies allowed the first observation [2] of the small quadratic *diamagnetic shift* of excitons in the monolayer TMDs: $\Delta E_{dia} = e^2 \langle r^2 \rangle B^2/8m_r$. This crucial parameter has not yet been measured in any monolayer TMD, likely due to the large reduced mass m_r, the small radii r of tightly-bound excitons in these materials, and to the modest magnetic fields used in studies to date. Note that diamagnetic shift measurements have long been used to infer exciton size, binding energy, and dimensionality in conventional semiconductors.

We use the measured diamagnetic shift to directly calculate A and B exciton radii of 1.53 nm and 1.16 nm in monolayer WS_2. Further, we show that diamagnetic shifts can constrain estimates of the *exciton binding energy* ––– a subject of considerable recent interest in monolayer TMDs. Within the context of the non-local dielectric screening potential that is believed to exist in these 2D semiconductors [3], Fig. 2 shows that the exciton binding energy is constrained to lie along the contours of constant diamagnetic shift that are overlayed on a 2D color plot of calculated binding energy. Our data suggest exciton binding energies of ~410 meV and ~470 meV for the A and B exciton in monolayer WS_2. These measurements highlight the utility of very large magnetic fields for understanding new 2D materials.

[1] *see, e.g.*, X. Xu, W. Yao, D. Xiao, T. F. Heinz, *Nature Physics* **10**, 343 (2014).
[2] A. V. Stier *et al.*, *submitted. See preprint on www.arXiv.org*
[3] T. C. Berkelbach *et al.* PRB 88, 045318 (2013).

Tu1145

Abstract focus area: Graphene and other 2D materials

Hybrid, gate-tunable, van der Waals p-n heterojunctions from pentacene and MoS_2

Deep Jariwala[1†*], Sarah L. Howell[1†], Kan-Sheng Chen[1], Junmo Kang[1], Vinod K. Sangwan[1], Stephen A. Filippone[1], Riccardo Turrisi[2], Tobin J. Marks[1,2], Lincoln J. Lauhon[1] and Mark C. Hersam[1,2]

[1]Department of Materials Science and Engineering, Northwestern University, Evanston, Illinois 60208, USA.
[2]Department of Chemistry, Northwestern University, Evanston, Illinois 60208, USA.

† These authors contributed equally.
* Presenting author, e-mail: deepjariwala2015@u.northwestern.edu

The emergence of a wide variety of two-dimensional (2D) materials has created new opportunities for device designs and applications. In particular, the availability of semiconducting transition metal dichalcogenides,[1] in addition to semi-metallic graphene and insulating boron nitride, has enabled the fabrication of 'all 2D' van der Waals heterostructure devices. However, the concept of van der Waals heterostructures[1, 2] has the potential to be significantly broadened beyond layered solids. This principle has been exploited to fabricate heterojunctions between conventional silicon and 2D materials[3] as well as carbon nanotubes with 2D materials[4] and amorphous oxide semiconductors.[5] Similarly, molecular and polymeric organic solids, whose surface atoms possess saturated bonds, have the potential to interact via van der Waals forces and thus offer an alternative for scalable integration with 2D materials. Despite this potential, the integration of organic semiconductors with 2D materials for optoelectronic devices has thus far been limited. Here, we demonstrate the integration of an organic small molecule p-type semiconductor, pentacene, with a 2D n-type semiconductor, MoS_2. The resulting p-n heterojunction diode is gate-tunable and shows asymmetric control over the anti-ambipolar transfer characteristic. The operating principles and band profiles of this system are characterized by direct charge transport measurements, scanning photocurrent microscopy, electrostatic force microscopy and finite element modeling. This comprehensive experimental and computational study reveals that pentacene forms a type-II heterojunction with MoS_2 exhibiting a photovoltaic effect, thereby demonstrating n-type MoS_2 as a candidate non-fullerene acceptor in organic photovoltaics.

References:

1. Jariwala D., Sangwan V.K., Lauhon L.J., Marks T.J., Hersam M.C. Emerging device applications for semiconducting two-dimensional transition metal dichalcogenides. ACS Nano 8, 1102–1120 (2014).
2. Grigorieva I.V., Geim A.K. Van der Waals heterostructures. Nature 499, 419-425 (2013).
3. Yang H., Heo J., Park S., Song H.J., Seo D.H., Byun K.-E., et al. Graphene Barristor, A Triode Device with a Gate-Controlled Schottky Barrier. Science 336, 1140-1143 (2012).
4. Jariwala D., Sangwan V.K., Wu C.-C., Prabhumirashi P.L., Geier M.L., Marks T.J., et al. Gate-Tunable Carbon Nanotube–MoS2 Heterojunction p-n Diode. Proc. Nat. Acad. Sci. USA 110, 18076–18080 (2013).
5. Jariwala D., Sangwan V.K., Seo J.-W.T., Xu W., Smith J., Kim C.H., et al. Large-Area, Low-Voltage, Antiambipolar Heterojunctions from Solution-Processed Semiconductors. Nano Lett. 15, 416-421 (2015).

Tu1150

Nanoscale Chemical and Electronic Properties of Methyl-Terminated Germanane

T.J. Asel[1], X. Yang[2], S. Jiang[3], K. Krymowski[4], O. Restrepo[4], W. Windl[4], J. Goldberger[3], and L.J. Brillson[1, 2]
[1] The Ohio State University, Department of Physics, 191 West Woodruff Ave., Columbus, OH 43210 USA
[2]The Ohio State University, Department of Electrical and Computer Engineering, 205 Dreese Lab, 2015 Neil Ave., Columbus, OH 43210 USA
[3] The Ohio State University, Department of Chemistry, Newman and Wolfrom Lab,100 West 18th Ave., Columbus, OH 43210 USA
[4] The Ohio State University, Department of Materials Science and Engineering, 117 Watts Hall, 2041 N. College Rd., Columbus, OH, 43210

We have used a combination of surface science and depth-resolved techniques to study the nanoscale chemical and electronic properties of a chemically functionalized two-dimensional (2D) material, methyl-terminated germanane (Ge CH_3). With the discovery of graphene, two-dimensional (2D) materials have attracted high interest due to their many unique properties and the ability to further manipulate them chemically and mechanically. Germanane is a 2D material like graphene and MoS_2 but has a direct band gap that can be manipulated by attaching new ligands, making it an attractive candidate for optoelectronic applications. $GeCH_3$ is synthesized by de-intercalating $CaGe_2$ with CH_3I to produce $GeCH_3$ [1]. Germanane is prone to oxygen contamination which can alter its electronic properties. Here we use x-ray photoelectron spectroscopy (XPS) to guide our efforts to produce a clean $GeCH_3$ surface. Once a clean surface has been obtained, we apply depth-resolved cathodoluminescence spectroscopy (DRCLS) [2] to measure the electronic transitions of "bulk" $GeCH_3$ flakes and their sensitivity to oxidation.

2D materials such as Ge CH_3 are challenging to synthesize without introducing impurities. Our XPS measurements reveal that, after refinement of the synthesis, impurities such as Ca and I can be minimized and using a pressurized glove bag to cleave samples without air exposure, they show minimal oxygen adsorption. Such adsorption has major effects on surface electronic properties. XPS shows that brief (minutes) air exposure produces adsorbed oxygen on Ge CH_3, while surface-sensitive DRCLS measurements of the air-exposed surface reveals the formation of a nanometer-thick surface layer with the optical properties of GeO_2 [3] and which is distinct from the Ge CH_3 below the surface.

DRCLS using incident beam energies of 1.0-3.0 kV reveal the optical emissions of $GeCH_3$. Density functional theory (DFT) calculations predict a band gap of 1.56 eV for hydrogenated germanane, while CH_3 termination is predicted to increase its band gap energy to 1.82 eV. Our measurements show a band gap of approximately 1.60 eV, and a possible increase with increasing excitation depth. Further, DRCLS reveals above-band-gap optical transitions at 2.72 and 3.11 eV that correspond to higher lying conduction-band-to-valence band states as predicted by DFT and which up until now have never been observed at the $GeCH_3$ or other functionalized 2D material surfaces. The energy and intensity of these features depend strongly on orbital symmetry and orientation, offering a new avenue for monitoring and controlling electronic structure in 2D materials using chemical functionalization, and opens up the possibility for further control by uniaxial strain.

[1] S. Jiang, S. Butler, E. Bianco, O.D. Restrepo, W. Windl, J. E. Goldberger, *Nat. Comm.* **5**, 3389 (2014).

[2] L. J. Brillson, *J. Phys. D: Appl. Phys.* **45**, 183001 (2012).

[3] E. Nogales, A. Montone, F. Cardellini, B. Mendez, and J. Piqueras, *Semiconductor Sci. Technol.* **17,** 1267 (2002)

in situ studies of thermal behavior of exfoliated black phosphorus

Matthieu Fortin-Deschênes,[1] Pierre Levesque,[2] Richard Martel,[2] Oussama Moutanabbir[1,*]

[1] Department of Engineering Physics, Polytechnique Montréal, 2900 boulevard Edouard Montpetit, Montréal, Canada
[2] Département de Chimie, Université de Montréal, 2900 boulevard Edouard Montpetit, Montréal, Canada

[*]Corresponding authors: oussama.moutanabbir@polymtl.ca

Abstract

Few-layer black phosphorus (bP) an emerging two-dimensional material which attracts a great deal of interest due to its interesting properties including tunable direct band gap, relatively high hole mobility, significant thermoelectric figure of merit, highly anisotropic properties and many other interesting characteristics. This makes bP suitable for applications in electronics, optoelectronics, and energy conversion. Developing these technologies requires an atomistic-level understanding of structural and morphological properties of bP both under ambient conditions and throughout thermal treatments. With this perspective, this work describes the dynamics of thermal decomposition of exfoliated bP layers during thermal annealing using low energy electron microscopy (LEEM) and scanning tunneling microscopy (STM). The ability to probe *in situ* the behavior of bP as a function of temperature provides unprecedented insights into its thermal stability as well as into the basic mechanisms underlying its sublimation. The investigated samples consist of exfoliated bP layers with a variable thickness transferred onto host silicon substrates. Thermal annealing was conducted under ultrahigh vacuum in LEEM chamber. The data indicate that the sublimation takes place around 400°C following two simultaneous but distinct atomic pathways at the edges and on the surface. Through the latter, the sublimation of bP induces asymmetric flakes along the [001] direction. These flakes propagate at a velocity on the order of nm/s. This dynamics of bP sublimation will be discussed and elucidated by combining LEEM, STM, DFT calculations, and kinetic Monte Carlo simulations. The quantitative description of these mechanisms is useful to define the optimal experimental parameters for fabrication and processing of bP-based materials and devices.

Tuesday Evening

Rump Session: Novel Energy Materials

Tu1900 Invited

Using Nanostructured Assemblies to Control the Physics of Energy Harvesting and Storage

Sarah H. Tolbert
Department of Chemistry and Biochemistry
Department of Materials Science and Engineering
The California NanoSystems Institute
UCLA

In this talk, we examine how nanostructured assemblies can be used to control fundamental physical processes, and how those processes can find practical applications in our quest to solve energy related issues in fields ranging from solar energy harvesting to electrochemical energy storage and electro-catalysis. We begin with assemblies of organic molecules that could find application in organic photovoltaics. Here we examine how amphiphilic assembly can be used to create well defined arrays of conjugated organic molecules (semiconducting polymers and fullerenes) that rapidly separate charge carriers upon photoexcitation and keep those carriers separated for extended periods of time. We then move to inorganic nanostructures and examine how architectural control can be used to enhance rate capabilities in battery systems and efficiency in electro-catalysts. In these systems, the challenge is to create assemblies that combine porosity for solvent diffusion, optimized composition, and electrical conductivity so that redox reactions are not limited by diffusion constraints. We will specifically focus on new oxide and sulfide materials for fast electrochemical energy storage. If time permits, we will also examine Ni/Fe based materials for the water splitting oxygen evolution reaction.

Tu1940 Invited

Modulating Charge Transport Mechanisms by Tuning the Architectures of Supramolecular Assemblies

James D. Batteas

Department of Chemistry, Texas A&M University
College Station, TX 77843

The use of molecules as the active components in electronic devices has been studied since the 1950s, and more specifically, since the seminal work of Aviram and Ratner on the design of molecular rectifiers. Molecules proffer exceptional capabilities for the design of organic electronic components or as integrated components in More than Moore applications based on the ability to readily tune their electronic states through controlled synthetic modifications. However, when tunneling is the dominant mechanism of charge transport, the conductivity is largely insensitive chemical and structural changes that do not alter the overall length of the junction, thus seemingly limiting the ability for synthetic changes to modulate conductivity. Recently we have been investigating how nearest neighbor interactions can be used to afford charge delocalization in molecular islands to shift transport out of the tunneling regime into the more chemically tunable charge-hopping regime. To explore this, the transport properties of a series of free-base and zinc coordinated tri-pyridyl and tri-phenyl porphyrin thiols inserted into a dodecanethiol matrix on Au(111) were studied using scanning tunneling microscopy (STM). For single molecules, the tunneling efficiency and I-V behvaiour was found to be dominated by through bond tunneling, dictated by the hydrocarbon tether used to bind the molecules to the surface. However, when the porphyrin thiols were driven to aggregate into islands on the surface (e.g. through pi-stacking), distinct changes in their charge transport properties were observed. The formation of nanoscale islands of ca. 5 -10 nm results in sufficiently reduced charge confinement energy to facilitate the transition from a purely tunneling mechanism to a charge-hopping mechanism. These results illustrate the impact of molecular aggregation and nearest neighbor interactions on charge transport of molecular assemblies, and demonstrate the effectiveness of using such aggregates to achieve single-electron transport characteristics from relatively simple, tunable subunits. Directing such assemblies into pre-designed architectures however still represents a significant challenge. Here, to further control the dimensionality and organization of such assemblies, combinations of nanofabrication (using electron beam and scanning probe lithographies) and click-chemistry have been employed to enable the construction of controlled assemblies. The fabrication and assembly process along with the corresponding changes in the observed electronic properties of the assembled island will be discussed.

Tu2020 Invited

Additive Printing of Flexible Electronics

Tse Nga Tina Ng[1], David Schwartz[2], Ping Mei[2], Gregory Whiting[2], Janos Veres[2]

[1]UC San Diego

[2]Palo Alto Research Center

Additive printing of soluble materials ranging from conductors, semiconductors and dielectrics has enabled rapid fabrication of electronic circuits. Through inkjet printing technique we have demonstrated mechanically flexible, n- and p- type field-effect transistors based on organic semiconductors. Design rules and device models have been developed based on these printed transistors to produce complementary logic circuits such as shift registers and voltage-dependent oscillators. The logic circuits have been integrated with printed sensors to form a sensor platform. These circuits can provide the signal processing capabilities required for applications such as health monitoring and item-level tracking based on flexible sensing systems.

Wednesday Morning

Oxides II

We0830 Invited

Effect of Oxygen Incorporation on the performance of Noble Metal Oxide Schottky Contacts to ZnO

Alana M. Hyland[1], Robert Makin,[2] Steven M. Durbin,[2] and Martin W. Allen[1]

[1]MacDiarmid Institute for Advanced Materials and Nanotechnology, University of Canterbury, Christchurch, New Zealand.

[2]Department of Electrical and Computer Engineering, Western Michigan University, Kalamazoo, MI, USA.

Non-stoichiometric noble metal oxide Schottky photodiodes fabricated on ZnO via reactive RF sputtering and pulsed laser deposition (PLD) show significantly enhanced performance metrics compared to those fabricated using conventional Schottky contact techniques. These include barrier heights in excess of 1.0 eV, ideality factors approaching unity, temperature stability up to 180 °C, strong UV responsivity, and reduced persistent photoconductivity.

In this paper, the effect of increasing oxygen incorporation on these figures of merit is systematically investigated, with the aim of optimizing ZnO photodiode performance and reliability.

Reproducible arrays of iridium, ruthenium, platinum, and palladium oxide Schottky contacts were fabricated on identical single crystal ZnO wafers, over a range of oxygen compositions, by controlling the oxygen:argon processing gas ratio during the reactive RF sputtering and PLD of the corresponding noble metal target.

The level of oxygen incorporation in these Schottky contacts was found to strongly influence the electrical and optical properties of the resulting photodiodes. For example, the rectification ratio of iridium oxide photodiodes (at +/- 1 V) increased from less than 4 orders of magnitude with no oxygen incorporation to more than 11 with the optimum non-stoichiometric composition, with a corresponding increase in barrier height from 0.53 to 1.10 eV. This effect was even more pronounced for platinum oxide contacts with barrier heights reaching 1.30 eV.

Transmission measurements also showed a significant increase in contact transparency with increasing oxygen incorporation, indicating considerable potential for their use in transparent electronics.

We0910

Laser Curing and Ink-Jet Processes for Fabricating SiOx RRAM Structures

Kwangsub Byun[1], Ying Wang[2], Bruce Adams[2], Jack Lee[1]
[1]*Department of Electrical and Computer Engineering, Microelectronics Research Center, University of Texas at Austin, Texas 78758, USA, Email: ksubbyun@utexas.edu*
[2]*Applied Materials Inc. Laser Lab, 21421 NW Jacobson Rd., Hillsboro, OR 97124*

Memory devices employing resistive switching have been attracting a great deal of attention [1]. Various dielectric oxide materials have shown resistive switching behavior. One of the mechanisms that have been suggested to explain this behavior is the formation of nanocrystal (NC) conductive filaments in the oxide layer. For this type of device, “defects” inside the oxide layer play an important role in forming the NC filament. Both unipolar and bipolar behaviors have been reported according to the dependence on polarity of the external bias to switch between high and low resistance states (HRS & LRS). Silicon oxide, one of the most common materials for CMOS technology, has also been reported to exhibit switching behavior. In this paper, we present fabrication techniques that are applicable for SiOx based RRAM structures and improve device performance.

Firstly, we introduce the application of laser radiation onto the silicon oxide layer. For this purpose, we prepared two different kinds of “poorly-working” RRAM devices, one with BOE (buffered oxide etch) treatment to etch the oxide layer and the other without BOE treatment to maintain as-deposited oxide layer as shown in Fig 1(a). For the BOE etched structure, we first treated it with increasing laser energy (table in Fig 1(b)), and observed the strikingly noticeable increasing yield rate with increasing total laser energy applied to the devices. Based on this result, we applied the determined optimum laser energy to the non-etched RRAM structure that didn’t show switching behavior before, and observed the switching behavior after laser treatment (Fig 1(c)). Considering the basic mechanism of the oxide-based RRAM, one can conclude that the laser treatment induces and increases potential sites for nanocrystal filament formation within the oxide layer and therefore improves the yield rate. Such laser-curing step can be easily inserted into the manufacturing flow.

Secondly, we introduce a low-cost ink-jet printing technique for fabrication of MIM SiOx RRAM structures. We used ink-jet printing to print top and bottom (TE & BE) electrode lines with silver (Ag) ink in a cross-bar structure, with SiOx layer deposited using e-beam evaporation (50 nm) between those electrodes. Then the oxide layer was etched away using the TE as a mask layer to make a “working” etched structure. The optical image of final Ag/SiOx/Ag structure is shown in Fig 2(a). After an electroforming scanning process (inset of Fig. 2(b)), we observed reasonable set and reset unipolar switching behavior in both positive and negative bias regions after voltage sweeping from 0 to 4V (or 0 to -4V) for the set process, and again swept from 0 to 6V (or 0 to -6V) for the reset process. The I-V curves show very high on/off ratio ($>10^3$). This I-V behavior indicates a “soft breakdown” of the oxide layer for the formation of nanocrystal (NC) conductive filaments producing switching behavior in this ink-jet printed device. To further examine the electrical characteristics, we did data retention and endurance tests. The retention test was conducted at a voltage bias of 1V, while for the endurance test, a pulse of 4V of 1 ms duration and a pulse of 12V of 10 ms duration were used for set and reset processes respectively. Excellent electrical characteristics were obtained, e.g. data retention (i.e. $>10^4$ s) and endurance ($>10^4$ cycles), which are comparable to the current flash memory devices [1].

In summary, laser curing and low-cost ink-jet printing processes have been developed for fabricating unipolar or bipolar RRAM structures with silicon oxide materials and for improving their performance. The results provide additional insights into the mechanism of switching behavior and improved fabrication of RRAM devices.

[1] J. Joshua Yang, Dmitri B. Strukov and Duncan R. Stewart, Nature Nanotechnology, Vol. 8, 13, Jan. 2013

We0920

Initial nucleation and bi-axial texturing of MgO thin-films assisted by ion-beam irradiation on amorphous Y_2O_3 layers

Hye-Jin Jin[1], William Jo[1,*], Janghyun Jo[2], Miyoung Kim[2], Boo Min Kang[3], Gwan-Tae Kim[3], Rock-Kil Ko[3], Young-Sik Jo[3], and Dong-Woo Ha[3]

[1]Department of Physics, Ewha Womans University, Seoul, 120-750, Korea
[2]Department of Materials Science and Engineering, Seoul National University, 151-742, Korea
[3]Superconductivity Research Center, Korea Electrotechology Research Institute, Changwon, 642-120, Korea

*E-mail: wmjo@ewha.ac.kr

It is desirable to achieve artificial crystalline surfaces of oxide materials with bi-axially aligned lattices. In the field of high temperature superconductors, several schemes of texturing methods have been well developed including ion-beam assisted deposition (IBAD)[1], inclined substrate deposition and rolling-assisted biaxial texturing. In this talk, we revisit the IBAD process of MgO to elucidate the nucleation and texturing on amorphous yttira or alumina layers, which were synthesized by solution-deposition process (SDP)[2]. In addition, planarization of the intermediate layer between IBAD-MgO and metal alloy substrates should be taken into account. In order to investigate the whole growth mechanism in IBAD-MgO on SDP-Y_2O_3, we monitored the crystallinity of the initial MgO by reflection high-energy electron diffraction (RHEED) during the deposition. All the materials were carefully characterized by transmission electron microscopy (TEM) and X-ray diffraction (XRD) patterns. We propose a competing mechanism between initial nucleation of MgO islands and coalescence of biaxially aligned MgO nano-domains.

[1]C. P. Wang, K. B. Do, M. R. Beasley, T. H. Geballe and R. H. Hammond, Appl. Phys. Lett. 71 (20), 2955-2957 (1997).
[2]Vladimir Matias, Jens Hänisch, E. John Rowley, Chris Sheehan, Paul G. Clem, Noriyuki Kumasaka and Ichiro Kodaka, MRS Proceedings http://dx.doi.org/10.1557/PROC-1001-M04-02 (2007).

Wednesday Morning

High-K

We0925

SOLUTION- PROCESSED ORGANIC-INORGANIC HYBRID GATE DIELECTRIC FOR FLEXIBLE THIN FILM TRANSISTORS

M.G.Syamala Rao[1], Rafael Ramírez Bon[1]

[1]Centro de Investigación y de Estudios Avanzados (CINVESTAV-IPN), Libramiento Norponiente#2000, Fraccionamiento Real de Juriquilla, C.P.76230, Santiago de Querétaro, Querétaro, México.

Solution processing has been recently considered as an option when trying to reduce the costs associated with deposition under vacuum. In this context, solution-processable organic-inorganic hybrid gate dielectrics are of significant interest because of their low-cost, low temperatures processing and applications to flexible thin film transistors. In this work we explore the sol gel synthesis to prepare hybrid dielectric films that allows enhancing the high capacitance of a gate dielectric to enable the transistors operating at low voltages. The organic-inorganic hybrid transparent dielectrics composed of hafnium Chloride ($HfCl_4$) and (3-Glycidoxy propyl) trimethoxysilane (GPTMS).The hybrid HfO_X-GPTMS dielectric films are readily grown by spin coating with controlled thickness. After deposition, the wet hybrid films were cured at low annealing temperatures ($\leq 150^0$C) for compatibility deposition on plastic substrates. Addition of sol-gel derived hybrid films improved the film density. The representative films are characterized by UV-Vis spectroscopy, AFM, SEM and XPS respectively. The hardness of the films was studied by Nanoindentation. The surface morphology of hybrid dielectric films are amorphous, smooth enough, homogeneous and very low roughness to be used as a gate dielectric for TFTs. Additionally these hybrid amorphous films are desired for electrical properties such as reduced leakage current and Capacitance –voltage properties of TFT.

Key Words: Sol-gel, Dielectrics, TFTs.

We0930

Self-cleaning and unexpected surface chemistry during atomic layer deposition revealed by time-resolved XPS

S. McKibbin, S. Yngman, A. Head, J. Knutsson, J. Schnadt, A. Mikkelsen, and R. Timm

NanoLund, Department of Physics, Lund University, 221 00 Lund, Sweden
rainer.timm@sljus.lu.se

Atomic layer deposition (ALD) has been established as the main technique for creating metal-oxide-semiconductor structures. In order to achieve superior device performance based on III-V semiconductors, a precise control and profound knowledge of the semiconductor/oxide interface is crucial, but not fully reached yet. One of the great challenges is to characterize the chemical reactions taking place at the interface between the semiconductor, its native oxide, and the high-k dielectric material during the ALD process. X-ray photoemission spectroscopy (XPS) has successfully been used to investigate this interface before and after individual steps of the ALD reaction [1,2], but was until now limited to ultrahigh vacuum conditions.

Here we present near-ambient pressure XPS (AP-XPS) studies of the ALD of HfO_2 on InAs, using tetrakis-(dimethylamino)-Hafnium (TDMA-Hf) and water precursors: By performing subsequent half-cycle steps of the ALD process within the reaction cell of an AP-XPS system [3], we were able to monitor the slowed down ALD reaction by XPS and thus obtain fully in-situ and real-time XPS measurements of the high-k deposition on III-V semiconductors. Figure 1 shows the temporal evolution of the As 3d core-level components during the first half-cycle of TDMA-Hf deposition: A full removal of the As-oxides can be seen, which has been reported before as the so-called self-cleaning effect of ALD. By obtaining alternating series of As 3d and In 3d spectra during the deposition, we can now resolve that As^{5+} oxides are removed slightly prior to As^{3+} and In-oxides upon the self-cleaning.

Furthermore, monitoring the Hf signal during deposition reveals a period of Hf precursor chemisorption on the surface prior to ligand split-off and Hf-oxide formation, as can be seen in Fig. 2 by the shift in Hf binding energy. Interestingly, the oxide removal occurs already during this chemisorption period, indicating that the previously accepted simple picture of ligand exchange as the only ALD reaction responsible for the self-cleaning has to be revised.

[1] Timm *et al.*, Appl. Phys. Lett. **97**, 132904 (2010)

[2] Timm *et al.*, Appl. Phys. Lett. **99**, 222907 (2011)

[3] Schnadt *et al*. J. Synchrotron Radiat. **19**, 701 (2012)

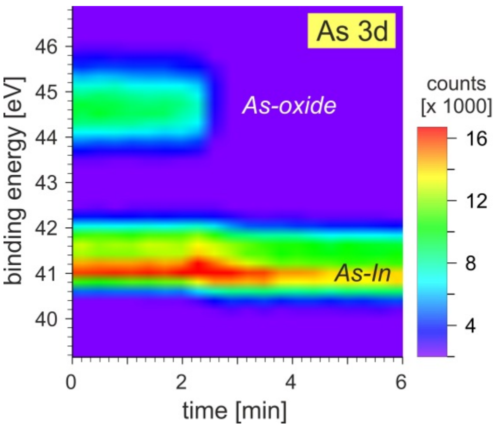

Figure 1: Time-resolved As 3d spectra, obtained during TDMA-Hf deposition.

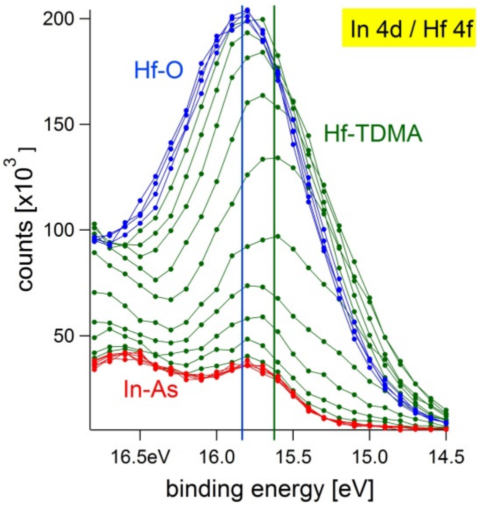

Figure 2: Subsequent Hf 4f / In 4d XPS spectra obtained during TDMA-Hf deposition, showing spectra before (red), during (green) and after (blue) the reaction.

Impact of D_2 High-pressure Annealing onto InGaAs MOSCAPs with Al_2O_3/HfO_2

[1]J. S. Kim*, [2]S.-H. Shin, [1]D. K. Kim, [3]Y. D. Cho, [3]C.-S. Shin, [3]W.-K. Park, [4]E. Chiu, [4]M. Rivera,
[4]J. I. Lew, [1]J. H. Lee, [2]S. K. Banerjee, [5]T.-W. Kim, and [1]D.-H. Kim

[1]School of Electrical Engineering, Kyungpook National University, Daegu, South Korea
[2]University of Texas at Austin, TX, USA
[3]KANC, Suwon, South Korea
[4]PoongSan Inc., CA, USA
[5]SEMATECH, NY, USA
*Email : dae-hyun.kim@ee.knu.ac.kr, TEL : +82-53-950-7844

INTRODUCTION: To fully benefit from using high-mobility III-V channel materials in InGaAs MOSFETs, it is important to minimize the interface trap density (D_{it}) at the III-V gate stack interface which degrades subthreshold-swing (SS), carrier transport property at ON-state and hence I_{ON}/I_{OFF} ratio [1]. Furthermore, the charge-trapping in dielectrics, so called 'Border-Traps', can cause a frequency dispersion and threshold voltage (V_T) shift from the reliability perspective [2-3]. However, it is difficult to achieve sub-1-nm EOT and low leakage current with a single dielectric material due to the inherent trade-off between band-gap and dielectric constant. Therefore, bi-layer gate stacks, such as Al_2O_3/HfO_2, have been explored from the EOT scaling and leakage current perspective [4]. In this paper, we address the benefit of high-pressure-annealing (HPA) on D_{it} in planar InGaAs MOSCAPs with Al_2O_3/HfO_2 stack, in an effort to further improve the quality of the high-k and InGaAs interfaces.

EXPERIMENT/RESULT: ***Figure 1*** shows a cross-sectional schematic and band diagram of $In_{0.53}Ga_{0.47}As$ MOSCAPs with bilayer Al_2O_3/HfO_2 gate stack. The layer structure is grown by molecular beam epitaxy (MBE) on InP substrate. From top to bottom, the epi wafer consists of an n-$In_{0.53}Ga_{0.47}As$ channel (300 nm) and an n^+ $In_{0.53}Ga_{0.47}As$ contact (150 nm), on n^+ InP (100) substrate. The device fabrication is similar to our previous report [3]. Using a diluted HCl solution, the n- $In_{0.53}Ga_{0.47}As$ channel surface is cleaned, and ALD Al_2O_3/HfO_2 is deposited at 250 °C. Subsequently, a TiN metal gate is deposited with ALD system in an *in-situ* manner. Then, a Ti/Au gate metal pad is deposited by e-beam evaporation. Finally, High-pressure Annealing (HPA) is performed for the InGaAs MOSCAPs with process conditions of 400 °C, 100 % Deuterium (D_2) ambient, 20 atm and 30 minutes, using a "Poongsan GENI-SYS" equipment. ***Figure 2*** shows cross-sectional TEM images for the InGaAs gate stack before and after HPA. The TEM image for the sample with HPA shows a very sharp interface with an indistinguishable interfacial layer. ***Figure 3*** shows a hysteresis behavior of the capacitance-voltage (CV) responses for the InGaAs MOSCAPs. The MOSCAP with HPA process exhibits less hysteresis behavior in CV. In fact, the hysteresis decreases from 84 mV to 72 mV after D_2 HPA, meaning that the HPA process helps to decrease the D_{it} at the interface. ***Figure 4*** shows multi-frequency CV responses for the MOSCAPs before and after D_2 HPA process. Note that a frequency dispersion in an accumulation regime also decreases after D_2 HPA process, revealing that trap densities inside the high-k dielectric layers, so called "border traps", also decrease. ***Figure 5*** shows the extracted D_{it} for the MOSCAPs with Al_2O_3/HfO_2 before and after D_2 HPA, using a conductance method [5]. Consistent with the improvement in the border traps, the value of D_{it} considerably improves from 7×10^{11} $cm^{-2}eV^{-1}$ to 4.2×10^{11} $cm^{-2}eV^{-1}$ after D_2 HPA. To the knowledge of the authors, the value of D_{it} achieved in this work is the lowest ever reported. Indeed, the HPA process in this work would be an effective remedy to reduce both interfacial and oxide trap densities of the InGaAs/high-k gate stacks in InGaAs MOSFETs.

CONCLUSION: We have investigated the effect of D_2 HPA process onto the InGaAs MOSCAPs with Al_2O_3/HfO_2 gate stack. We find that D_2 HPA process is effective in reducing both border trap and interfacial trap densities. We believe that the HPA process in this work will also be beneficial for future non-planar InGaAs MOSFET architectures and a backbone to overcome the reliability issues of InGaAs MOSFETs..

Acknowledgement : This work was supported by the BK21 Plus project funded by the Ministry of Education, Korea (21A20131600011).

We0940

Impact of surface treatments on high-k dielectric integration with Ga-polar and N-polar GaN

C.R. English[1], V.D. Wheeler[2], Nelson Y. Garces[3], Neeraj Nepal[4], Anindya Nath[5], Jennifer K. Hite[2], Michael A. Mastro[2], Charles R. Eddy, Jr.[2]

[1]University of Wisconsin, Department of Chemistry, 1101 University Avenue, Madison, WI 53706

[2]Electronics Science & Technology Division, U.S. Naval Research Laboratory, 4555 Overlook Ave., SW, Washington DC 20375

[3]U.S. Patent & Trademark Office, Alexandria, VA 22314

[4]Sotera Defense Solutions, 2200 Defense Hwy. Suite 405, Crofton, MD 21114

[5]American Society for Engineering Education, 1818 N Street NW, Washington, DC 20036, residing at NRL

Gallium- and nitrogen-polar GaN surfaces are subjected to a variety of pretreatments, including oxidation, before the application of high-k dielectrics by atomic layer deposition (ALD) in order to assess the “best” preparation of smooth, clean and electrically high-performing dielectric semiconductor interfaces. In terms of topographical and chemical cleanliness, a pretreatment with a wet chemical piranha etch (H_2SO_4:H_2O_2) was found to be optimum for both surfaces and, additionally, $(NH_4)_2S$ is effective for N-polar surfaces. Both thermal and plasma oxidations were employed for controlled growth of native oxides. For Ga-polar surfaces, all native oxides were as smooth as pretreated surfaces, while for N-polar surfaces all native oxides are much rougher except for very short, high temperature oxidations. ALD Al_2O_3 films on Ga-polar surfaces are smoother for pre-treated surfaces than for as-received surfaces, whereas for N-polar surfaces the opposite is true. In general, ALD HfO_2 films on Ga-polar surfaces are rougher (0.8 nm rms) than Al_2O_3 films (0.1 nm rms), whereas for piranha treated N-polar surfaces HfO_2 films are smoother than Al_2O_3 films. For Ga-polar surface, capacitance-voltage measurements of simple Al_2O_3 (measured k = 9) capacitors show the smallest hysteresis for unintentionally oxidized surfaces (0.37 V), whereas simple HfO_2 (measured k = 14) capacitors show the smallest hysteresis for a thermal GaO_x at the interface (0.1 V). In both cases, the thicker the GaO_x at the interface the larger the negative threshold voltage shift – suggesting an electron trap. Calculated total trapped charges associated with the dielectrics range from 3.2×10^{11} cm^{-2} (for HfO_2 on thermally oxidized GaN) to 1×10^{12} cm^{-2} for Al_2O_3 on thermally oxidized GaN and HfO_2 on plasma oxidized GaN. Finally, the leakage current density for nearly all capacitors is <10^{-5} A-cm^{-2} for up to a +8V bias.

We0950 Late News

Film-substrate interfacial engineering for accurate determination of the near-bandgap optical properties using spectroscopic ellipsometry

Sukgeun Choi[1], Jian Li[2], and Ingrid L. Repins[3]

[1]Department of Electrical and Computer Engineering, University of California, Santa Barbara, CA 93106, USA

[2]Department of Physics and Astronomy and Wright Center for Photovoltaic Innovation and Commercialization, University of Toledo, Toledo, OH 43606, USA

[3]National Renewable Energy Laboratory, Golden, CO 80401, USA

For the development of high-performance photonic and photovoltaic devices, accurate knowledge of near-bandgap (E_0) optical properties is of great importance. To measure the E_0, photoluminescence (PL) and optical absorption spectroscopy are frequently used. However, it is often challenging to unambiguously identify the origins of PL peaks when multiple peaks associated with various types of defect structures present. To estimate the E_0 in optical absorption spectrum, on the other hand, a straight segment of the absorption coefficient curve needs to be defined, which is somewhat arbitrary process leading to an inaccurate value.

Spectroscopic ellipsometry (SE) is known to be an excellent technique of determining optical function spectra over a wide range of photon energy. In SE measurements of thin films grown on flat substrates, the light reflected from the film surface and film/substrate interface interferes with each other and generates oscillatory patterns below the E_0 of the film. In theory, the multilayer modeling procedures can remove the thickness fringes and the E_0 energy can be obtained. In practice, however, a number of non-idealities, such as 1) possible formation of unidentified thin interfacial layer between the film and substrate and 2) unknown optical characteristic of the substrate, exist that makes accurate determination of the near-E_0 optical function data a nontrivial task and the model-determined E_0 energy can be influenced by the types of model functions and initial parameters.

To reduce complications in mathematical modeling of SE data and improve the accuracy of results, a direct method has recently been developed. Here, the front surface of substrate is first mechanically roughened using abrasive alumina powder followed by the deposition of a film on top of it. During SE measurement, the probing light penetrating through the film scatters in random directions at the roughened substrate surface, which suppresses the secondary reflections from the film/substrate interface. Consequently, the thin film can now be treated as a “pseudobulk” whose optical thickness is semi-infinite, and the E_0 is directly seen without being obscured by the oscillatory patterns.

In this presentation, we demonstrate successful applications of the pseudobulk method in SE studies of several polycrystalline thin-film photovoltaic absorber materials. We also discuss the technical merits, detailed procedures, and limitations.

Probing Human Pluripotent Stem Cell Neurons: Electrical Modeling and Physiological Measurements

Ahmed T. E. Youssef,[1] Renjie Chen,[1] Ren Liu,[1] Sang Heon Lee,[1] Massoud L. Khraiche,[1] Sandy Hinckley,[2] Yoontae Hwang,[1] Atsunori Tanaka,[3] Yun Goo Ro,[1] Keisuke Matsushita,[3] Anne Bang,[2] and Shadi A. Dayeh[1,3,★]

[1]Integrated Electronics and Biointerfaces Laboratory
Department of Electrical and Computer Engineering, University of California San Diego, 9500 Gilman Dr., La Jolla CA 92093

[2]Conrad Prebys Center for Chemical Genomics
Sanford Burnham Prebys Medical Discovery Institute
10901 North Torrey Pines Road, La Jolla CA 92037

[3]Graduate Program of Materials Science and Engineering, University of California San Diego, 9500 Gilman Dr., La Jolla CA 92093

Electro-neural interfaces play the most crucial role in elucidating the fundamental mechanisms of mapping and processing neuronal activities that can open the gate for a wide range of applications in electrophysiology and drug screening. The development of such electro-physiological technologies at the nanometer scale involves homogenous blend of neuro-science and engineering ranging from understating the cell physiology, firing mechanisms through ion channels, and the response to different stimulation techniques, up through system level modeling and signal processing. In this paper, we report on electrophysiological measurements on human cortical and induced pluripotent stem cell (iPSC) derived neurons. A detailed electrical model is developed that accounts for the electrochemical effects and parasitic components along the recording's path. In addition, the model accounts for the dynamic process of firing an action potential (AP) by considering specific Na+ and K+ ionic current conductances through the cell membrane which in turn dictate the temporal response of the system.

The electro-neural interface system is divided into three stages i) the neural cell membrane, ii) the electrolyte/electrode interface, and iii) the sensing amplifier, each stage is characterized separately.

The model is mostly constructed of elementary electrical components of resistors and capacitors and their values are derived based on specific characterization techniques at the respective interface. The signal processing and analysis are carried out in both time and frequency domain, where an overall all transfer function (TF) is derived to quantify the network's effect on the frequency ranges of interest for the physiological recording. Deconvolution method is used to reverse such effects quantified by the overall TF of the system, and validated against Cadence TCAD simulations. In addition, a parametric study for individual network components and their impact on the recordings coupling coefficient is included that gives insights about the quality of physiological measurements with technology scaling.

We1000 Late News

Strain Engineering for Beyond 10 µm Thick Crack-Free GaN Growth on Si for High Power Device Applications

Atsunori Tanaka, Renjie Chen, and Shadi A. Dayeh
Univ. of California San Diego
Department of Electrical and Computer Engineering
La Jolla, California 92093, USA
Phone: +1-858-534-5171 E-mail: sdayeh@ece.ucsd.edu

GaN holds a great potential for next generation efficient high power devices due to a number of attributes including the large bandgap which can support high breakdown fields and small thermally generated leakage currents, and high carier density and mobility/saturation velocity which provide low dynamic on-resistance. However, due to the relatively high cost of bulk GaN and the lack of appropriate substrate for its monolithic integration, the full potential of GaN for commercial applications is yet to be realized. One approach that has potential for a disruptive high power GaN technology is its growth on cheap and technologically well-developed substrates such as Si. However, the growth of thick GaN layers on Si is hindered by the thermal (and lattice) mismatches which result in generating cracks in the GaN layer for thicknesses exceeding ~3 µm and using well-optimized AlGaN transition layers.

In this work, we analyzed the selective area growth (SAG) of GaN on Si and performed mechanistic studies to understand cracking associated with thermal stresses and created structures to accommodate them in order to grow over 10 µm thick crack-free GaN on Si in circular openings in SiO_2 with diameters of over 350µm. We observed that cracks are initiated on $\{1\bar{1}00\}$ planes and propagate in $<1\bar{2}10>$ directions. We therefore have grown structures that have $\{1\bar{1}01\}$ which shared dislocation burgers vectors with $\{\bar{1}010\}$ plane and relieve the stresses in the $<1\bar{2}10>$ orientation. Our time-dependent growth and facet evolution supported our hypothesis of stress relaxation. In addition, our SAG on different mask patterns further validated the importance of having the $\{1\bar{1}01\}$ facet planes. While our optimized mask design eliminated cracks in GaN by minimizing the thermal stress in the grown GaN layer, the stress in turn concentrated in the Si substrate and cracking in Si was observed for some dots. We then studied the cracking in the Si substrate and minimized the cracks by engineering the base Si substrate. Using these techniques, thick crack-free GaN structures on the Si substrate were obtained. The Selective area diffraction (SAD) by high resolution TEM verified the high crystalline quality throughout the structure of the 10 µm thick GaN and indicated a dislocation density is $2\text{-}3\times10^{8}$ cm^{-2} at the GaN surface, comparable to and lower than that in highly efficient GaN light emitting diodes on sapphire. Schottky diodes with 10 µm thick GaN on Si has potential to have very high breakdown voltages in excess of 1kV; our devices have not yet reached this milestone. The Schottky diode fabrication and electrical characteristics will be reported.

Ex-situ and In-situ TEM studies of Ni-InGaAs reaction in InGaAs Fins

Renjie Chen, and Shadi A. Dayeh
Department of Electrical and Computer Engineering
University of California, San Diego, La Jolla, CA, United States

The Ni-InGaAs (nickelide) contact technology has been demonstrated as a suitable self-aligned contact technology for InGaAs channels with record small specific contact resistivity.[1] However, little studies focused on the contact metallurgy specific to ultra-scaled devices at nanoscale, where crystal orientation, size, and structural phase play dominant roles in the reaction kinetics and thermodynamics and the resultant morphology and interfaces determine the device performance. Here, we utilized a novel wafer bonding technique to transfer thin (50 nm) $In_{0.53}Ga_{0.47}As$ layers onto SiO_2/Si substrates and onto SiO_2/Si transmission electron microscopy (TEM) aperture frames, and fabricated the InGaAs Fin channels with variable widths and orientations through a combination of electron-beam lithography and top-down dry etching steps.[2] After Ni contact deposition at the two ends of InGaAs Fin channels, the solid-state reaction was performed under rapid thermal annealing (RTA) in a furnace for ex-situ TEM studies on focused ion beam (FIB) cut samples. The interfacial relationship was found to be $Ni_4InGaAs_2$ (0001) || $In_{0.53}Ga_{0.47}As$ (111) with a single $Ni_4InGaAs_2$ phase whose [0001] axis exhibit a peculiar rotation away from the nickelide/InGaAs interface due to surface energy minimization. This crystalline interfacial relationship is responsible for introducing a uniaxial height expansion of 33% ± 5% in the formed nickelide segments.

Samples fabricated on the SiO_2/Si TEM aperture frame were directly annealed inside the TEM chamber with a Gatan in-situ heating stage. The nickelide ledge was found to propagate along the (111) plane of InGaAs, and the nickelide nucleus predominantly starts at the interface in between the gate dielectrics and InGaAs Fins with each step of few atomic layers. Interestingly, different gate dielectrics altered the nucleation and ledge propagation behaviors due to the varying bond strength at the dielectric/InGaAs interface. The COMSOL simulation further suggested that the stress built up during nickelide formations may further tune the nickelide/InGaAs interface profiles beside the crystallographic preferred interface, providing the way to engineer the interface strain. These timely observations advance our understanding and development for self-aligned contacts to III-V nanochannels, and for engineering new processes that can maximize their device performance.

1. Abraham, M.; Yu, S.-Y.; Choi, W. H.; Lee, R. T.; Mohney, S. E. *Journal of Applied Physics* **2014,** 116, (16), 164506.

2. Dai, X.; Nguyen, B. M.; Hwang, Y.; Soci, C.; Dayeh, S. A. *Advanced Functional Materials* **2014,** 24, (28), 4420-4426.

3. Chen, R.; Dayeh, S. A. *Nano Lett.*, **2015**, 15 (6), 3770–3779.

Mechanistic studies for the development of thin Si microwire solar cells for wearable electronics

Yun Goo Ro, Renjie Chen, Ahmed T. E.-T. Youssef, Namseok Park, Ren Liu and Shadi A. Dayeh

Univ. of California San Diego
Department of Electrical and Computer Engineering
La Jolla, California 92093, USA
Phone: +1-858-534-5171 E-mail: sdayeh@ece.ucsd.edu

It is well recognized that one of the main obstacles to overcome for flexible and wearable electronic devices is power management. This work seeks the development of the fundamental science that is required to realize thin Si solar cells that are co-integrated side by side with processing electronics for compact, flexible, and wearable electronics.

Silicon microwire solar cells have long promised reducing the optical absorption length in Si and enhancing photovoltaic activity in thin Si materials but have been limited to less than 10% power conversion efficiencies. Surface and Auger recombination losses of photogenerated carriers are the major components for degrading microwire solar cell performance. Controlling the microwire facets on crystal planes that are known to have low interface state densities may help in reducing surface recombination and recovering the promised performance of microwire solar cells. Here, we studied the solar cell performance in {100} and {110} square Si microwires and in arbitrary faceted Si circular microwires with similar surface area. We performed a systematic study to minimize the surface recombination effect by fabricating microwires with clean and smooth surfaces and we demonstrated that with appropriate surface passivation, solar cell performance can be enhanced from 3% to over 9% efficiency. Additional tuning of optical absorption and junction formation resulted in further increase of current density and efficiency to over 15%.

To enable this relatively high efficiency, we performed systematic studies to investigate the effect of structural design of Si microwire array in surface recombination and to determine the optimal design can yield the highest efficiency. We have first changed the diameter of Si microwires (2, 4, 6, 8, 10 μm) and then changed the side-to-side spacing of each Si microwire by 2, 4, 6, 8 μm for a fixed diameter of 2 μm. We found that as the diameter and spacing become bigger, the open circuit voltage increases. This is due to the fact that the entire surface area of each microwire array decreases resulting in lower recombination currents and therefore higher open circuit voltage. At the same time, the current density decreased due to a red shift in the absorption spectrum that reduces the absorbed photon flux. These dependencies indicate that there are tradeoffs between short circuit current density and open circuit voltage in choosing the optimal design. With our current iterations, 10 μm high vertical junction Si microwire solar cells resulted in efficiency of > 15 % for the best performing device.

Wednesday Morning

Novel Semiconductors

We1100

Temperature-dependent photoluminescence studies of $Ge_{1-y}Sn_y$ direct bandgap semiconductors

Mee-Yi Ryu[1], Thomas R. Harris[2], Buguo Wang,[2] Yung Kee Yeo[2] and John Kouvetakis[3]

[1]Kangwon National Univ.

1 Kangwondaehak-gil, Chuncheon, Kangwon-do 200-701, Korea

[2] Air Force Institute of Technology

2950 Hobson Way, Wright-Patterson AFB, OH 45433, USA

[3]Arizona State Univ.

551 E University Dr, Tempe, Arizona 85287, USA

A significant breakthrough has been made on device quality $Ge_{1-y}Sn_y$ material growth and optical and electrical characterization has been reported by several research groups. As a result of intensive effort, Si photonics has achieved significant progress through the development of Si-based various devices such as light emitting diode, laser diodes, and photodetectors. Furthermore, the lasing in direct-bandgap GeSn alloy grown on Ge-buffered Si was demonstrated at low temperatures and relatively high optical pumping, and the indirect-to-direct bandgap transition was found at ~9% Sn for fully relaxed samples. In spite of the tremendous recent progress in crystal growth and device fabrication of the $Ge_{1-y}Sn_y$ and $Ge_{1-x-y}Si_xSn_y$ materials, the development of true direct bandgap semiconductors from these Ge-Si-Sn systems is still far from complete, and most of the important properties of these materials are largely remained uncharacterized. Recently, the temperature- (T-) and excitation laser power-dependent photoluminescence (PL) studies for $Ge_{1-y}Sn_y$ alloys with various Sn compositions up to 10% have been carried out. From indirect $Ge_{1-y}Sn_y$ alloys with lower Sn compositions than the crossover values, the dominant direct PL emissions were observed at higher temperatures (Ts) up to room temperature due to the thermally populated carriers into the direct band (Γ valley), indicating the competition between the indirect and direct band transition. Moreover, the strain-split direct band transitions to the light-hole and heavy-hole bands for the tensile-strained GeSn (0.03% Sn) were demonstrated by the comprehensive PL studies with varying excitation power and temperature. Compared the optical characterization studies of these $Ge_{1-y}Sn_y$, the electrical properties have been investigated very few. For the successful development of electronic and optoelectronic devices based on $Ge_{1-y}Sn_y$ alloys, it is very important to know the electrical and optical properties of $Ge_{1-y}Sn_y$. Therefore, T-dependent PL and Hall-effect measurements have been made on $Ge_{1-y}Sn_y$ alloys grown on Ge-buffered Si substrates as a function of Sn composition from 1.7% to 7.5%. The direct (E_D) emission PL peak associated with the direct transition from the minimum of conduction band (Γ-valley) to the maximum of valence band starts to appear for the $Ge_{1-y}Sn_y$ with Sn of 5.2% at 10 K while at 300 K all $Ge_{1-y}Sn_y$ samples with Sn content of 1.7%-7.5% exhibit the predominant E_D emission. In spite of the fact that the $Ge_{1-y}Sn_y$ alloys with lower Sn (≤5.2%) are still indirect material, the superior E_D emission is obtained from the $Ge_{1-y}Sn_y$ alloys with lower Sn (≤5.2%) under certain conditions such as high excitation density and/or high temperature, indicating the competition between the direct and indirect transition. The T-dependent electron concentration increases initially from 10 K, indicating no degenerate conducting layer relevant to dislocation density, and then raises more rapidly at higher temperatures due to the ionization of deeper donors. These T-dependent PL and Hall-effect results show that the optical and electrical properties of $Ge_{1-y}Sn_y$ alloys are strongly dependent on temperature. It should be taken into account for the development of optoelectronic and electronic devices.

Silicon-Germanium-Tin Semiconductors: Growth and Properties

J.-H. Fournier,[1] S. Mukherjee,[1] B. Meynard,[1] M. Fortin-Deschênes,[1] S. Wirths,[2], J. M. Hartmann,[3] P. Desjardins,[1] D. Buca,[2] and O. Moutanabbir[1],*
1: Department of Engineering Physics, Ecole Polytechnique de Montreal, Montréal, C.P. 6079, Succ. Centre-Ville, Montréal, Québec H3C 3A7, Canada
2: Peter Grünberg Institute 9 and JARA-FIT, Forschungszentrum Juelich, 52425 Juelich, Germany
3: CEA, LETI, Minatec Campus, 17 rue des Martyrs, 38054 Grenoble, France
4: Département de Chimie, Université de Montréal, C.P. 6128, succ. Centre-Ville, Montréal, (Québec), Canada H3C 3J7

*Corresponding authors: oussama.moutanabbir@polymtl.ca

Compound semiconductor alloys have been successfully used for a precise and simultaneous control of lattice parameters and bandgap structures bringing to existence a variety of functional heterostructures and low-dimensional systems. Extending this paradigm to group IV semiconductors will be a true breakthrough that will pave the way to creating an entirely new class of silicon-compatible electronic, optoelectronic, and photonic devices. With this perspective, germanium-tin ($Ge_{1-x}Sn_x$) and germanium-silicon-tin ($Ge_{1-x-y}Si_xSn_y$) alloys have recently been the subject of extensive investigations as new material systems to independently engineer lattice parameter and bandgap energy and directness. The ability to incorporate Sn atoms into silicon and germanium at concentrations about one order of magnitude higher than the equilibrium solubility is at the core of these emerging potential technologies. In this presentation, we will address the epitaxial growth and stability of these metastable semiconductors. We will also discuss the optical and electronic properties as well as the nature of the atomic order in Sn-rich $Ge_{1-x-y}Si_xSn_y$. Moreover, based on *in situ* electron microscopy, we will present real time studies of their thermal behavior which reveal unprecedented insights into the key phenomena that govern the thermal decomposition and phase separation in these materials. These studies define the temperature window for the processing of $Ge_{1-x-y}Si_xSn_y$ -based devices.

We1110

Investigation of the half-Heusler CoTiSb/III-V heterointerfaces

S. D. Harrington,[1] A. Rice,[1] T. McFadden,[2] J. K. Kawasaki,[1]
and C. J. Palmstrøm[1,2]

[1]*Materials Department, University of California, Santa Barbara, CA*
[2]*Department of Electrical & Computer Engineering, University of California, Santa Barbara, CA*

Half-Heusler compounds are an exciting class of intermetallics due to their diverse electrical and magnetic properties, including semiconducting [1], half metallic [2], and thermoelectric [3]. Additionally, a number of the half-Heusler compounds have been predicted to be topological insulators [4]. Their crystal structure and lattice parameters are closely related to III-V compound semiconductors, suggesting the possibility of half-Heusler/III-V semiconductor heterostructures with unique properties. Integration of epitaxial half-Heusler compounds with existing III-V technologies requires a deeper understanding of their interface. Most experimental studies of half-Heusler compounds have been limited to bulk polycrystalline samples, which cannot be used for measurements of interface properties. CoTiSb has been extensively studied in the bulk and recently in molecular beam epitaxy (MBE) grown films where record high carrier mobilities were demonstrated [5]. However, no studies to date have measured the interface properties and resulting electrical characteristics.

In this presentation, the heterointerfaces formed between the semiconducting half-Heusler CoTiSb with the III-Vs InAlAs and InGaAs are investigated. Lattice matched $In_{0.52}Al_{0.48}As$ and $In_{0.53}Ga_{0.47}As$ layers were epitaxially grown on InP (001) substrates in a dedicated III-V MBE system. The epitaxial CoTiSb layers were grown in a separate dedicated MBE system. The valence-band discontinuities in abrupt CoTiSb/InGaAs and CoTiSb/InAlAs heterojunctions were determined using x-ray photoemission spectroscopy (XPS). By combining these measurements with available XPS valence band offsets for $In_{0.52}Al_{0.48}As/In_{0.53}Ga_{0.47}As$, we find that the band offset transitivity is satisfied. Here it was found that CoTiSb has a type I and type II band alignment with InAlAs and InGaAs respectively. Using these results, a variety of heterojunctions between CoTiSb and the III-Vs were designed and grown. Heterointerfaces between CoTiSb (intrinsically n-type) and n-InGaAs, p-InGaAs, and unintentionally doped InGaAs were formed. Temperature dependent vertical transport I-V measurements of the n-n and n-p structures were performed for etched mesas of a variety of sizes. The n-n heterostructures display Ohmic behaviour at room temperature, but small variations are observed at 30K indicative of a small barrier present at the interface. Current rectification is present in the n-p heterojunctions in good agreement with expectations from the band-offset measurements. Temperature and area dependence of measured I-V characteristics will be discussed.

[1] H. Kandpal, C. Felser, and R. Seshadri, J. Phys. D. Appl. Phys. **39**, 776 (2006).
[2] M. Katsnelson, V. Irkhin, L. Chioncel, a. Lichtenstein, and R. de Groot, Rev. Mod. Phys. **80**, 315 (2008).
[3] S. Chen and Z. Ren, Mater. Today **16**, 387 (2013).
[4] H. Lin, L. A. Wray, Y. Xia, S. Xu, S. Jia, R. J. Cava, A. Bansil, and M. Z. Hasan, Nat. Mater. **9**, 546 (2010).
[5] J. K. Kawasaki, L. I. M. Johansson, B. D. Schultz, and C. J. Palmstrøm, Appl. Phys. Lett. **104**, (2014).

This is work was supported by ARO W911NF-12-1-0459, ONR-NSSEFF N0014-15-1-2845 and NSF graduate student research fellowship

We1115

Half-Heusler/Heusler Interfaces: Stability and Electronic Properties

A. D. Rice,[1] **S.D. Harrington**[1], **J. K. Kawasaki**,[1] **N. Verma**[2], **B. D. Schultz**,[3] **and C. J. Palmstrøm**[1,3+]
[1]*Materials Department, University of California Santa Barbara*
[2]*Material Research Laboratory, University of California Santa Barbara*
[3]*Department of Electrical and Computer Engineering, University of California Santa Barbara*

The Half Heuslers are an attractive family of compounds for a number of applications due to their wide range of properties, including half-metals and topological insulators. In particular, those containing 18 valence electrons per formula unit typically show a semiconducting band gap. [1]. This all suggests the possibility of a single multifunctional structure with the same crystal structure throughout to be synthesized. An understanding of their interfaces will be critical for structural stability as well as to account for possible effects separate from bulk behavior, such as in GaAs/AlGaAs, ZnO/ZnMgO, and a number of perovskite oxide systems.

Using the Ni-Ti-Sn system, which contains both a narrow-band gap semiconducting hH phase and a metallic fH phase, we report the growth of hH/fH layered structures along with a study of their strain, stability, and electronic properties. Relaxation appears to occur via misfit dislocation formation above the predicted critical thickness predicted by Matthews-Blakeslee. Structures remain stable after 12 hour anneals through at least 550°C, with signs of roughening and strain but no detectable intermixing, confirmed with both Rutherford backscattering spectroscopy and TEM-EDS.

Layered structures with CoTiSb, another 18 valence electron semiconducting half-Heusler, have also been successfully grown. The structures are metallic with sheet densities that double in magnitude going from 20K to 300K and are orders of magnitude lower than typical values for either pure semiconductor structure. XPS has been performed to understand electronic interaction and interface stability and gives an approximate band offset resulting in a type-II interface. Further investigation is underway to determine the exact nature of this behavior.

This work was supported in part by the ARO (W911NF-12-1-0459) and NSF-MRSEC (DMR-1121053). The UCSB MRL Shared Experimental Facilities are supported by the MRSEC Program of the NSF under Award No. DMR 1121053; a member of the NSF-funded Materials Research Facilities Network. A part of this work was performed in the UCSB Nanofabrication Facility which is a part of the NSF funded National Nanotechnology Infrastructure Network.

[1] T. Graf, C. Felsar, and S. Parkin. Progress in Solid State Chemistry 39 (2011) 1-50

+ Author for correspondence email: cpalmstrom@ece.ucsb.edu

Wednesday Morning

2D Materials II

We1120 Upgraded

2D Nitrides beyond hBN: The case of 2D GaN

Zakaria Y. Al Balushi[1,2,*], Ke Wang[3], Ram Krishna Ghosh[2,4], Rafael A. Vilá[1,2], Sarah M. Eichfeld[1,2,3], Dennis F. Paul[5], Suman Datta[2,3,4], Joshua A. Robinson[1,2,3,a] and Joan M. Redwing[1,2,3,4,b]

[1] *Department of Materials Science and Engineering, The Pennsylvania State University, University Park, PA 16802*
[2] *Center for 2-Dimensional and Layered Materials, University Park, PA 16802*
[3] *Materials Research Institute, University Park, PA 16802 USA*
[4] *Department of Electrical Engineering, The Pennsylvania State University, University Park, PA 16802*
[5] *Physical Electronics USA, 18725 Lake Drive East, Chanhassen, MN, 55317*

* Presenting author.
Corresponding authors: [a] e-mail: jrobinson@psu.edu; [b] e-mail: jmr31@psu.edu

In recent years, the spectrum of two-dimensional (2D) and layered materials “beyond graphene” has been continually expanding. The realization of wide bandgap 2D layered materials “beyond hexagonal boron nitride (hBN)”, however, has been limited. Group-III nitride semiconductors such as indium nitride (InN), gallium nitride (GaN), and aluminum nitride (AlN) are proposed to have thickness tunable energy bandgaps ranging from ~0.7 – 7.0 eV as a result of quantum confinement. Despite the immense computational discovery of 2D materials, the synthesis of 2D III-nitrides “beyond hBN” is still elusive. Here we demonstrate experimentally, for the first time, that 2D atomic layers of GaN not only can be stabilized, but also exhibit extraordinary properties from that of bulk material. Our work utilizes a novel migration enhanced encapsulated growth process that involves the use of graphene. We elucidate the mechanism of 2D GaN formation and discuss graphene’s ability in providing sufficient thermodynamic stabilization of the (direct bandgap) 2D buckled structure both experimentally and theoretically with density functional theory (DFT). Our results from high resolution auger electron spectral mapping and energy-dispersive x-ray spectroscopy in an aberration corrected transmission electron microscope (TEM), provides evidence that during growth process, a layer of gallium intercalates between graphene and the supporting substrate, and is subsequently nitrided to form crystalline 2D GaN. Theoretically we show that current 2D GaN models may not properly describe the layered crystal structure, in which we verify our findings from the positions of the (heavy and light) atomic columns in the 2D GaN structure using aberration corrected scanning TEM (STEM) in annular bright field (ABF) mode. Additionally, we correlate theoretical results with experimental spectroscopy and show bandgap tunability in GaN due to quantum confinement. Our results demonstrate a pathway towards stabilizing new 2D III-nitrides that are not naturally layered in bulk crystals. Recognizing the impact of 2D III-nitrides, it can be expected that the addition of 2D GaN and related materials will open up new avenues of research in novel electronic and optoelectronic devices, such as miniaturized deep ultra violet (DUV) light emitters and lasers, composed of new heterostructures of 2D atomic layers of group III-nitride semiconductors.

We1140

Observation of friction between gold nanocrystals and graphene using quartz crystal microbalance

Michael Lodge, Brandon Blue, B.D. Dawson and Masa Ishigami

Department of Physics and Nanoscience Technology Center, University of Central Florida, Orlando, FL 32816

A simple phenomenological formula, $F = \mu N$, where μ is the coefficient of friction and N is the normal force, governs macroscopic friction. Nanoscale contacts between surface asperities are assumed to determine μ, but the fundamental science of friction at the nanoscale is still in its infancy. From an engineering standpoint nanoscopic friction at speeds between 1 mm/s and 1 m/s are most technologically relevant. However, existing experimental methods are limited to slower speeds, and theoretical methods are limited to systems that are too small to realize experimentally at these speeds [1].

Our recent results using quartz crystal microbalances (QCM) show that experimental measurements of nanoscale friction at speeds up to 1 m/s are possible [2]. QCMs are thin quartz crystal disks that oscillate in shear mode when an oscillating voltage is applied across them. Surfaces of QCMs can reach peak velocities of m/s with amplitudes in the range of 1-10 nm. QCMs are extremely sensitive to mass adsorption and changes in dissipation at the surface because of their high quality factors. We used the QCM technique to measure the friction of gold nanocrystals with a narrow diameter distribution on graphene, which acts as a model system, to enable simulations that precisely match experimental parameters. We measure that the sliding nanocrystals exhibit viscous friction behavior with a drag coefficient of $\xi = 3 \times 10^{-13}$ kg/s.

This work is based upon research supported by the National Science Foundation under Grant No. 0955625.

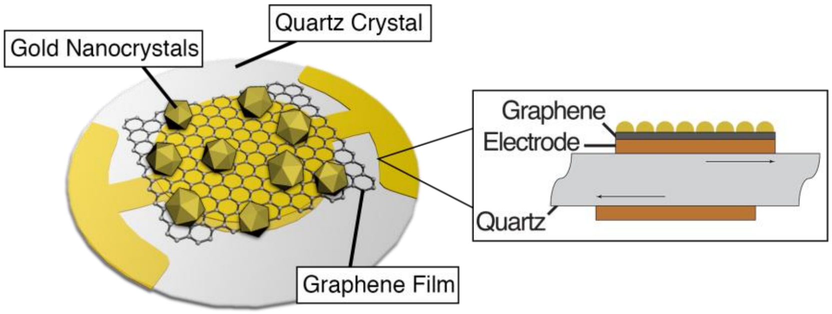

Figure 1| Graphene-laminated QCM with gold nanocrystals. (Inset) Cutaway view illustrating layer ordering and motion of the quartz

References

1. Y. Dong, Q. Li, and A. Martini, *Molecular dynamics simulation of atomic friction: A review and guide.* Journal of Vacuum Science & Technology A, 2013. **31**: p. 030801.
2. M.S. Lodge, B.T. Blue, C. Tang, W.A. Hubbard, B.C. Regan, A. Martini, B.D. Dawson, and M. Ishigami, *Direct measurement of friction between gold nanocrystals and graphene using quartz crystal microbalance.* In preparation, 2015.

We1145

Development of Water Soluble Polyvinyl Alcohol Assisted Transfer Technique for 2-Dimensional Materials for High-performance Graphene Field Effect Transistors

Huynh Van Ngoc and Dae Joon Kang*

Department of Physics, Sungkyunkwan University, Suwon 440-746, Republic of Korea

Abstract

Hexagonal boron nitride (h-BN) has emerged as an exceptional dielectric for graphene based field effect transistor (GFET). GFETs based on mechanically exfoliated h-BN dielectric were found to exhibit an order of magnitude improvement in device mobility, reduced carrier in-homogeneity, lower extrinsic doping, reduced chemical reactivity, and improved high-bias performance when compared to FET devices fabricated with conventional oxide dielectrics. However, the chemical vapor deposition (CVD) growth of h-BN dielectric has not been fully explored yet for high-performance GFETs. This is mainly due to residues originated from incomplete etching of polymethylmethacrylate (PMMA) during a typical PMMA-assisted transfer on to the surface of transferred h-BN. This creates additional trapping sites, thus degrading the performance of GFETs. In this report, we demonstrate that GFETs based on CVD grown h-BN dielectric layer can show excellent electrical properties by adding a water soluble polyvinyl alcohol (PVA) layer in-between PMMA and 2D materials, graphene and h-BN. This transfer method allows not only an effective transfer of 2D materials to various target substrates with a high degree of freedom but also an metal etching-free process of PMMA-assisted-transfer, minimizing the effects of undesirable contaminations on the surface. This facile transfer technique presents a great potential for future research and application suitable for high performance large area mechanical, optical and electronic devices based on graphene/h-BN heterostructures.

---

* Corresponding author: djkang@skku.edu

Defect Controlled Addition of Nitrogen into Aromatic Configurations in CVD-Grown Graphene by Microwave Flowing Afterglow Plasma Exposure

Germain Robert Bigras[1], Leron Vandsburger[1], Luc Stafford[1] and Andranik Sarkissian[2]

[1]Département de Physique, Université de Montréal, Montréal, QC, Canada
[2]PLASMIONIQUE Inc, Varennes, QC, Canada

The tuning of graphene electronic properties via a fine and controlled Nitrogen doping is promising for multiple domains including: digital electronics, optoelectronic and bio-sensors. Using variable-bias ion bombardment on graphene enables a controlled formation of reactive defects and therefore the tuning of the number of sites where chemical bonds can be formed by Nitrogen [1,2]. The cleaning and reconstitution of graphene achieved by Nitrogen plasma treatment in combination to annealing processes allows the formation of surface engineered defect free Nitrogen doped graphene sheets [3]. Unlike wet-chemistry treatment, the plasma approach requires no acidic environment, is less time consuming, easily adapted to clean-room conditions in addition to being more eco-friendly. In this work, a dual source plasma system was developed to examine the role of defect density in determining aromatic nitrogen content in graphene films. A primary plasma source, consisting of a 600 MHz surface wave generator (surfatron) was used to produce an ion-rich argon plasma. A secondary source consisting of a 2.45 GHz surfatron was used to produce the nitrogen plasma flowing afterglow used for downstream treatment. In this system, samples were mounted in direct contact with a biased sample holder, which was biased at -100 VDC during exposure to Ar plasma. Based on literature published on defects in Ar ion treated graphene, a timeframe of 1-10 seconds of treatment under Ar bombardment conditions was investigated. All nitrogen treatment parameters where held constant to isolate the effect of ion bombardment treatment defect density. Following treatment, samples were analyzed by XPS and compared to data collected from untreated samples. High resolution XPS analysis demonstrated that treatment by ion bombardment prior to N_2 flowing afterglow exposure had a significant and dramatic effect on aromatic content. In particular, there was a 300% increase in pyridinic N content, while amine and pyridinic N content was relatively unaffected by Ar ion treatment. The largest change was seen in adsorbed N content in films. This phenomenon is explained by activation of the graphene film by ion bombardment, leading to an increase in the sticking coefficient and stabilization of N chemisorption processes. Over the first two seconds of Ar bombardment, the content of aromatic pyridinic N increases relatively linearly, which supports a hypothetical hypothesis of incorporation at point defects. The stability of amine bonding is explained by the fact that N_2 treatment parameters were held constant. These data represent a conclusive demonstration of defect-limited low energy incorporation of N atoms into graphene by downstream plasma treatment. Adsorbed and amine nitrogen content can be removed selectively by substrate transfer and thermal treatments, respectively. This allows the approach to produce a graphene film with significant aromatic N content as well as tightly controlled composition, through a completely integrated post-growth process.

[1] Imre Bertóti, Miklós Mohai, and Krisztina László, Carbon, 84:185–196, 2015.
[2] Lucchese, Márcia Maria, F. Stavale, EH Martins Ferreira, C. Vilani, M. V. O. Moutinho, Rodrigo B. Capaz, C. A. Achete, and A. Jorio, Carbon 48, no. 5 (2010): 1592-1597.
[3] Nikolaos Peltekis, Shishir Kumar, Niall McEvoy, Kangho Lee, Anne Weidlich, and Georg S. Duesberg. Carbon, 50(2):395–403, 2012.

We1155

Etching-free transfer of highly-aligned bottom-up graphene nanoribbon arrays on Au(788) template.

Manabu Ohtomo[1], Yoshiaki Sekine[1], Hiroki Hibino[1,2], and Hideki Yamamoto[1]

[1]*NTT Basic Research Laboratory, 3-1 Morinosato-Wakamiya, Atsugi, Kanagawa 243-0198, Japan*
[2]*Kwansei Gakuin University, 2-1 Gakuen, Sanda, Hyogo 669-1337, Japan*

Bottom-up fabrication of extremely-narrow graphene nanoribbons with seven carbon atoms across (7-ACGNRs) has been reported by utilizing on-surface polymerization and graphitization of 10,10'-dibromo-9,9'-bianthracene (DBBA) molecules[1] (Fig.1(i)). In this research, we present novel method to transfer highly-aligned, densely-distributed nanoribbon arrays grown on Au(788) template[2] onto SiO_2 surfaces. By utilizing intercalation of alkanethiol self-assembled monolayers (SAMs) between GNRs and Au, the densely-distributed GNR arrays are delaminated without etching Au single crystals.

The nanoribbon arrays were grown as described in previous reports[2]. As a support layer of GNRs during transfer process, hydrogen silsesquioxane (HSQ) film was spin-coated and annealed at 300°C, which makes the HSQ films nanoporous[3]. The sample was then immersed in 1 M 1-octanethiol solution in ethanol for >12 hours. After immersion, the HSQ layer was peeled off using thermal release tapes and laminated onto SiO_2 substrate. The HSQ layer was removed by TMAH developer.

Fig. 1 shows the polar plots of Raman D and G peak intensity of (ii) as-grown GNRs on Au(788) and (iii) after transferred onto SiO_2, as a function of the angle θ, where θ is the angle between the incident polarization direction and the GNR edges orientation. The black solid line is a fit to the experimental data, $I \propto \cos^2\theta + R$, where I and R are raman peak intensity and constant, respectively. Both D and G peak intensity showed similar anisotropic θ dependence derived from the so-called depolarization effect[4]. After transferred onto SiO_2 substrate, the anisotropy was weakened, probably due to the weakened depolarization effect on SiO_2 surface[5]. The removal of 1-octanethiol SAMs by means of electrochemical reduction of Au-S bond, and the reuse of Au crystals is also demonstrated.

[1] J. Cai *et al.* Nature **466**, 470 (2010). [2] S. Linden *et al.* Phys. Rev. Lett. **108**, 216801 (2012). [3] W.-C. Liu *et al.* Journal of Non-Crystalline Solids **311**, 233 (2002). [4] G. S. Duesberg *et al.* Phys. Rev. Lett. **85**, 5436 (2000). [5] A. Grüneis *et al.* Chemical Physics Letters **387**, 301 (2004).

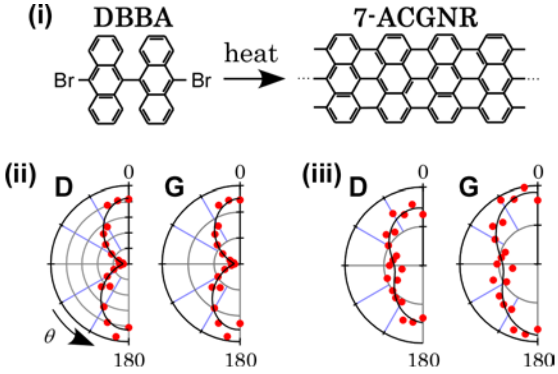

Figure 1 (i) The schematic diagram of the bottom-up fabrication process. (ii,iii) The polar plots of D and G peaks of (ii) as-grown and (iii) transferred GNR arrays on SiO_2.

Wednesday Afternoon

Semiconductor Interfaces & Devices II

We1400 Invited

Phosphorene as a New 2D Material for Device Applications

Peide D. Ye

School of Electrical and Computer Engineering, Purdue University, West Lafayette, IN 47907
Tel: 1-765-494-7611, Fax: 1-765-496-6443, Email: yep@purdue.edu

Phosphorus is one of the most abundant elements preserved in earth, constructing with a fraction of 0.1% of the earth crust. In general, phosphorus has several allotropes including white, red, and black phosphorus. Black phosphorus, though rarely mentioned, is a layered semiconductor as shown in Figure 1 and have great potentials in optical and electronic applications. Remarkably, this layered material can be reduced to one single atomic layer as shown in Figure 2 in the vertical direction owing to the van der Waals structure, dubbed phosphorene, where the physical properties can be tremendously different from its bulk counterpart and needed to be further explored. In this talk, we trace back to the 100 years research history on black phosphorus from the synthesis to material properties, and extend the topic from black phosphorus to phosphorene. The physical and transport properties are highlighted, aiming at further applications in electronic and optoelectronics devices.

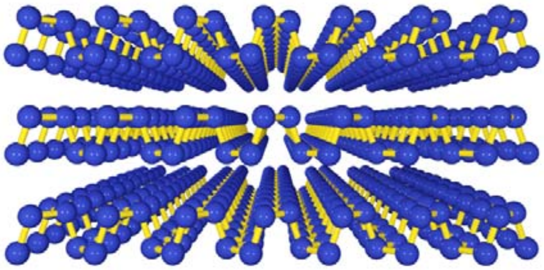

Figure 1: Crystal structure of few layer phosphorene. The ridged layers are bonded by the van der Waals force.

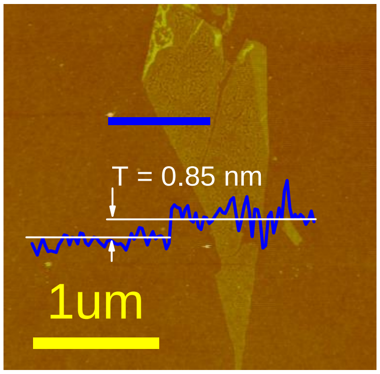

Figure 2: Atomic Force Microscopy image of a single-layer phosphorene crystal with the measured thickness of ~ 0.85 nm.

Interface Improvement in AlGaN/GaN HFETs Using TMAH Pre-treatment

Do-Kywn Kim, Won-Sang Park, Young-In Jang, Jin-Su Kim, Young-Jun Yun, In-Man Kang,
Dae-Hyun Kim and Jung-Hee Lee
School of Electrical Engineering, Kyungpook National University, Daegu, 702-701, Korea
*E-mail: jlee@ee.knu.ac.kr, Tel: +82-53-940-8655

INTRODUCTION: AlGaN/GaN-based heterojunction field-effect transistors (HFETs) are well known as one of the most promising devices for high-power and high-frequency applications, due to their excellent material properties, such as wide bandgap, high breakdown voltage and high 2-DEG density [1]. Recently, researches on the interfacial properties between gate metal and (Al)GaN layer have been extensively explored, aiming to improve the Schottky characteristics, which is critical in mitigating the gate leakage current (I_G) and the off-state drain leakage current (I_{OFF}) [2]. Meanwhile, various dielectric materials, such as SiO_2, SiN and Al_2O_3 are widely utilized to protect the surface of a thin AlGaN barrier layer, especially during high-temperature RTP step for a formation of S/D ohmic contacts [3]. In doing so, it is known that the (Al)GaN surface can be reacted with oxygen atoms in the dielectric layer by forming nonuniform interfacial oxides such as GaO_x and AlO_x during high temperature RTP. Unfortunately, this deterioates the surface morphology with poor roughness after the removal of the dielectric layer. Now, a remaining challenge is how to remove the interfacial oxide layer and to recover the degraded surface prior to the gate metallization, since the bad interfacial properties can significantly deteriorate the overall device characteristics [4]. In this paper, we have developed a new method of wet-chemical treatment in a TMAH solution prior to the gate metallization, which completely removes the interfacial oxide layer and also effectively recover the device surface compared to the conventional wet etching in a BOE solution.

EXPERIMENT/RESULT: ***Figure 1 (a)*** shows a cross-sectional schematic of a fabricated GaN-cap (2 nm)/AlGaN (15 nm)/GaN HFET with L_g = 2 µm on sapphire substrate. The device surface was covered with ALD Al_2O_3 layer to protect the surface during ohmic RTP. Prior to the gate metallization, two different types of pretreatments were investigated for the device fabrication; one with TMAH pretreatment and the other with the conventional BOE pretreatment, as shown in ***Fig. 1 (b)***. ***Figure 2*** displays AFM images (2 µm x 2 µm) after both pretreatments. The THAH-treated HFET yields better surface roughness (RMS = 0.36 nm) than the BOE-treated one (RMS = 0.5 nm). ***Figure 3*** shows the transfer and transconductance (g_m) characteristics for both devices. The TMAH-treated HFET shows a positive shift of V_T compared to the BOE-treated HFET. This is in part because the schottky barrier height (SBH, Φ_B = 0.74 eV) of the TMAH-treated HFET is higher than that (Φ_B = 0.53 eV) of the BOE-treated HFET. The barrier height of both devices were extracted from the gate leakage currents shown in ***Fig. 4***. The reasons why the TMAH-treated device exhibits higher barrier height are as follows: First, the TMAH solution is likely to completely remove the undesirable interfacial GaO_x and AlO_x layers between Al_2O_3 layer and GaN-cap layer which are formed during high-temperature RTP [5]. Secondly, it also effectively recovers the degraded GaN surface thanks to a strong lateral etching nature of the TMAH solution which makes the device surface very smooth and defect-free [6]. In contrast, the BOE solution can also remove both interfacial oxide layers, but cannot recover the degraded surface because the BOE does not etch the GaN layer. As a result, the g_m of the TMAH-treated HFET is improved by 10 %. This, in turn, can be manifested in the the reduction of the gate leakage current (I_G) and the off-state drain leakage current (I_{off}), compared to the BOE-treated HFET. Hence, the TMAH-treated HFET exhibits a lot lower off-state performances. ***Figure 5*** shows the subthreshold characteristics for both devices at V_{DS} = 0.1 V. Consistent with the improved leakage currents (I_G and I_{off}), the THAH-treated HFET shows much better subthreshold-swing (SS) of 72 mV/decade and I_{ON}/I_{OFF} ratio of 10^6. We believe that these improvements arise from the effective removal of the interfacial GaO_x layers with smoother surface morphology by TMAH solution. Moreover, these yield larger SBH and better ideality factor (η) in the TMAH-treated HFET, as summarized in ***Table 1.***

CONCLUSION: We have developed a new method of using the TMAH pretreatment prior to the gate metallization and characterized the electrical properties of the fabricated AlGaN/GaN HFETs with two different types of surface pretreatments (THAH and BOE). Clearly, the THAH treatment provides much better electrical properties in the AlGaN/GaN HFETs, such as lower I_G and I_{OFF}, much better SS, I_{ON}/I_{OFF} ratio, and schottky interface characteristics. We believe that these improvements stem from the smooth surface and effective removal of GaO_x layer by TMAH solution.

Acknowledgement : This work was supported by the BK21 Plus project funded by Ministry of Education, Korea (21A20131600011).

References:

[1] Y.F Wu, *IEEE Electron Device Lett.* **48**, 586 (2001).
[2] D. Qiao, *Journal of Applied Physics* **87**, 801 (2000).
[3] D.K Kim, *Solid-State Electron*. **100**, 11 (2014).
[4] J. Oh, *Journal of the electrochemical Society*, **158**, D217 (2011).
[5] S. Ozaki, *CS MANTECH conference, USA* (2012).
[6] K.W Kim, *IEEE Electron Device Lett.* **32**, 1376 (2011).

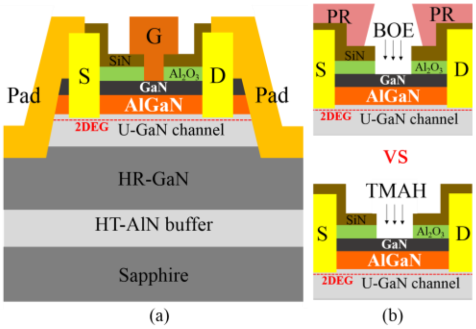

Fig. 1. Cross-sectional schematic of fabricated AlGaN/GaN HFETs with TMAH and BOE treatment

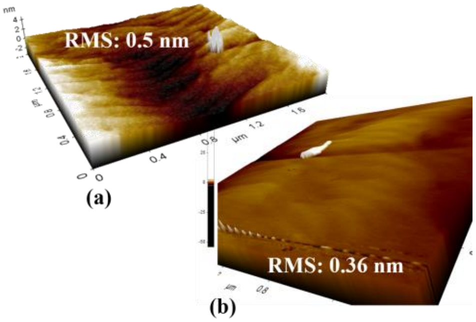

Fig. 2. 3D views of measured AFM images for (a) BOE and (b) TMAH treatment

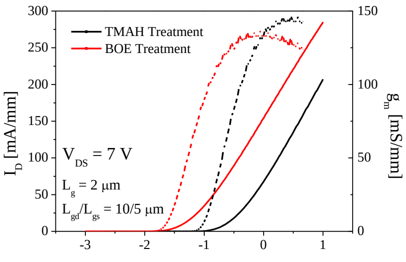

Fig. 3. Transfer and transconductance characteristics of two types of AlGaN/GaN HFETs: Red is for BOE and black for TMAH

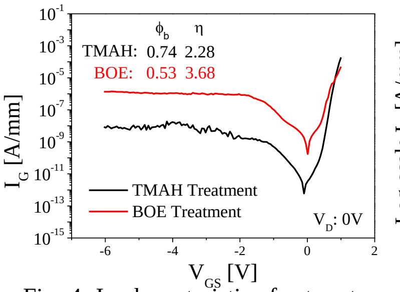

Fig. 4. I_G characteristics for two types of AlGaN/GaN HFETs: Red is for BOE and black for TMAH

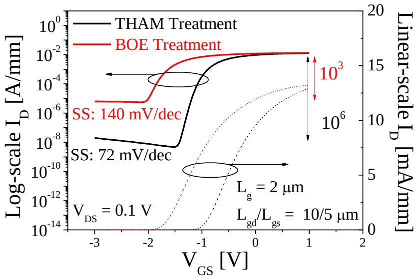

Fig. 5. SS and on/off ratio characteristics for two types of AlGaN/GaN HFETs: Red is for BOE and black for TMAH

Table. 1 Summary of device parameters from two types of GaN/AlGaN/GaN HFETs

	RMS [nm]	g_m [mS/mm]	SS [mV/dec]	I_{ON}/I_{OFF}	I_G [A/mm]	Φ_B [eV]	Ideality factor (η)
BOE-treated HFET	0.5	132.3	140	10^3	1.35×10^{-6}	0.53	3.68
TMAH- treated HFET	0.36	145.7	72	10^6	8.66×10^{-9}	0.74	2.28

Assessment of substrate surface pretreatment for epitaxial growth of III-nitrides at low temperatures

N. Nepal[1], V. R. Anderson[1], V.D. Wheeler[1], J. K .Hite[1], S. D Johnson[1], D.J. Meyer[1], B.P. Downey[1], A. DeMasi[2], K.F. Ludwig[2], and C.R. Eddy, Jr[1]

[1]*U.S. Naval Research Laboratory,* 4555 Overlook Avenue SW, *Washington, DC 20375, USA*

[2]*Physics Department, Boston University, Boston, Massachusetts 02215, USA*

A challenge with integration of III-N semiconductors (AlN, GaN and InN) is the requisite heteroepitaxy on foreign substrates, compounded by ever increasing device structure complexity. State-of-the-art device structure heterojunctions require nanometer-thick binary and single-phase ternary layers (as for example those required for normally-off power switches). To address ternary layer miscibility gaps, substrates versatility and low strain heterojunctions the growth temperature has to be reduced. However, at low growth temperatures, high quality epitaxy is challenged by the reduced thermal energy needed for adatom mobility. Thus, to initiate epitaxial nucleation and growth processes at low temperatures, substrate surfaces have to be properly prepared.

In this talk we report *ex situ* and *in situ* substrate surface pretreatment for low temperature atomic layer epitaxy (ALEp) of III-N semiconductors. The surface pretreatments were optimized by *in situ* and *ex situ* characterizations. For *ex situ* characterization atomic force microscopy and x-ray photoelectron spectroscopy were used. For *in situ* characterizations, grazing incident small angle x-ray scattering (GISAXS), anti-Bragg x-ray diffraction and x-ray reflectivity measurements were used to monitor the effect of plasma treatments on *a*-sapphire and GaN/*a*-sapphire templates. Based on these surface characterizations, optimal wet chemical treatments resulting in the smoothest and least contaminated surfaces are: (a) dilute HF (10:1) dip for Si(111); (b) piranha clean at 80°C/10 min for GaN/*a*-sapphire templates; (c) 20 min UV ozone at room temperature plus 10 sec 10% HCl dip for GaN/Si(111) templates; and (d) 10 min each acetone and isopropanol clean at 40°C for *a*-plane sapphire. Optimally *ex situ* cleaned substrates were loaded in the ALEp reactor and then *in situ* cleaned. An emulated Ga flash-off, H_2 plasma, and N_2 plasma sequences were done just before epitaxial growth of III-N layers on GaN/*a*-sapphire templates. GISAXS shows that the emulated Ga-flash-off process is very similar to the conventional molecular beam epitaxy (MBE) Ga flash-off version. For *a*-plane sapphire H_2 plasma and N_2 plasma clean sequence were used before III-N growth. X-ray diffraction (XRD) measurements on ALEp grown InN at 180 – 240°C on pretreated *a*-sapphire and AlN at 500°C on pretreated GaN/*a*-sapphire templates show high crystalline quality (full-width at half maximum of 262 arc-sec for InN and 670 arc-sec for AlN layer). In- and out-of-plane XRD results show sharp epitaxial InN peaks. Furthermore, transport measurements show an electron mobility of 50 cm^2/V-s for a 5.6 nm thick InN film on pretreated *a*-plane sapphire, which is higher than the reported value of 30 cm^2/V-s for a 1300 nm thick InN film grown by MBE directly on sapphire [1]. It is believed that the surface cleaning removes substrate polishing damage, thin top native oxide layers, and carbon and absorbed impurities producing high quality surface for the low temperature epitaxial growth of III-Ns.

1. Kuo et al., Diamond & Related Materials **20**, 1188 (2011).

Direct ohmic contact to p-AlGaN and its application to 365 nm AlGaInN/InGaN light-emitting diodes

TaeHo Lee[1], Dae Yun Kang[1], Tae Geun Kim[1]

[1]School of Electrical Engineering, Korea University, Anam-ro 5-ga, Sungbuk-gu, Seoul 136-701, Republic of Korea

To improve the performance of GaN-based light-emitting diodes (LEDs), particularly in the ultraviolet (UV) region [1], it is important to form ohmic contact between p-AlGaN and transparent conductive electrodes (TCEs) having high optical transmittance and low electrical resistance. However, trade-offs between the conductivity and transmittance have made it difficult to make it. Recently, we have reported a universal method to make ohmic contact between p-AlGaN and metal oxide/nitride using electrical breakdown (EBD) methods, and successfully demonstrated its validity for vertical-type GaN LEDs using SiN-based TCEs [2].

In this report, we demonstrate improved performance of lateral-type GaN LEDs emitting at 365 nm using AlN-based TCEs. We inserted a thin conductive layer below AlN TCE to enhance the current spreading effect. In addition, to mininize the electrical shock during the EBD process, we conceived a unique bias method to form conducting paths in the TCE via a thin conductive layer. As a result, we accomplished much higher light-output power (~8.5 % ↑) and lower forward voltage (~2.8 % ↓) for 365 nm near UV LEDs with AlN TCEs, when compared to those of the UV LED with reference ITO. This improvement is attributed to enhanced current spreading (via insertion layers) as well ass higher optical transmittance (> 93% at 365 nm) and lower contact resistance via conducting filament (3.7×10^{-2} Ωcm^2). More details on the experimental result will be presented at the conference.

[1] J. Y. Kim, J. H. Jeon, M. K. Kwon., ACS Appl. Mater. Interfaces, 7, 7945-7950 (2015).

[2] S. J. Kim, H. D. Kim, K. H. Kim, H. W. Shin, I. K. H., T. G. Kim., Scientific Reports, 4, 5827-5829 (2014)

We1455

Epitaxial lateral overgrowth of ZnTe on sapphire substrates using SiO_2 mask

S. Hattori[1*], T. Nakasu[1], T. Kizu[1], Y. Hashimoto[1], W. Sun[1], F. Kazami[1],
M. Kobayashi[1, 2], T. Asahi[3],
Waseda Univ. Dept. of Elec. Eng. & Biosci.[1], Res. Inst. for Mat. Sci. & Technol.[2],
JX Nippon Mining & Metals Corporation [3]
※shota-wahaha@ruri.waseda.jp

ZnTe has attracted attention for use in various novel devices including terahertz wave detector. Toward the application to detect terahertz wave, ZnTe films were grown on transparent sapphire substrates. Although there is a large lattice mismatch between ZnTe and sapphire, the crystal quality of the ZnTe film was improved by the insertion of a low temperature buffer layer at the interface [1]. In this study, we focused on an epitaxial lateral overgrowth (ELO) method to utilize the variation of surface chemistry and further improve the crystal quality of the ZnTe film. The dislocation density of grown films can be decreased by the ELO, and improvement of the crystal quality can be expected [2]. ELO of ZnTe on patterned substrates ideally requires a vanishingly small sticking coefficient of incident Zn and Te atoms on a mask surface and a near unity sticking coefficient on an open sapphire substrate surface (selective growth). Higher growth rate of ZnTe in the lateral direction is also expected than in the vertical direction (anisotropic growth). Since SiO_2 mask and sapphire have different chemical and physical surface properties, incident atoms of Zn and Te would show different behaviors for different surfaces.

The c-plane sapphire substrates were used to deposit a 50nm thick SiO_2 film by the sputtering. The 5~50μm wide stripe opening patterns were then formed by a standard photolithography. The intervals of the openings were various form 10μm to 100μm. MBE growth was performed on the patterned substrate, and the substrate temperature was set to 340~360℃. The flux ratio J_{Te}/J_{Zn} was varied from 0.67~1.33, and growth rate was varied from 0.2~0.5 μm/h. The target film thickness was kept constant at 1μm. The surface and cross-sectional states were observed by SEM.

When ZnTe layers were grown at a low flux ratio (0.83) and a low growth rate (0.2 μm/h), non-deposition of ZnTe on the SiO_2 was observed even though ZnTe growth on sapphire was realized, hence the selective growth of ZnTe was confirmed. On the other hand, when ZnTe grown at either high flux ratio (≥1.0) or high growth rate (≥0.4 μm/h), the deposition of ZnTe were formed on both SiO_2 and sapphire. These results showed that amount of Te-flux significantly affected selective growth of ZnTe. Since Te has lower vapor pressure than Zn, Te atoms could have a longer surface lifetime. Therefore the sticking coefficient of Te atoms on SiO_2 was probably larger than that of Zn. Selective growth of ZnTe was realized because of the dominant behavior of Te desorption from the SiO_2 surface. From the cross-sectional SEM images, it was confirmed that the sidewalls of the lateral direction growth of ZnTe were both inclined in the same direction. Therefore, an anisotropic growth in the lateral direction was taking place. The direction adjustment of the opening would improve the degree of the anisotropy.

This work was supported in part by Waseda Univ. Research Initiatives, "Early Bird" grant for young researcher at Waseda Research Inst. for Sci. & Eng., collaboration between Mitsubishi Mat. Corp. & Faculty of Sci. & Eng., Waseda Univ., JSPS Research Fellowships for Young Scientists, and the Foundation of Ando Laboratory.

[1] T. Nakasu et al. Appl. Phys Express 5 (2012) 095502.
[2] K. Hiramatsu et al. J. Cryst. Growth 221.1 (2000) 316-326.

Wednesday Afternoon

New Techniques & Devices

We1500

Nanoscale imaging of local few-femtosecond near-field dynamics within individual nanostructures.

Erik Mårsell[1], Arthur Losquin[1], Robin Svärd[1], Miguel Miranda[1], Chen Guo[1],
Anne Harth[1], Eleonora Lorek[1], Johan Mauritsson[1], Cord L. Arnold[1], Hongxing Xu[2], Anne L'Huillier[1], Anders Mikkelsen[1]
[1]*Department of Physics, Lund University, Box 118, 221 00 Lund, Sweden*
[2]*School of Physics and Technology, and Institute for Advanced Studies, Wuhan University, China*

Email: anders.mikkelsen@sljus.lu.se

The local enhancement of few-cycle laser pulses by nanostructures opens up for spatiotemporal control of optical interactions on a nanometer and few-femtosecond scale. However, spatially resolved characterization of few-cycle field dynamics poses a major challenge due to the extreme length and time scales involved. Using 5.5 fs laser pulses with a central energy around 1.6 eV in an interferometric time-resolved photoemission electron microscopy (ITR-PEEM) setup, we are capable of addressing this issues for a variety of nanostructures. As the photoemission probability scales to the power of ~3 with laser power, ITR-PEEM is an extremely sensitive probe of near-field enhancement.

We experimentally demonstrate local variations in the dynamics during the few strongest cycles of plasmon-enhanced fields within both individual rice-shaped silver nanoparticles [1] and focused ion beam (FIB) defined gold bowtie antennae [2]. The experiments are supported by finite-difference time-domain simulations of similar structures and laser fields. The observed differences in the field dynamics across a single silver rice particle do not reflect differences in plasmon resonance frequency or dephasing time. They instead arise from a combination of retardation effects and the coherent superposition between multiple plasmon modes of the particle, inherent to a few-cycle pulse excitation. For the bowtie antennae we observe that bowties with the same overall dimensions and good central field enhancement can have a different time structure already within the first few cycles of the laser field. These differences can be attributed to the small inherent structural variations due to the lithographic process used. The ability to detect and predict local variations in the few-femtosecond time evolution of multi-mode coherent plasmon excitations in rationally designed nanostructures can be used in the tailoring of nanostructures for ultrafast and nonlinear plasmonics.

Using high intensity ultra short laser pulses we find that field enhancement effects can also be observed in a wide range of III-V semiconductor nanowires in ITR-PEEM. While the time structure on the few femtosecond scale is governed by the very fast multi-photon photoemission processes involved, we observe a rich variety in polarization behavior of the nanowires. In the future these IR pulses will be combined with XUV pulses for investigations of photon excitations with sub-femtosecond precision [3,4]

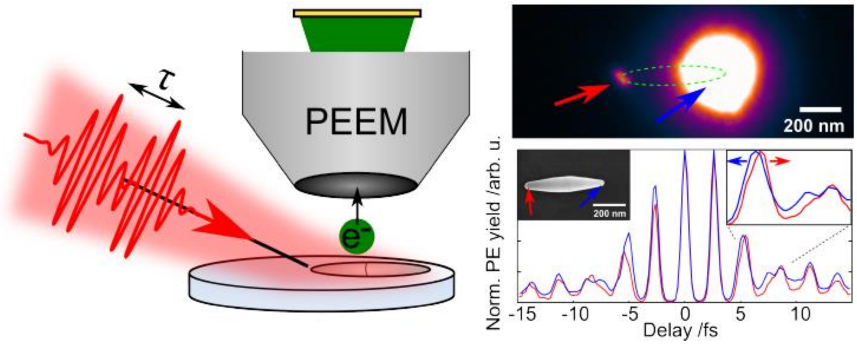

Figure 1: Schematic of the ITR-PEEM experiment and results from nano rice particles[1]

References

[1] E. Mårsell et al *Nano Letters 15 (2015) 6601*
[2] E. Lorek et al, *submitted (2015)*
[3] A. Mikkelsen *et al.*, *Rev. Sci. Instrum. 80 (2009) 123703*.
[5] E. Mårsell *et al.*, *Annalen der Physik, 525 (2013) 162*.

We1505

Time of Flight Backscattering Spectrometry and Secondary Ion Mass Spectrometry in a Helium Ion Microscope Enabling Chemical Analysis on the nm Scale

N. Klingner[1], *R. Heller*[1], *G. Hlawacek*[1], *P. Gnauck*[2], *S. Facsko*[1], *and J. von Borany*[1]

[1]Helmholtz-Zentrum Dresden-Rossendorf, Bautzner Landstr. 400, 01328 Dresden, Germany
[2]Carl-Zeiss-Microscopy GmbH, D-73447 Oberkochen, Germany

Helium ion microscopes (HIM) are commonly used high resolution imaging devices within several laboratories around the world. Beside a sub nano-meter resolution and a high depth of field latest generation of HIM devices (Zeiss Orion NanoFab) make use of both Helium and Neon ions as well, thus enabling various possibilities for local surface modifications [1].

While the image generation in a HIM is realized by evaluating the amount of secondary electrons (SE) the energy of backscattered He or Ne projectiles is rarely taken into consideration so far. However, this energy contains information on the chemistry of surface and sub-surface as well and it provides an additional mechanism of contrast generation. Early attempts to measure BS energy spectra were carried out by Sijbrandij *et al.* [2] and gave evidence for the general feasibility but also revealed that a quantitative chemical analysis of thin layers would require the development of more sophisticated detection concepts.

In this contribution we present an experimental approach and the corresponding results of performing backscattering spectrometry (BS) in a HIM with a lateral resolution < 55 nm and an energy resolution < 2 keV (example seen in fig. 1). We show that pulsing the primary ion beam and measuring the Time of Flight (ToF) of the BS He/Ne enables BS spectrometry in a HIM without disturbing its excellent imaging capabilities. Since our approach enables us also to perform Secondary Ion Mass Spectrometry (SIMS) by biasing the sample to a positive potential, elemental contrast in chemical analysis is further increased.

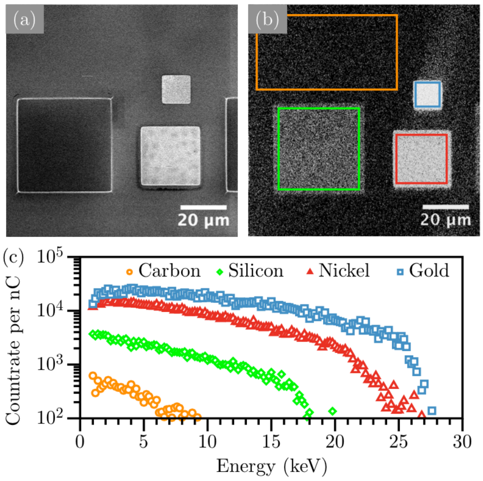

Figure 1: Images of a carbon sample covered with rectangular patterns of Si, Ni and Au acquired in standard SE mode (a) and in ToF-BS mode (b). The color scale in (b) corresponds to the time of flight of the BS particles. In contrast to SE imaging this technique reveals well-defined elemental contrast. ToF-BS spectra from within different regions in (b) - marked by rectangles - are plotted in (c). The color of the spectra equals the color of the rectangles in (b). The ToF-BS spectra allow clearly distinguishing between different elements.

Both techniques SIMS and BS together with the high-resolution imaging by SEs reveal a "complete" picture of the sample in terms of topography and chemistry. Further the evaluation of BS spectra generates access to the sub-surface chemistry by measuring elemental depth profiles.

REFERENCES

[1] [1] G. Hlawacek, V. Veligura, R. van Gastel, and B. Poelsema, J. Vac. Sci. Technol. B **32**(2), 2014, 020801.

[2] [2] S. Sijbrandij, B. Thompson, J. Notte, B. W. Ward and N. P. Economou, J. Vac. Sci. Technol. B, **26**(6), 2008, 2103-2106

We1510

Nanoscale Imaging of Defects in CdTe Photovoltaic Devices Using Two Novel Optical Spectroscopies

Yohan Yoon[1, 2], Jungseok Chae [1, 2], Aaron Katzenmeyer[1], Heayoung P. Yoon[1, 2], Joshua Schumacher [1], Sangmin An[1, 2], Andrea Centrone[1], Nikolai Zhitenev[1]

[1]Center for Nanoscale Science and Technology, National Institute of Standards and Technology, Gaithersburg, MD 20899, USA
[2]Maryland Nanocenter, University of Maryland, College Park, MD 20742, USA

Polycrystalline thin film technology has shown great promise for low cost, high efficiency photovoltaics. To further increase the power efficiency, a firm understanding of microstructural properties of the devices is required. In this work, we investigate the inhomogeneous properties of CdTe photovoltaic devices using two optical spectroscopies. The first technique is photothermal induced resonance (PTIR) used to obtain absorption spectra and maps over a broad range of wavelengths. In PTIR, a wavelength tunable pulsed laser is used in combination with an atomic force microscope tip to detect the local thermal expansion of lamella CdTe sample induced by light absorption. The nano-scale high-resolution PTIR images show a variation of local absorption in a range of wavelengths near the CdTe bandgap energy, implying an inhomogeneous composition of CdTe absorber layer corresponding to a band gap variation of 20 meV. PTIR data were compared with the absorption/transmission spatial maps obtained by a complementary local excitation technique, near-field scanning optical microscope (NSOM), that generate excess carriers by a near-field light illumination using NSOM probe with near-IR lasers (850, 905, and 980 nm) close to CdTe band-gap energy (1.5 eV). A sub-micron thickness lamella CdTe sample was prepared by focused ion beam (FIB) and cleaned by low energy ion milling as a post-FIB processing. The lamella was transferred to a high efficiency photodetector and then illuminated with an optical fiber probe (200 nm in diameter) mounted on a tuning fork. The transmitted power throughout the lamella sample was detected by photodetector. The resolution and the sensitivity of these two approaches are compared.

We1515

Title: **"Overcoming Interface Oxidation via Melt Mixing during LPE of AlGaAs Multi-Layer Structures."**

Authors: Jerry M. Woodall and Xin Zhao
Institution: ECE Department, UC Davis, Davis CA 95616
Contact email: jwoodall@ucdavis.edu

Abstract:

It is well known that aluminum (Al) has a great affinity for oxygen. All air or water exposed Al surfaces form either a robust passivating oxide, Al_2O_3, or $Al(OH)_3$, thus enabling global scale applications for Al.

Therefore, it should be no surprise that AlGaAs liquid phase epitaxy (LPE) was the seminal technology that launched many heterojunction technologies. It is now clear in hind sight that both MBE and MOCVD AlGaAs device technology was slow to emerge owing to the fact that for both MBE and MOCVD, epilayers of AlGaAs are susceptible to both ambient and materials contamination occurring at either the gas or vacuum solid crystal growth interface. This is in contrast to the beneficial LPE solid-liquid interface, which protects the growing epilayer from both oxygen-producing defects and, via melt segregation, unwanted impurities.

This presentation continues the exploitation of the beneficial aspects of the solid-liquid interface during the growth of AlGaAs epilayers. The justification for the materials science of our project is the possible realization of an $Al_{0.2}Ga_{0.8}As$ solar cell whose band gap energy is 1.72 eV. A high efficiency cell with this band gap energy as the top cell of a tandem stack with a Si solar cell at the bottom, is expected to have a 100x solar concentrator efficiency of > 40 %.

The initial approach for this project was to use a three bin, vertical LPE system, in which a GaAs substrate was rotated into a given Al-Ga-As melt to form the desired n-type AlGaAs layer. After the growth of this epilayer, the substrate plus AlGaAs epilayer was rotated into another melt chamber whose Al-Ga-As composition and Zn doping results in a p-type $Al_{0.9}Ga_{0.1}As$ "window" layer. The purpose of this layer is to reduce surface carrier recombination loses while allowing solar photons reach the 1.72 eV band gap layer. During the formation of the window layer, Zn diffuses into the AlGaAs active layer forming a p-n junction in the active AlGaAs structure. This method produced high efficiency p-p-n AlGaAs-GaAs-GaAs solar cells. However, it did not work for the AlGaAs cell project.

It was found that when the epilayer was rotated from one AlGaAs LPE melt into another, the solid-liquid interface was lost. As a result a passivating AlGaAs-oxide film formed during the rotation. The resulting cells showed poor performance. Attempts to removed this passivating film by using an under saturated melt to dissolve the film were not generally successful.

A novel solution was developed that maintained a solid-liquid interface during epilayer formation. This was done using a recessed substrate holder, which allowed for the epilayer to be covered with a thin layer of melt during transfer. Devices made by this simple but fundamentally profound method are now approaching state of the art. The details of the materials science of this technique will be described at the conference.

Application of metal-insulator-metal single electron transistors for characterization of ultrathin dielectrics grown by atomic layer deposition.

Golnaz Karbasian, Michael S. McConnell, Alexei O. Orlov, Alexander Mukasyan, Sergei Rouvimov, and Gregory L. Snider

The development of emerging technologies in microelectronics such as magnetic tunnel junction (MTJ) devices, tunneling field-effect transistors (TFETs), and single-electron tunneling transistors (SETs) calls for precise fabrication of ultrathin films down to a few atomic layers. A deep understanding of the physical and chemical mechanisms involved in the formation of such layers is required for successful device fabrication. One popular technique for the formation of thin dielectric barriers critical to MTJs, TFETs, and SETs is atomic layer deposition (ALD), which enables the precise growth of a number of materials down to a few monolayers. We report the use of ALD for SET fabrication to form ultra-thin (≈ 1 nm) SiO_2 and Al_2O_3 dielectric barriers in metal-insulator-metal (MIM) tunnel junctions. The nanoscale-sized (≈ 20 x 20 nm^2) tunnel junctions were fabricated on thermally grown SiO_2 substrates by using a combination of high resolution electron beam lithography and metal evaporation to define metal electrodes (source, drain, gate and SET island) and ALD to form tunnel barriers. Several metals (Ni, Pt, Pd) were tested to produce the devices which were electrically tested at temperatures from 300K down to 0.3K. The experimental results reveal the formation of thin layers of non-metal compounds that modify and impede the operation of the devices (e.g. by exponentially increasing device resistance). Several treatment techniques were investigated in order to recover the desired properties of MIM junctions, including hydrogen-based treatments that enable decomposition and/or reduction of parasitic native oxides formed during the ALD process. We report two major research findings. First, our results show that by optimization of device definition techniques and post fabrication treatments it is possible to achieve nearly ideal MIM junction behavior. Second, we demonstrate that MIM SET devices offer a uniquely sensitive characterization platform, enabling the detection of interstitial layers and non-uniformities in nanoscaled tunnel junctions.

Wednesday Afternoon

Semiconductor Interfaces

We1625 Invited

Engineering interfaces for memristive devices

J. Joshua Yang[1*]

[1]*The Department of Electrical and Computer Engineering, University of Massachusetts, Amherst, Massachusetts 01002, USA*

*E-mail: jjyang@umass.edu

Existing technologies for the current computing system are approaching their physical limits, and novel device concepts are required as device sizes continuously decrease. Under these new concepts, the devices need to be not only increasingly infinitesimal and simple but also increasingly capable. Memristive devices (RRAM) seem to fulfill these goals well for the next generation computing system. These devices are electrical resistance switches that can retain a state of internal resistance based on the history of applied voltage or current. Memristive devices can store and process information, and offer several key performance characteristics that exceed conventional integrated circuit technology. An important class of these devices is two-terminal resistance switches based on ionic motion, which are built from a simple conductor/insulator/conductor thin-film stack.

The electrode/metal-oxide interface of memristive switches plays a crucial role in the switching mechanism as well as in the i-v characteristics of the devices. We demonstrate here that a rich set of device behaviors can be obtained by engineering the two interfaces of the device. Using TiOx and TaOx based devices, we show that the work function of the metal electrode has a surprisingly minor effect in determining the electronic barrier at the interface. In contrast, the oxides can be readily reduced by most electrode metals. The amount of oxygen vacancies created by these chemical reactions essentially determines the electronic barrier at the device interfaces. The virgin resistance, electroforming and switching performance depend heavily on the chemical property of the top electrode materials. In addition, a highly nonlinear i-v relation in the low resistance state can be achieved by using some special electrode materials, such as V, Nb or graphene. The high linearity provides a built-in selector for those devices to reduce the sneak path current in a crossbar array for real applications.

Supplementary materials: Epitaxial Al-InAs two-dimensional systems: a platform for gate-able topological superconductivity

J. Shabani[1], M. Kjaergaard[2], H. J. Suominen[2], Y. Kim[3], F. Nichele[2], K. Pakrouski[4], T. Stankevic, , R. Lutchyn[5], P. Krogstrup[2] , S. Kraemer[4] , C. Nayak[3,5], M. Troyer[4], C. M. Marcus[2], C. J. Palmstrøm[1,4,6]

[1]*California NanoSystems Institute, University of California, Santa Barbara, USA*

[2]*Center for Quantum Devices, Niels Bohr Institute, University of Copenhagen, Copenhagen, Denmark*

[3]*Physics Department, University of California, Santa Barbara, USA*

[4]*Institute for Theoretical Physics, ETH Zurich, CH-8093 Zurich, Switzerland*

[5]*Materials Research Laboratories, University of California, Santa Barbara, USA*

[6]*Microsoft Station Q, Santa Barbara, USA*

[7]*Department of Electrical Engineering, University of California, Santa Barbara, USA*

Figure 1 shows a brief presentation of our work. Fig. 1a presents the schematic of the Al-InAs structure. Figure 1b shows the weak antilocation signal analyzed to determine the strength of the spin-orbit interaction. A transmission electron microscope image of the interface between Al and InGaAs materials is shown in Fig. 1c.

Superconducting-semiconductor-semiconductor junctions fabricated on these structures, such as the one shown in Fig. 1d, show supercurrent with unprecedented interface properties.

We1735

Schottky Barrier Diodes with in-situ Grown Single Crystal Aluminum on GaN by Plasma-Assisted Molecular Beam Epitaxy

H. Y. Tseng, W. C. Yang, P. Y. Lee, C. W. Lin, K. C. Hsieh and K. Y. Cheng
Department of Electrical Engineering, National Tsing Hua Universit,y
Hsinchu, Taiwan 30013, Republic of China

Schottky barrier diodes (SBDs), with low carrier storage time, are widely used in microwave devices and millimeter wave devices. Recently, the electrical properties of n-GaN SBDs have been studied using current-voltage (I-V) and capacitance-voltage (C-V) methods [1]. However, the contamination from exposing semiconductor surface to atmosphere is almost unavoidable in fabricating Schottky diodes, leading to high interfacial trap states. In this work, *in situ* single crystal aluminum layer is epitaxially grown on GaN by plasma-assisted MBE (PAMBE) to overcome this problem [2].

After the growth of a 300nm n^+-GaN layer on the GaN template, a 500nm undoped GaN layer is grown. The substrate is subsequently cooled down to room temperature. In the meantime, the Al effusion cell is heated to 1100°C to achieve a deposition rate of about 2600Å/h. The growth of the Al layer is monitored by *in situ* reflection high-energy electron diffractions (RHEED) and *ex situ* high-resolution x-ray diffractions (HRXRD). Both (002) diffraction of GaN and (111) diffraction of single crystal Al are observed in HRXRD rocking curves (Fig. 1). In addition, the RHEED patterns in $[1\bar{1}00]$ azimuth are performed, from which the lattice arrangement variance during the deposition of Al is observed. During the initial deposition of Al (up to ~10Å), the Al surface diffraction pattern is the same as GaN indicating the same lattice registrations (Fig. 2a). After that, extra weak streaks outside the bulk diffraction streaks appear, which suggests the existence of two different lattice arrangements of Al (Fig. 2b). With an additional ~5Å Al deposition, the bulk diffraction pattern disappears entirely and replaced by the extra streaks (Fig. 2c). In other words, the strain of Al on GaN is totally released retaining its nature lattice constant of 4.048Å . The single crystal Al is oriented along [111] on (0001) GaN without rotation. The 10% lattice mismatch between Al and GaN is accommodated within ~15Å by registering every 5th Al atoms with every 9th Ga atoms (Fig. 3).

For device fabrication, the as-grown Al layer (130nm) and undoped-GaN layer are patterned and dry etched using BCl_3+Cl_2 plasma by reactive ion etching (RIE) and inductively coupled plasma RIE techniques, respectively. Multiple layers of Ti/Al/Ti/Au are deposited as the ohmic contact to complete the quasi-vertical SBD structure. The interface quality of SBDs is examined by I-V technique. The SBD exhibits better Schottky rectifying characteristic for the *in-situ* deposited Al as seen an increase in Schottky barrier height from 0.47eV (*ex-situ* deposited Al) to 0.68eV and more than 2-orders of magnitude reduction in leakage current. Furthermore, the ideality factors of nine randomly selected diodes are compared. The average ideality factor values of 1.3 and 1.75, and standard deviations of 0.09 and 0.24 for *in-situ* deposited and thermal deposited Al SBDs are measured, respectively (Fig. 4). The narrow distribution of the ideality factor values and greatly reduced leakage current in the *in-situ* MBE grown Al-SBDs on GaN represents a high quality and uniform metal-semiconductor interface without contamination from the atmosphere. Furthermore, the noise performance of both types of SBDs is under evaluation and will be reported.

kycheng@ee.nthu.edu.tw

How Surface Leakage and Dislocations Affect Diode Behavior in Micrometer-Sized SiGe/Si Heterostructures

A. Jung,[1,*] F. Isa,[1] T. Kreiliger,[1] Y. Arroyo Rojas Dasilva,[2] R. Erni,[2] P. Niedermann,[3] G. Isella,[4] and H. von Känel[1]

[1] *Laboratory for Solid State Physics, ETH Zürich, Otto-Stern-Weg 1 CH-8093 Zürich, Switzerland.*
[2]*Electron Microscopy Center, Empa-Swiss Federal Laboratories for Materials Science & Technology, Switzerland*
[3]*CSEM, Rue Jaquet-Droz 1, CH-2002 Neuchâtel, Switzerland*
[4]*L-NESS, Department of Physics, Politecnico di Milano, via Anzani 42, I-22100 Como, Italy.*

Tel: + 41 44 633 23 39, Email: junga@phys.ethz.ch

The growth of lattice mismatched materials remains one of the major challenges in semiconductor heteroepitaxy due to defects resulting from lattice and thermal misfits. Thick and defect free heterolayers are particularly interesting for applications such as efficient LEDs and sensitive photodetectors requiring perfect crystal quality. Substrate patterning, together with an out-of-equilibrium deposition technique [1], provides a way to circumvent the obstacles of heteroepitaxy by growing space filling arrays of relaxed micro-crystals even tens of micrometers tall [2]. We apply this peculiar approach to the archetypal example of germanium on silicon heterointegration and demonstrate that by combining a very shallow Ge grading rate together with high aspect ratio structures, a complete suppression of misfit and threading dislocations is achieved by pure elastic relaxation.

Here, we focus on the effect of misfit dislocations at the SiGe/Si heterojunction on the leakage current of SiGe/Si heterojunction diodes in such tall micro-crystals (Fig 1a). The impact of pattern dimensions and grading rate, both affecting the dislocation density and thus the leakage current, is elucidated. We demonstrate the significance of surface passivation for those structures having a very high surface to volume ratio. Electrical investigations of the microcrystals' Si/SiGe interface is done by contacting with a tungsten tip within a scanning electron microscope (SEM) chamber (Fig 1b, c). The dislocation density is quantified by etch pit counting and transmission electron microscope investigations.

Our results show the feasibility of integrating thick SiGe micro-crystals on patterned Si with drastically reduced dislocation densities and its impact on pn-diodes realized in those. We think this approach may provide new possibilities for high-end optoelectronic applications such as the realization of a monolithically integrated Ge X-ray absorber on Si that yields superior sensitivity and resolution.

References

[1] C. Rosenblad et al. Appl. Phys. Lett 76, 427 (2000)
[2] C. V. Falub et al. Science **335**, 1330 (2012).

We1745

Hot electron transport studies of W/Si and Cr/Si diodes using Ballistic Electron Emission Microscopy

Christopher Durcan, Westly Nolting, Avery Green, Brendan O'Brien

College of Nanoscale Science and Engineering, SUNY Albany, 253 Fuller Rd. Albany, NY 12203

Nicholas Pieniazek, Dr. Vincent P. LaBella

Colleges of Nanoscale Science and Engineering, SUNY Polytechnic Institute,

257 Fuller Rd. Albany, NY 12203

Electron scattering in nanoscale materials is of fundamental and technological importance as well as the transport of carriers across metal semiconductor interfaces. We utilize an STM based technique called ballistic electron emission microscopy (BEEM) to measure the hot electron attenuation length of metals as well as map the Schottky barrier height to nanoscale resolution, as is shown in Fig. 1. By injecting electrons from the tip in the energy range 200meV - 1.5V and measuring the BEEM current as a function of tip position a map of the Schottky barrier height can be measured. In addition, by measuring the decay in BEEM current vs. metal thickness, a hot electron attenuation length can be measured. The Schottky barrier acts as an electron filter to extract only unscattered electrons. By varying the metal thickness, an attenuation length is measured.

To understand the relationship between bulk resistivity and the attenuation lengths measured with BEEM, attenuation lengths of W and Cr are studied as they have larger resistivities: 5.6 μΩ-cm, 12.6 μΩ-cm, respectively than what has been studied previously (e.g. Cu, Au: 1.7 μΩ-cm, 2.3 μΩ-cm, respectively)[1,2]. This allows for the comparison of BEEM attenuation lengths to resistivity over an order of magnitude, showing an inverse relationship between the two. This indicates that BEEM measurements are sensitive to the intrinsic properties of the metal and not solely the structure of the films. In addition, fluctuations in the Schottky barrier height at the interface at the nanoscale will be presented [3].

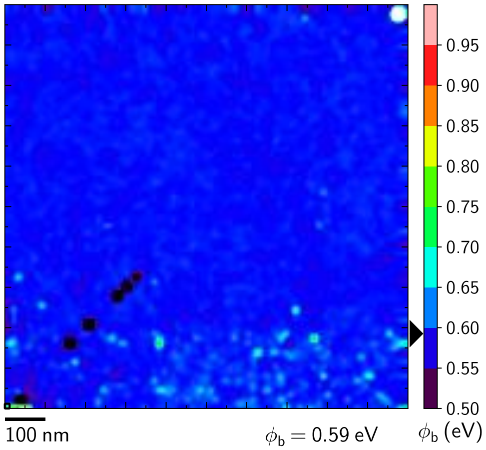

Fig.1 Schottky barrier height map of the Cr/Si(111) diode

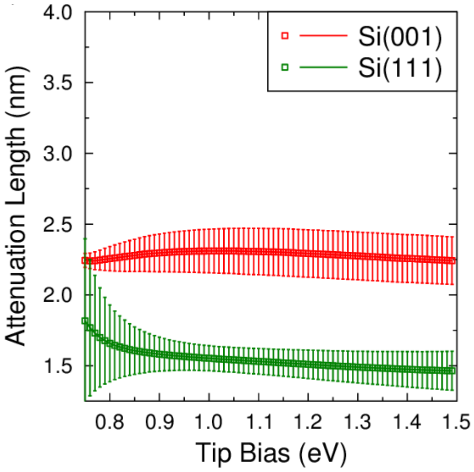

Fig.2 Hot electron attenuation length of W/Si(001) and W/Si(111) diodes

1) Garramone et all, Applied Physics Letters, 96 062105 (2010)
2) Stollenwerk et all, Physical Review B, 77 033416 (2008)
3) Durcan et all, Journal of Applied Physics, **117** 245306 (2015)

We1750

Charge transport mechanisms in p-i-n anisotype GaSb/GaAs hetrojunctions

A. Sellai[1], M. Aziz[2], M. Henini[2] and A. Mesli[3]

[1]Department of Physics, Sultan Qaboos University, Oman
[2]School of Physics and Astronomy, Nottingham Nanotechnology and Nanoscience Center, University of Nottingham, NG7 2RD, United Kingdom
[3]IM2NP, CNRS (UMR 7334), and Université Aix-Marseille, 13397 Marseille Cedex 20, France Marseille Cedex 20, France

Abstract:
Due its narrow direct low band gap, GaSb have shown potentiality for applications in high speed devices, infrared optoelectronic devices and photovoltaic cells. GaSb can be grown on low-cost GaAs substrates using the interfacial misfit growth mode to relieve the strain between the mismatched GaAs substrate and the GaSb epitaxial layer but often results in interface states made mainly of Ga-dangling bonds localized at the GaSb/GaAs interface [1]. It is of relevance to study the electronic properties and current transport mechanisms, likely to be affected by the properties at the interface, in these structures. In this context, the current-voltage (I-V) characteristics were measured at temperatures between 40 K and 300 K for a p-n junction diode made of p-GaSb and n-GaAs contact layers separated by very thin undoped GaSb and GaAs spacers. The I-V data is initially analyzed within the framework of thermionic emission theory and used to extract salient parameters of the diode and to study their dependence on temperature.

First, a quantitative estimation of the distance between the misfit dislocations and the related density of surface states yielded the respective values of 7.8 nm and $1.65\text{x}10^{12}$ cm^{-2}.

The temperature dependence of the potential barrier-height is found to be well described by the linear relationship: $\varphi_0(T)=\varphi_0(0)-\beta T$, $\Phi(T) = \Phi(0) - \beta T$ with a temperature coefficient $\beta \sim 2.2\text{x}10^{-3}$ eV K^{-1} and a potential barrier at T = 0 K of $\varphi_0(0) = 1.14$ eV.

The derived ideality factor shows temperature dependence and increases significantly at lower temperatures indicating the predominance of a conduction mechanism other than thermionic emission. The standard Richardson plot of $\text{Ln}(I_0/T^2)$ versus 1/T, which should be linear if thermionic emission is the prevailing current conduction process, is only linear over a certain temperature range and yielded a modified Richardson's constant A* = $2.65\text{x}10^2$ $\text{A/m}^2\text{K}$, which is orders of magnitudes lower than that of either GaAs (8 $\text{x}10^4$ $\text{A/m}^2\text{K}$) or GaSb (5 $\text{x}10^4$ $\text{A/m}^2\text{K}$). The drawbacks that arise when considering only thermionic emission in data analyses could be conveniently addressed if an alternative thermionic-field-emission conduction process in which tunneling plays a key role is used instead. The ideality factor variations with temperature could then be well fitted over the entire temperature range to an analytical expression derived on the basis of this alternative model with the assumption of a doping density that is one order of magnitude higher than what it was initially supposed to be. Also, a modified Richardson's plot shows perfect linearity over the whole temperature range considered with a slope yielding an activation energy from which the band gap discontinuity between GaSb and GaAs could be estimated.

[1] M. Aziz et al., J. Appl. Phys. 114, 134507 (2013)

Keywords: GaSb/GaAs heterojunction, Current conduction mechanism, Thermionic field emission, interface properties in misfit growth heterojunctions.

Structural Properties of β-FeSi$_2$ Thin Films on Si(111) Substrate and Electrical Transport Properties of n-Type β-FeSi$_2$/p-Type Si Heterojunctions Prepared by Radio Frequency Magnetron Sputtering

Nathaporn Promros[1], Ryuji Baba[2], Hirokazu Kishimoto[2], Phongsaphak Sittimart[1], Weerasaruth Kaenrai[1], Takanori Hanada[2], Abdelrahman Zkria[2], Mahmoud Shaban[3], and Tsuyoshi Yoshitake[2]

[1]Department of Physics, Faculty of Science, King Mongkut's Institute of Technology Ladkrabang, Bangkok 10520, Thailand
Email:nathaporn_promros@kyudai.jp

[2]Department of Applied Science for Electronics and Materials, Kyushu University, Kasuga, Fukuoka 816-8580, Japan

[3]Department of Electrical Engineering, Aswan Faculty of Engineering, Aswan University, Aswan 81542, Egypt

Using radio frequency magnetron sputtering, β-FeSi$_2$ thin films were deposited on p-type Si(111) substrates at a substrate temperature of 560 °C. From the XRD pattern, a weak 404/440 peak and strong 202/220 peak, which are typical peaks for β-FeSi$_2$ thin films epitaxially grown on Si(111) substrates, were evidently observed. The pole figure concerning the β-440/404 peak showed the existence of three types of epitaxial variant that are rotated at an angle of 120° with respect to each other. n-Type β-FeSi$_2$/p-type Si heterojunctions, which exhibited typical rectifying action, were investigated for the possible mechanisms of current transport by estimation of the ideality factor from the slope of the linear part of the forward *I-V* characteristics at low temperatures. At 300 K, the ideality factor was calculated to be 1.95 and it was almost constant at temperatures between 300 K and 120 K. This suggests that the predominant transport mechanism through the n-type β-FeSi$_2$/p-type Si heterojunctions was a recombination process. At temperatures below 120 K, the values of ideality factor were higher than two and the parameter *A* was almost constant. Concerning the temperature dependent ideality factor and the constant value of parameter *A*, it was expected that the current transport was dominated by a trap-assisted multi-step tunneling process.

We1800

Lead telluride through transformation of plumbonacrite in CVD process And its behavior as part of PbTe-Si diode

I.R. Chávez Urbiola[1], R. Ramírez Bon[1], Y.V. Vorobiev[1]

[1]CINVESTAV-IPN, Unidad Querétaro, Libramiento Norponiente 2000, 76230 Querétaro, México.

Abstract

Plumbonacrite $Pb_{10}(CO_3)_6O(OH)_{60}$ is a natural lead salt which is produced by lead degradation. The plumbonacrite can be used as a multifunctional material due to its potential to be transformed into different functional material as PbO, PbS, PbSe and PbTe. Therefore a synthetic plumbonacrite-film represents an alternative way to obtain lead chalcogenides which are used in a technological gadgets. The plumbonacrite film synthesis in this work is carried out by Photo Chemical Bath Deposition (PCBD) over silicon (n-type) substrate. The deposition process took place at room temperature in flat baker with a total area of 20 cm^2, the deposition area is just limited by the size of the baker and the radiation area therefore this process can be reproduced in large scale. The plumbonacrite film is transformed into a PbTe film by interaction with a tellurium hot gas in a CVD reactor. The deposited plumbonacrite and PbTe films were characterized by X-ray diffraction; morphology and thickness of samples were verified by Scanning Electron Microscopy (SEM). The chemical composition was measured by Energy dispersive X-ray spectroscopy. Optical reflection spectra were recorded in the wavelength range $4000cm^{-1}$–$400cm^{-1}$ with FTIR Spectrum. Electrical properties were obtained from Hall measurements, which were performed at room temperature, in accordance with the standard Van der Pauw configuration. XRD shows a hexagonal structure for the plumbonacrite film (Powder Diffraction File 19-0680), and after telluride gas treatment the plumbonacrite structure suffers a change turning from hexagonal structure to cubical structure of lead telluride. Scanning electron microscopy images shows that the plumbonacrite film is composed of thin circular flakes with approximate thickness of 133 nm and diameter 3.4 micrometers, there is no space between flakes. The plumbonacrite films suffer a morphological transformation when placed under tellurium hot gas, the flakes start to transform into cubical grains which is a typical morphology of a PbTe film. Hall measurements showed that our PbTe films had p-type conduction. The device Si (n-type) / PbTe (p-type) shows a satisfactory behavior as diode at 300K (saturation current of 2.66E-8 and ideality diode factor of 3) and presents photoelectric effect that we hope to improve optimizing the structure and technological procedure.

Key words: PbTe film, diode PbTe/Si, CVD, PCBD, Plumbonacrite.

Thursday Morning

2D Materials III

Th0830 Invited

Excitonic Effects in 2D Semiconductor Layers

Tony F. Heinz

Departments of Applied Physics and Photon Science
348 Via Pueblo Mall, Stanford, CA 94305, USA
Email: tony.heinz@stanford.edu

In this paper we discuss recent advances in our understanding of the optical properties of monolayers of the transition metal dichalcogenide (TMDC) materials, including MoS_2, $MoSe_2$, $MoTe_2$, WS_2, WSe_2. These materials share several unusual characteristics, including a transition from an indirect-gap material in the bulk to a direct-gap, emissive material at monolayer thickness. They also exhibit selectivity to excitation of the degenerate K or K' valley under circularly polarized radiation. In our discussion, we will focus on their unusually strong and distinctive excitonic effects. These materials exhibit greatly enhanced excitonic interactions both as a consequence of the 2D quantum confinement of the carriers and of the reduced dielectric screening associated with their ultrathin character. We will describe the manifestations of these excitonic effects in terms of the binding energy and anomalous Rydberg spectrum of the excitons, as well as screening of the excitons induced be free charges. We will also discuss the formation of stable charged excitons (trions) and of biexcitons. At high excitation densities, we have identified the signatures of a Mott transition, including the disappearance of excitonic correlations and the emergence of a very large band-gap renormalization.

Optical spectroscopy in monolayer transition metal dichalcogenides: Excitonic properties and valley dynamics

Bernhard Urbaszek

Université de Toulouse, INSA-CNRS-UPS, LPCNO Toulouse, France

Transition metal dichalcogenides (TMDCs) such as WSe_2 and MoS_2 are layered semiconductors, with strong in-plane bonds and Van-der-Waals bonding between the individual layers. Although indirect semiconductors in bulk form, when thinned down to one monolayer (ML) they become direct semiconductors in the visible/IR region of the optical spectrum [1]. These atomically flat 2D materials have unique physical properties for manipulating electrons in non-equivalent valleys in momentum space and can potentially serve as building blocks in Van-der-Waals heterostructures for optoelectronics applications. In this talk we will review the optical properties of ML TMDCs governed by robust excitons, Coulomb bound electron-hole pairs. We discuss valley state manipulation with polarized lasers and the numerous open questions and challenges in this fast growing field.

ML TMDCs share common properties: The ML crystals have no inversion centre, contrary to graphene or bilayer TMDCs. In addition, the spin-orbit (SO) coupling is strong due to the heavy transition metal atoms. This combination leads to a unique coupling of electron spin and k-space valley physics, initially described in a single particle picture [2]. When electrons and holes are simultaneously present, they will form excitons as the Coulomb interaction is enhanced by the strong quantum confinement, the large effective masses, and the reduced dielectric screening in these ideal 2D systems. Excitons with typical binding energies of 500 meV dominate the optical properties of ML TMDCs as the 1s, 2s, 2p…. exciton states are resonantly excited, also Raman scattering amplitudes are strongly affected by exciton resonances [3]. Due to the high oscillator strength of excitonic transitions, the intrinsic radiative lifetimes are expected to be short, and in time resolved photoluminescence experiments on ML MoS_2, WSe_2 and $MoSe_2$ we find indeed luminescence emission times in the ps range [4].

In addition to these common properties for ML TMDCs we also discuss important differences. We show how valley polarization and coherence can be optically initialized in ML WSe_2 but not ML $MoSe_2$. We also discuss the competition between bright and dark excitons that determines the light emission yield in these binary materials and their ternary alloys $MoWSe_2$ [5].

References
[1] Mak et al, PRL 105, 136805 (2010); Lezema et al, NanoLett 15, 2336 (2015)
[2] Di Xiao et al, PRL 108, 196802 (2012)
[3] Wang et al, PRL 114, 097403 (2015) & Wang et al PRL 115, 117401 (2015)
[4] Lagarde et al, PRL 112, 047401 (2014) & Wang et al PRB 90, 075413 (2014)
[5] Wang et al, Nat. Comms (in press, arXiv 1506.08114)

Th0950

Imaging Spin Dynamics in Monolayer WS_2 by Time-Resolved Kerr Rotation Microscopy

Elizabeth Bushong,[1] Kelly Yunqiu Luo,[1] Kathleen M. McCreary,[2] Michael Newburger,[1] Simranjeet Singh,[1] Berend Jonker,[2] and Roland K. Kawakami[1]

[1]*Department of Physics, The Ohio State University, Columbus OH, 43210*
[2]*Materials Science and Technology Division, Naval Research Laboratory, Washington DC, 20375*

Transition metal dichalcogenides (TMDs) such as WS_2 offer a unique platform to probe spin and valley degrees of freedom in two-dimensional condensed matter systems. Monolayer WS_2 and related TMDs (e.g. MoS_2, $MoSe_2$, WSe_2) are of great interest because they have a direct band gap and optical selection rules that permit the excitation of valley-polarized and spin-polarized electrons using circularly polarized light. Strong spin-orbit coupling leads to valley-dependent spin-splitting in both the conduction and valence bands, which may suppress spin relaxation and inhibit intervalley scattering, thereby increasing both the spin and valley lifetimes. However, most experimental studies of spin/valley dynamics have observed short lifetimes (<50 ps).

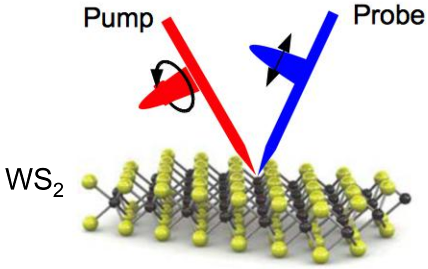

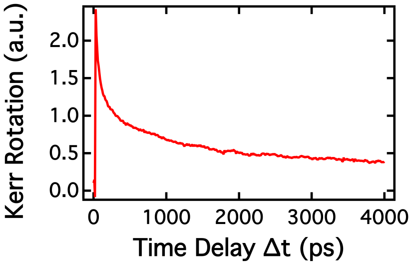

To measure the spin and valley dynamics of WS_2, we have developed time-resolved Kerr rotation microscopy with spatial resolution better than 1 micron and temporal resolution of 150 fs. WS_2 samples are grown by CVD and exhibit native n-type doping. Spin/valley-polarized excitons are generated by the absorption of a circularly-polarized pump pulse tuned near the exciton absorption peak, as determined by photoluminescence spectroscopy. These excitons interact with resident conduction electrons in the WS_2 and transfer some of their spin/valley polarization to the electrons. A time-delayed, linearly polarized probe pulse measures the spin/valley polarization of both the excitons and the resident electrons via Kerr rotation of the linear polarization axis. The spin dynamics are determined by varying the time delay between the pump and probe pulses. Interestingly, we observe a long spin lifetime of 5.1 ns in WS_2 at $T = 6.5$ K, which is similar to very recent reports of long spin lifetimes in MoS_2 by other groups [L. Yang, N. A. Sinitsyn, W. Chen, J. Yuan, J. Zhang, J. Lou, and S. A. Crooker, *Nature Phys.* **11**, 830-834 (2015)].

To investigate the nature of the long-lived spin states in WS_2, we perform, for the first time, high resolution imaging of the spin dynamics. We find a strong spatial dependence of the spin lifetimes with regions of spin lifetime less than 100 ps and regions of spin lifetime greater than 5 ns separated by only a few microns. In order to understand the origin of the long-lived spins, we investigate the relationship between spin lifetime and the photoluminescence intensity. Preliminary results suggest that the transfer of spin angular momentum from the exciton to the resident electrons is the crucial step to realize the long-lived states. Application of in-plane magnetic fields shows an oscillatory component and a non-oscillatory component, indicating two types of spin populations that experience different internal effective fields.

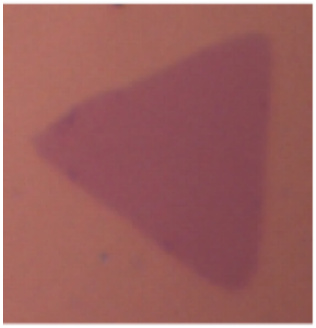

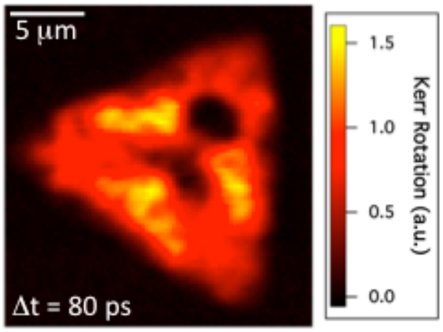

Measuring band alignment of transition metal dichalcogenides and graphene using low-energy electron microscopy

Sergio C. de la Barrera[1], Patrick C. Mende[1], Jun Li[1], Yu-Chuan Lin[2],
Suresh Vishwanath[3], Joshua A. Robinson[2], Huili Xing[3], and Randall M. Feenstra[1]

[1]Carnegie Mellon University, Department of Physics, Pittsburgh, PA 15213
[2]The Pennsylvania State University, Materials Science and Engineering,
State College, PA 16801
[3]Cornell University, Electrical and Computer Engineering, Ithaca, NY 14850

January 17–21, 2016

Abstract

Determining accurate experimental band offsets between graphene and 2D semiconducting transition metal dichalcogenides (TMDs) is crucial for the study of 2D heterostructures. Traditional methods for measuring band offsets between semiconductors include photoemission spectroscopy, optical techniques, and electrical transport measurements. Each method has its advantages and disadvantages depending on the material system, geometry, and required resolution. Measuring the band alignment at the interface of layered 2D heterostructures, for instance, requires extreme surface sensitivity and fine lateral resolution for small crystals. Furthermore, charge transfer between 2D layers can shift the band alignment from the ideal scenario suggested by alignment of electron affinities. Here, we report effective conduction band offsets and carrier densities for TMDs grown on epitaxial graphene obtained by spectroscopic analysis of low-energy electron microscopy (LEEM) images. LEEM utilizes a focused beam of electrons in the 0–20 eV range to interact with only the outer-most atomic layers of a sample surface, ideal for probing 2D materials. The lateral resolution of LEEM, comfortably below 100 nm, allows for spatial study of the electrostatic potential variation across the sample surface by comparing the work function difference between the electron gun and sample at various points on the surface. The potential difference between a 2D crystal and an exposed region of the layer below can be used to infer the effective band offset due to charge transfer between the two layers, and subsequently the carrier density or unintentional doping of the TMD layer. This technique is applied to WSe_2 on epitaxial graphene (EG), WSe_2 on quasi-freestanding EG, and $MoSe_2$ on EG to show that measured values differ significantly from simple differences of electron affinities, depending on the sample preparation. The ramifications of these values for the behavior of electronic devices based on such heterstructures are discussed.

Thursday Morning

Spintronics II

Th1100 Invited

FMR-Drive Pure Spin Transport in Metals and Antiferromagnetic Insulators

Fengyuan Yang, Department of Physics, The Ohio State University

Spintronics relies on the generation, transmission, manipulation, and detection of spin current mediated by itinerant charges or magnetic excitations. In recent years, pure spin transport driven by ferromagnetic resonance (FMR) spin pumping or a thermal gradient has attracted intense interest and become one of the most active frontiers in condensed matter physics. In both of these regimes a dynamic excitation of the magnetization results in the transfer of spin angular momentum in the absence of net charge flow, a long-sought goal for the field. Extensive research efforts over the last few years have demonstrated pure spin currents in a broad range of materials. These advances significantly enrich our understanding of dynamically-driven spin transport in heterostructures and open new paradigms for energy-efficient, spin-based information processing, data storage and sensing applications.

Building on the high-quality $Y_3Fe_5O_{12}$ (YIG) films [see Figs. 1(a)-1(c)] grown by a unique sputtering technique and the large inverse spin Hall effect (ISHE) signals enabled by these films, we have characterized pure spin currents in several classes of materials with different magnetic structures, including: nonmagnetic (NM) metals, ferromagnetic (FM) metals, nonmagnetic insulators, and antiferromagnetic (AF) insulators. The spin Hall angles determined for a series of 3*d*, 4*d*, and 5*d* NM metals show that both atomic number and *d*-electron count play important roles in spin Hall physics. By inserting an insulating spacer of various materials between YIG and Pt [Fig. 1(d)], we are able to probe the mechanism of spin pumping and the spin propagation. More interestingly, we observed robust spin current from YIG to Pt across AF insulators, which initially enhances the ISHE signals and can transmit spin currents up to 100 nm thickness, demonstrating highly efficient spin transport through an AF insulator carried by magnetic excitations. Our results show a strong correlation between spin propagation lengths in the AF insulators with the AF ordering temperatures [Fig. 1(e)]. An excellent linear relationship between the spin decay length in the AF insulators and the damping enhancement in YIG was observed, which suggests the critical role of magnetic correlations in the AF insulators as well as at the AF/YIG interfaces for spin transport in magnetic insulators. This offers a powerful platform for studying AF spin transport and AF dynamics as well as for exploration of spin manipulation in tailored structures comprising metallic and insulating FMs, AFs, and NMs.

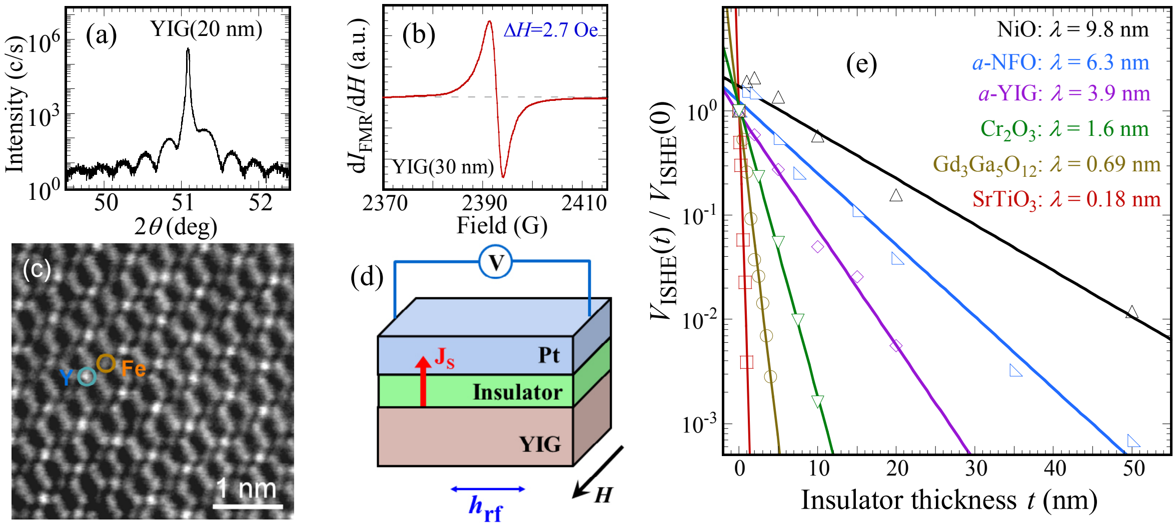

Fig. 1. (a) An x-ray diffraction scan of a 20-nm YIG epitaxial film on $Gd_3Ga_5O_{12}(111)$ shows clear Laue oscillations, indicting uniform single-crystalline structure. (b) Derivative of an FMR absorption scan of a 30-nm YIG film with a narrow linewidth of 2.7 Oe. (c) A scanning transmission electron microscopy (STEM) image of a YIG film shows clearly ordered Y and Fe atoms in garnet structure. (d) Schematic of ISHE measurement on Pt/insulator/YIG structures. (e) Semi-log plot of ISHE voltage (V_{ISHE}) as a function of the insulator thickness for the six series normalized to the values for the corresponding Pt/YIG bilayers, where the straight lines are exponential fits to each series, from which the spin decay lengths λ are determined.

Th1140

Spin injection in self-assembled InAs/GaAs quantum-dot molecular structures

Y. Q. Huang, Y. Puttisong, I.A. Buyanova, W.M. Chen
Department of Physics, Chemistry and Biology, Linköping University, S-581 83 Linköping, Sweden

While conventional electronics only relies on manipulation of electronic charge, a promising direction for next-generation electronic and photonic devices is expected to benefit additionally from exploiting the spin degree of freedom. Among vital ingredients in achieving spin functionalities are efficient injection of spin polarized carriers or excitons, prolonged spin dephasing/relaxation time as well as our ability to manipulate spin in a desirable way. Semiconductor quantum dots (QDs) have emerged as an excellent materials system in this context, as motion-induced spin relaxation that is dominant in bulk and 2D semiconductor structures is quenched due to the three-dimensional confinement. Indeed, appreciably long spin lifetimes have been reported in semiconductor QDs and a high degree of electron spin polarization has also been demonstrated through optical orientation under resonant excitation of QD excitons. However, upon spin injection from adjacent layers such as a wetting layer (WL) and a barrier layer, that is a necessary step required for operation of most envisaged spintronic devices based on QDs, reported values of electron spin polarization degree of QDs remain very low so far. The exact physical mechanism for the observed low spin injection efficiency is still not understood, unfortunately, though it was generally believed to be associated with accelerated spin relaxation in WL and barrier layers when carrier and exciton motions (i.e. with a non-zero momentum ***k***) promote spin-orbit mediated spin relaxation. Up to now, WL and barrier layers surrounding QDs are commonly regarded as being of “ideal” 2D and 3D characters, respectively.

In this work we examine the exact path of spin injection from WL and barriers into QDs in self-assembled InAs/GaAs QDs and lateral QD molecular structures (QMSs), by employing optical orientation, single-dot photoluminescence (PL) and PL excitation spectroscopy. The studied QDs and QMSs include single quantum dots (SQDs), laterally-aligned double QDs (DQDs), quantum rings (QRs), and quantum clusters (QCs). We find, surprisingly, that exciton spin injection in these QDs and QMSs is dominated by localized excitons confined within the QD-like regions of the WL and GaAs barrier layer immediately surrounding QDs and QMSs that in fact lack the commonly believed 2D and 3D character with an extended wavefunction. We identify the microscopic origin of the observed severe spin loss during spin injection as being due to a sizable anisotropic exchange interaction of the localized excitons in the WL and GaAs barrier layer, which has so far been overlooked. We find that the AEI of the injected excitons and thus the efficiency of the spin injection processes are directly correlated with the overall geometric symmetry of the QMSs, namely, spin injection is more efficient in the QMSs with a higher symmetry in geometric arrangement such as QRs and QCs as compared with the lower-symmetry DQDs. This correlation is attributed to the fact it is the symmetry of the QMSs that largely defines the anisotropy of the confinement potential of the localized excitons in the surrounding WL and GaAs barrier, which governs the AEI. This work represents a significant advance in our understanding of the spin injection processes and spin loss mechanism in QDs and QMSs, and it also provides a useful guideline in designing strategies to improve spin injection efficiency by optimizing the lateral arrangement of the QMSs, thereby overcoming a major obstacle in utilizing semiconductor QDs and QMSs for device applications in spintronics and quantum information processing.

Th1145

THE ROLE OF INTERFACE DIPOLE FOR SWITCHING SPIN STATE OF SPIN CROSSOVER MOLECULES

Xin Zhang[1], Yang Liu[1], Alpha N'Diaye[2], Jean-François Létard[3], Bernard Doudin[4], Peter A. Dowben[1]
[1] Department of Physics and Astronomy, University of Nebraska – Lincoln, United States
[2] Advanced Light Source, Lawrence Berkeley National Lab, United States
[3] CNRS, ICMCB, Université de Bordeaux, France
[4] CNRS, IPCMS, Université de Strasbourg, France

If the dipole and molecular band offsets that result from a molecular hetero-interface can be manipulated, there is an unparalleled opportunity to build novel organic devices. The engineering of these interfaces and possible voltage control of the hetero-interface also provides means for voltage controlled surface chemistry at a hetero-interface [1]. The spin crossover molecules form a significant class of organic materials for which the magnetic structure can be altered at the atomic level by an external stimulus. The spin state of [Fe($H_2B(pz)_2)_2$(bipy)] thin film is mediated by changes in the electric field a the interface of organic ferroelectric polyvinylidene fluoride with trifluoroethylene (PVDF-TrFE). Signatures of the molecular crossover transition are evident in the placement of the unoccupied states and associated with changes in electronic structure in the transition from diamagnetic to paramagnetic [2]. Consistent with the observation that dipole at interface can control the spin crossover molecule spin state, we have found that the molecule was locked at low spin states when grown on the SiO_2/Si substrate, but can be excited to high spin state by X-ray irradiation in a temperature range from 20 K to 350 K. The locking of the spin state in either a low spin diamagnetic state or high spin paramagnetic state implies there is an activation barrier to the spin crossover transition. The existence of such an activation barrier is confirmed by time dependent X-ray absorption spectroscopy (XAS). The time dependent spin crossover transition (Figure 1) is likely due to the surface charge that builds up at the interface during the X-ray photoemission process. On a conducting substrate, like Au(111), the molecule stays in a fixed spin state and no such time dependent spin cross over transition is observed [3]. These results demonstrate that the interface dipole plays an important role, affecting the molecule electronic structure and spin state.

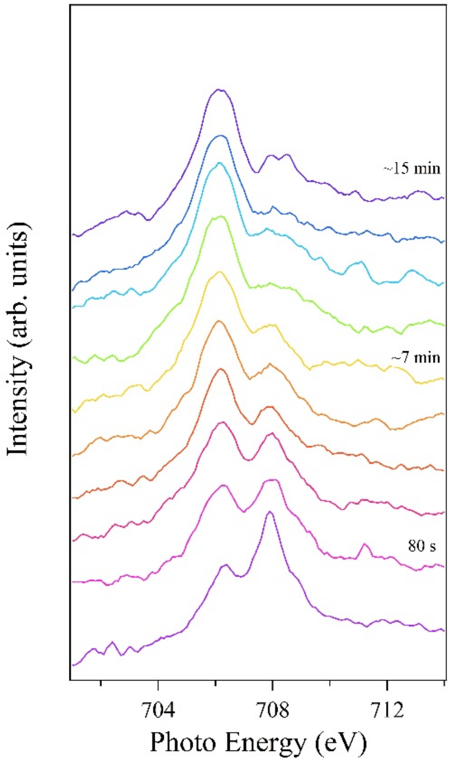

Figure 1. X-ray absorption spectroscopy of 5 nm [Fe($H_2B(pz)_2)_2$(bipy)] molecule thin film on SiO_2/Si substrate at 200 K. The time dependent XAS spectra shows the dynamic process of unoccupied orbitals when the molecule spin stated was excited from low spin to high spin state by X-ray irradiation.

[1] Z. Zhang, R. Gonzalez, G. Diaz, L. G. Rosa, I. Ketsman, X. Zhang, P. Sharma, A. Gruverman, and P. A. Dowben, ***J. Phys. Chem. C***, 2011, 115, 13041–13046.

[2] X. Zhang, T. Palamarciuc, J.-F. Létard, P. Rosa, E. V. Lozada,a, F. Torres, L. G. Rosa, B. Doudin and P. A. Dowben, ***Chem. Commun.***, 2014, **50**, 2255-2257

[3] S. Beniwal, X. Zhang, S. Mu, A. Naim, P. Rosa, G. Chastanet, J.-F. Létard, J. Liu, G. E. Sterbinsky, D. A. Arena, P. A. Dowben, and A. Enders, “Substrate-induced spin state locking of the [Fe($H_2B(pz)_2)_2$(bipy)] spin crossover complex”, submitted 2015.

Frequency-dependent current hysteresis measurements for alternating current (AC) characterization of organic/carbon nanotube thin-film transistors by applying sinusoidal wave drain voltage signals

Kazuhiro Watanabe, Ken Tanoue, Yasunori Taki, Kei Noda and Yuji Awano[a)]
Keio University, 3-14-1 Hiyoshi, Kohoku-ku, Yokohama, Japan, [a)]Email: awano@elec.keio.ac.jp

I. INTRODUCTION

Organic/carbon nanotube thin-film transistors (OTFTs/CNT-TFTs) have attracted much attention as light, low cost, flexible, and printable devices in large-area electronics applications. However, their alternating current (AC) characteristics have not yet been well understood, and a measuring method for them has still not been established. Because of their high impedance, conventional AC characterization methods for inorganic field-effect transistors (FETs), such as S-parameter extraction, are not suitable. The hysteresis effect in the current-voltage (I-V) characteristics of OTFTs, which is often observed, should be completely eliminated for reliable and stable circuit operation. In this paper, we propose a method for AC characterization of OTFTs, which uses this effect effectively. By using a sinusoidal wave signal as a terminal voltage, together with a measuring circuit considering the high impedance of OTFTs, we investigated the frequency-dependent current hysteresis phenomena in OTFTs to reveal the underlying effects related to the trapping and de-trapping phenomena of mobile charges at the material interfaces.

II. EXPERIMENTAL

Figure 1 shows a schematic of the measuring setup, where the sinusoidal wave is applied as drain voltage Vds. By applying sinusoidal wave signals as terminal voltages, we can measure the frequency-dependent electrical properties of OTFTs. Even if a pulsed input signal is often used for electron device measurements and the sinusoidal wave input signal is little known, the latter signal is useful for directly measuring the frequency-dependent phenomena, for example, trap-related phenomena. In a conventional measuring circuit, a current path junction to the measurement unit is put upstream of the TFT. However, in the case of OTFTs, we cannot accurately differentiate the current in an OTFT, as it is comparable with the leak current passing through the measurement equipment, because the OTFT impedance is nearly as high as that of the measurement equipment. Therefore, we propose putting the current path junction downstream of the FET, as shown in Fig. 1. The pentacene, dinaphtho[2,3-b:2',3'-f]thieno[3,2-b]thiophene (DNTT), and CNT-TFTs with a bottom-gate bottom-contact (BGBC) structure were fabricated. In the case of CNT-TFTs, we used an inkjet process with semiconductor-enriched single-walled nanotube (SWNT) ink to form a position-controlled thin film channel on 3-aminopropyltriethoxysilane (APTES) - functionalized SiO_2.

III. RESULTS AND DISCUSSION

Figure 2 shows the frequency dependence of the drain current-voltage (Ids-Vds) characteristics of a pentacene TFT in atmosphere at room temperature. A larger hysteresis in the Ids-Vds characteristics was initially observed then became smaller as the frequency became higher, which is normally not observed in FETs. Some of the mechanisms that cause hysteresis are already quite well described in literature on inorganic FETs, such as interface-trapped charges, fixed charges in oxide, and trapped charges in oxide. The hysteresis phenomena in OTFTs are partly based on dynamic processes, such as trapping and de-trapping, which depend on the measurement time and duration of the applied voltage. In other words, these phenomena exhibit frequency dependence and voltage dependence of the input signal. The dynamic process for a wide range of operation frequencies and voltages should be avoided for reliable and reproducible AC operation. The terminal capacitances, such as Cgs, Cgd, and Csd, can also cause hysteresis in the I-V characteristics in OTFTs because the channel impedance of OTFTs is extremely high. We discuss how to separate the contributions of the terminal capacitance.

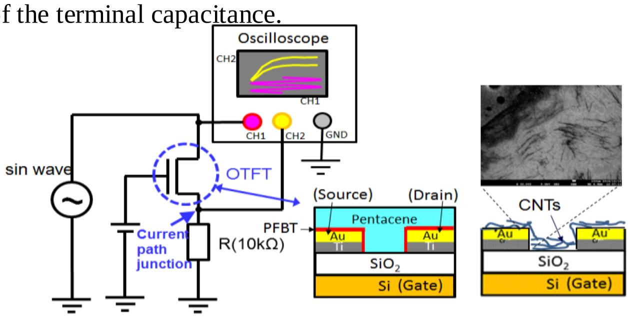

Fig. 1 Schematic of AC characteristics measurement setup for OTFTs

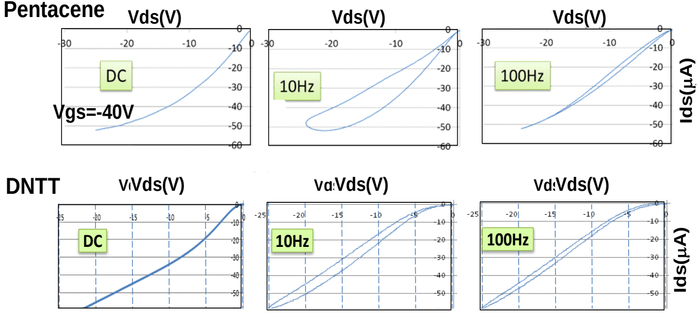

DNTT-TFTs

References

[1] T. Zaki et al., Organic Electronics 14, 1318 (2013)
[2] M. Egginger et al., Monatsh Chem. 140;735 (2009)

Th1155

Surface Composition and Atomic Structure of Single Crystal Bi_2Se_3 Investigated by Low Energy Ion Scattering

Weimin Zhou, Haoshan Zhu, Jory A. Yarmoff
Department of Physics and Astronomy, University of California, Riverside

A topological insulator (TI) is a two-dimensional material that behaves as an insulator in the bulk, but conducts along the surface via topologically protected surface states. TI's have attracted intense interest not only because of the novelty of their fundamental physics, but also because of their great potential in device applications. Because the critical electronic states in TI's are localized in the near-surface region, a complete description of these materials will only be possible if it is coupled with an understanding of the surface composition, surface atomic structure and surface chemistry.

We are using low energy ion scattering (LEIS) to investigate the surface composition and atomic structure of the prototypical TI material, Bi_2Se_3, prepared in different ways [1]. LEIS is uniquely suited to measure surface termination and atomic structure, as it provides the elemental identification of the near-surface region and can be deployed in such a way as to only probe the outermost atomic layer. Bi_2Se_3 is composed of Se-Bi-Se-Bi-Se quintuple layers (QL), so it has been assumed that cleaving leads to a Se-terminated surface. Although some surface structure studies have concluded that the cleaved surface is terminated by Se, other reports show either Bi- or mixed-terminations. We have compared surfaces prepared by *ex-situ* cleaving, *in-situ* cleaving and Ar^+ ion bombardment and annealing (IBA) in ultra-high vacuum. Surfaces prepared by *in-situ* cleaving have sharp 1x1 LEED patterns and are Se-terminated. Surfaces prepared by IBA are Bi-rich after ion bombardment, and the amount of Se in the near-surface region increases with annealing temperature. The angular dependence of the ion scattering yield, which is sensitive to the surface atomic structure, doesn't indicate any substantial differences between the Se-terminated surfaces prepared by IBA or *in-situ* cleaving. Samples inserted into the vacuum chamber following *ex-situ* cleaving have much dimmer LEED patterns, show carbon and oxygen contamination and can be either Se- or Bi-terminated, which suggests that the surface stoichiometry is critically dependent on the level of contamination. Future experiments will involve exposure of clean surfaces to gaseous species to investigate the surface chemical reactions that determine the ultimate termination.

[1] X. He, W. Zhou, Z. Y. Wang, Y. N. Zhang, J. Shi, R. Q. Wu and J. A. Yarmoff, Phys. Rev. Lett. **110**, 156101 (2013).

Th1200

Topological Surface States in Sb Quantum Wells on GaSb(111)A Substrates

K.S. Wickramasinghe, C.K. Gaspe, S. Cairns, N.D. Teasdale,
T.D. Mishima, J.C. Keay, M.B. Johnson, S.Q. Murphy, and M.B. Santos

Homer L. Dodge Department of Physics and Astronomy, University of Oklahoma

Bulk Antimony (Sb) is a semimetal with a negative indirect bandgap, with neither the conduction band minimum nor the valence band maximum at the Γ point. The large atomic number of Sb results in a large spin-orbit coupling for electrons in crystalline Sb, which in turn is predicted to lead to conducting surface states that are topologically protected from elastic backscattering. Angle-Resolved Photoemission Spectroscopy experiments have supported the existence of two types of topological surface states, electrons at the zone center (Γ point) and holes away from the zone center toward the M point, by mapping their dispersion relations [1, 2]. Recent theoretical studies have predicted that this topological semimetal will evolve into a 3D topological insulator when the Sb layer thickness is less than ~7.8 nm, where quantum confinement is sufficient to turn the negative bandgap into a positive bandgap [3]. A 2D quantum spin Hall state is predicted at a thickness of less than ~2.7 nm and a trivial semiconductor state is predicted for films thinner than ~1 nm [3]. Our goal is to enable transport measurements of topological surface states by suppressing the bulk conductivity through quantum confinement in thin Sb layers and enhancing the surface conductivity through remote n-type doping at the Γ point.

We report an experimental study of the growth and characterization of Sb quantum wells (QWs) grown on GaSb(111)A substrates. GaSb (111) is also chosen as the barrier material for Sb, which has a rhombohedral crystal structure, because both materials have a hexagonal arrangement of surface atoms with nearly identical nearest-neighbor distances. In our initial study [4] we used molecular beam epitaxy (MBE) to grow undoped Sb quantum wells on GaAs(111)A substrates. However, there was a high density of defects in these structures due to the 7.8% lattice mismatch between the substrate and epilayers. Because good crystalline quality is a necessity to probe topological surface states via transport measurements, we switched to GaSb(111)A substrates for further studies.

With the aid of *in situ* Reflection High-Energy Electron Diffraction (RHEED) measurements, we have developed a reliable growth method for Sb layers as thin as ~1nm (3 bilayers). The layer structures are shown in Figure 1. A 0.5 µm thick GaSb buffer layer was grown on a GaSb (111)A substrate by conventional MBE procedures at a substrate temperature of approximately 90-100°C below the oxide desorption temperature of the substrate. The Sb QW and GaSb cap layers were grown at 170°C to 200°C, and a migration enhanced epitaxy procedure was used for the GaSb cap. For some structures, we used Te to uniformly n-dope a section of the GaSb barrier below the Sb QW. Figure 2 is a high resolution transmision electron microscopy (TEM) image of a nominally 3.8 nm-thick Sb QW, which has an actual thickness ranging from 4.1 nm to 3.4 nm. This indicates that we have achieved a reasonably good thickness control for ultra-thin films. Atomic force microscopy (AFM) measurements of an uncapped Sb layer showed complete surface coverage of Sb and a root mean square roughness of 0.3 nm for the 3.8 nm-thick Sb QW (Figure 3).

Electrical conductivity measurements on undoped QWs of different thickness show a suppression of the bulk conductivity. This enables surface states to make a noticeable contribution to the conductivity, a ~20% contribution for the 3.8 nm QW for example [5]. The interpretation of Hall-effect measurements, which nominally indicate p-type conduction, is complicated by the presence of both electrons and holes in topological states. We have recently begun experiments to further populate the topological electron states by doping the GaSb barrier with Te atoms, which create donor states at the Γ point. At the Γ point of the Sb QW, the topological electron states have a lower energy than the conduction band minimum of the bulk. We observe clear n-type conduction for a remotely-doped Sb QW with a 94 nm spacer between the doped GaSb layer and the Sb QW. Figure 4 shows that the temperature dependence of the electron density and mobility are characteristic of a remotely-doped QW. We plan to make high-field magneto-transport measurements to verify that Sb surface states are populated rather than Sb bulk states.

Author Index

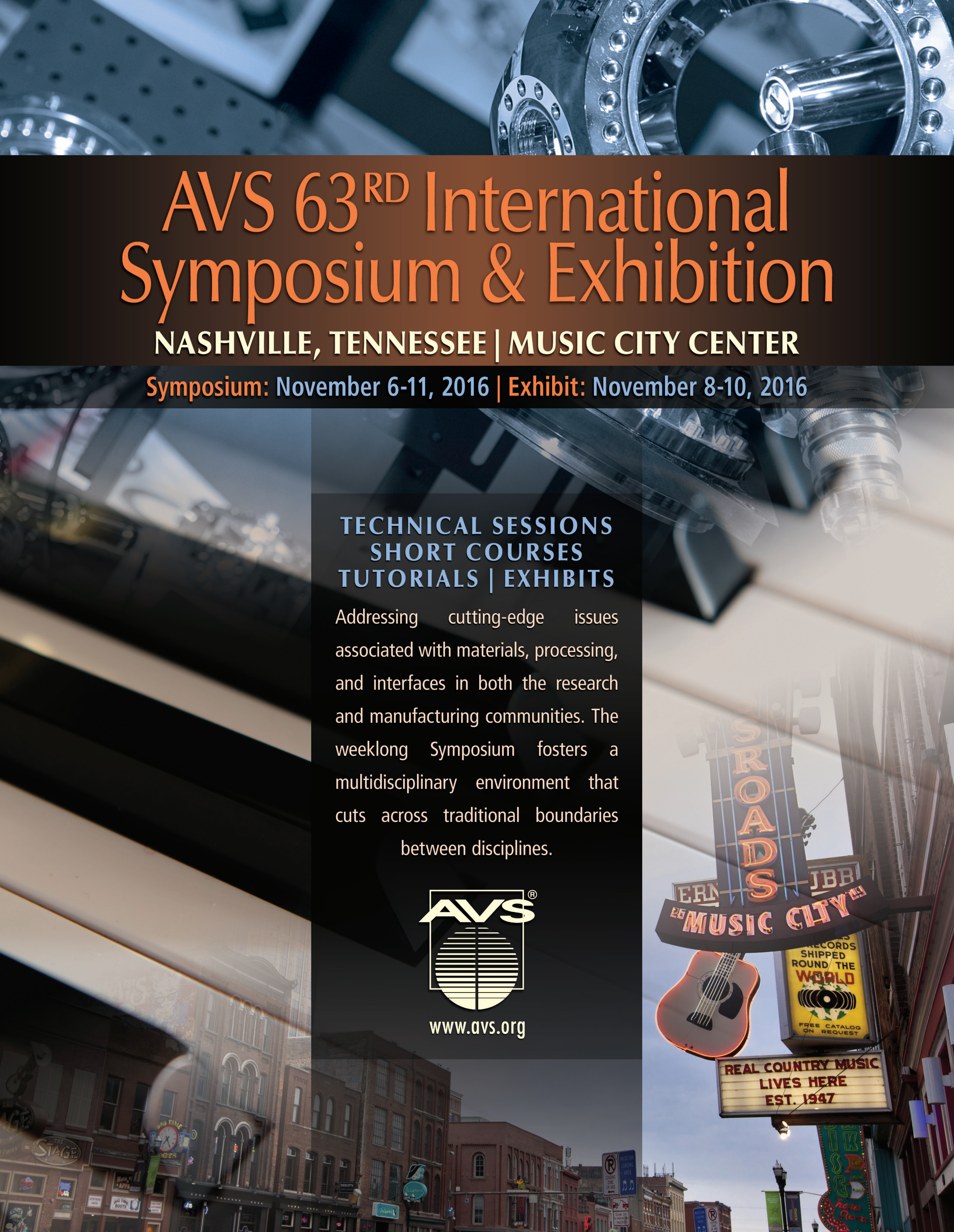

AVS 63RD International Symposium & Exhibition

NASHVILLE, TENNESSEE | MUSIC CITY CENTER

Symposium: November 6-11, 2016 | **Exhibit:** November 8-10, 2016

TECHNICAL SESSIONS
SHORT COURSES
TUTORIALS | EXHIBITS

Addressing cutting-edge issues associated with materials, processing, and interfaces in both the research and manufacturing communities. The weeklong Symposium fosters a multidisciplinary environment that cuts across traditional boundaries between disciplines.

AVS®

www.avs.org